

Lower Miocene carbonate platforms of the Falcón Basin (NW Venezuela) compared to the offshore Perla Field reservoir

Eduard Albert-Villanueva¹ Telm Bover-Arnal^{2,3} Carles Ferràndez-Cañadell⁴ Lenin González⁵ Mateu Esteban⁶ Ramon Salas^{2,3}

¹Denison Mines Corp.

345 4th Avenue South, Saskatoon, Saskatchewan S7K 1N3, Canada. Albert-Villanueva E-mail: eduard.albert21@gmail.com

²Departament de Mineralogia, Petrologia i Geologia Aplicada, Facultat de Ciències de la Terra, Universitat de Barcelona

Martí i Franquès s/n, 08028 Barcelona, Spain. Bover-Arnal E-mail: telm.boverarnal@ub.edu, Salas E-mail: ramonsalas@ub.edu

³Institut de Recerca GEOMODELS

Martí i Franquès s/n, 08028 Barcelona, Catalonia, Spain

⁴Departament de Dinàmica de la Terra i de l'Oceà, Facultat de Ciències de la Terra, Universitat de Barcelona

Martí i Franquès s/n, 08028 Barcelona, Spain. Ferràndez-Cañadell E-mail: carlesferrandez@ub.edu

⁵Departamento de Geología, Escuela de Geología, Minas y Geofísica, Facultad de Ingeniería, Universidad Central de Venezuela.

Ciudad Universitaria, Los Chaguaramos, 1050 Caracas, Venezuela. González E-mail: leningonzalez@hotmail.com

⁶Szalai Grup S.L.

Sant Jaume 11, 07314 Caimari (Selva), Mallorca, Spain. Esteban E-mail: mateu@szalai.es

ABSTRACT

Based on field data collected in the northern and southern Falcón Basin (Venezuela), this paper presents a comprehensive monograph that reports on the age and sedimentary evolution of the San Luis and Churuguara formations. It integrates platform-to-basin depositional models through facies distribution and stratal architecture, a palaeogeographic reconstruction, larger foraminifera biostratigraphy, sequence stratigraphy, and the evaluation of the accommodation history. An additional aim is to compare these onshore mixed carbonate-siliciclastic systems with the Oligo-Miocene subsurface carbonate reservoir of Perla in offshore Gulf of Venezuela, considered the largest gas discovery ever in Latin America. The carbonate platforms studied formed as a result of a second-order transgressive event, and corresponded to distally steepened or undifferentiated ramps dominated by coralline algae and larger foraminifera. The presence of *Miosorites americanus* and *Annulosorites spiralis* dates the San Luis and Churuguara formations to the Early Miocene. The miogypsinid associations identified further distinguish between the Aquitanian and Burdigalian stages. The San Luis and Churuguara platforms exhibit a general aggradational trend, while the Perla carbonates have been interpreted as a retrogradational unit. Third-order T-R sequences interpreted from these successions were mainly influenced by differential tectonic subsidence. Additionally, major regional regressive events in the Falcón Basin and Perla Field coincide with global glaciations, highlighting the influence of eustatic changes. However, the Perla reservoir exhibits significant differences in thickness, spatial extent and sedimentary architecture compared to the onshore equivalents. The differences arise from variations in tectonic and palaeotopographic settings, accommodation and sedimentation rates and influence of adjacent siliciclastic systems. As a result, predicting the sedimentary architecture of carbonate reservoirs in this region using a generalized depositional model has proven to be challenging.

KEYWORDS | Falcón Basin. Caribbean. Carbonate platform. Perla Field. Early Miocene

INTRODUCTION

The Oligocene-Lower Miocene Falcón Basin (Fig. 1) is considered a minor oil province of Venezuela, but contains significant gas reserves in the offshore region (Martínez *et al.*, 2007; Summa *et al.*, 2003). The first geological studies in the basin were carried out between 1912 and 1920 in parallel to the first oil-field discoveries in both Falcón and Maracaibo provinces (Boesi and Goddard, 1991). The geological knowledge of the basin resulting from this first exploration period was compiled by Senn (1935) and González de Juana (1938). Later on, and after

the exploration campaigns carried out by surface geologists from the Creole Petroleum Corporation, Wheeler (1963) established the stratigraphy of the Falcón Basin.

Based on planktonic foraminifera associations, Díaz de Gamero (1977, 1989) furnished the biostratigraphic framework of the Falcón Basin. In the 70's, the Venezuelan Petroleum Corporation started an offshore seismic campaign, continued by the Venezuelan companies Maraven and Corpoven during the 80's. Muessig (1984) and Macellari (1995) performed the first regional tectonosedimentary studies of the Falcón and adjacent

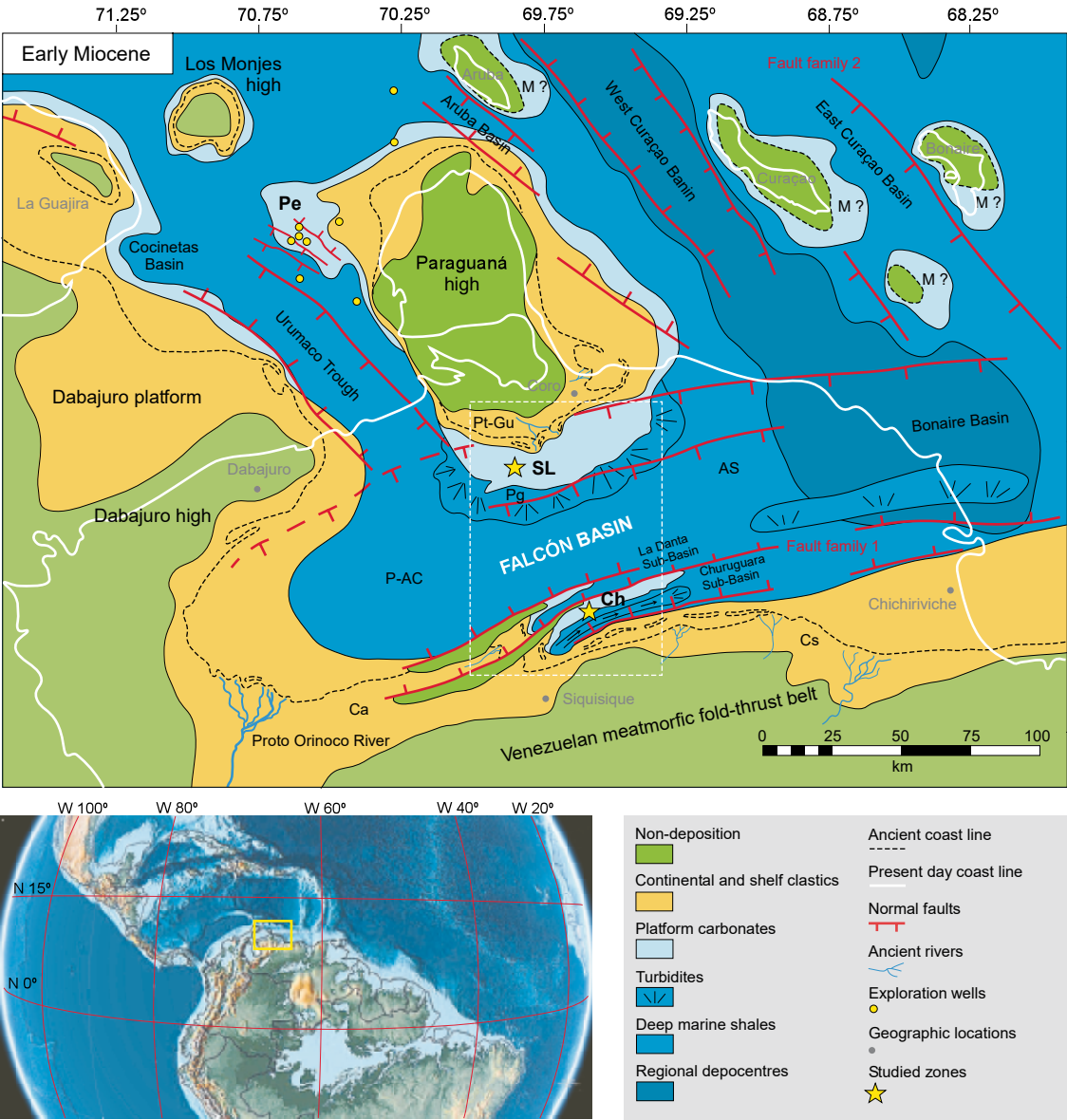


FIGURE 1. Main area: original early Miocene palaeogeography of northwestern Venezuela. The white dot-lined square indicates the location of the geological map shown in Figure 2. Bottom left: early Miocene palaeogeographic globe-map with the location of the study area (modified from Scotese, 2012). AC= Agua Clara Fm., AS= Agua Salada Fm., Ca= Castillo Fm., Ch= Churuguara Fm., Cs= Casupal Fm., Gu= Guarabal Fm., M= Miogypsina-rich carbonates, P= Pecaya Fm., Pe= Perla gas-field, Pg= Pedregoso Fm., Pt= Patieitos Fm., SL= San Luis Fm.

basins. Geodynamic models of the tectonic evolution of the South Caribbean margin and the associated basins are found in Audemard (1995), Mann (1999), Porras (2000), Summa *et al.* (2003), Baquero *et al.* (2009) and Escalona and Mann (2011). Recently, Albert-Villanueva *et al.* (2017) have contributed to the knowledge of the geology of the Falcón Basin through new detailed geological map and new structural model, age revisions of the lithostratigraphic units exposed in the northern and southern parts based on larger foraminifera associations, and a tectonostratigraphic reconstruction.

During the last decade, hydrocarbon discoveries in reservoir platform carbonates of Oligocene-Miocene age in the Gulf of Venezuela (*e.g.* Perla gas field, Borrromeo *et al.* 2011; Pinto *et al.*, 2011; Pomar *et al.*, 2015; Valencia and Laya, 2020) (Fig. 1) have raised interest in coeval intertidal to neritic carbonate rocks cropping out in the South-Caribbean region in order to establish analogues for these subsurface reservoirs. The Oligocene-Miocene platform carbonates of the Caribbean are characterized by the occurrence of abundant larger foraminifera, coralline algae, and colonial corals (Albert-Villanueva, 2016; Banerjee *et al.*, 2000; Curet, 1992; Iturralde-Vinent, 1972; Jones and Hunter, 1994; Mutti *et al.*, 2005; Pomar *et al.*, 2015). Similar biofacies are common in coeval tropical to subtropical carbonates worldwide (*e.g.* Bassant *et al.*, 2004, 2005; Bassi and Nebelsik, 2010; Bover-Arnal *et al.*, 2017; Brandano and Corda, 2002; Janson *et al.*, 2010; Kuss and Boukhary, 2008; Tomassetti *et al.*, 2018, 2021), and constitute important hydrocarbon reservoirs in Iran and Southeast Asia as well (*e.g.* Fournier *et al.*, 2005; Habibi and Bover-Arnal, 2018; Sharaf *et al.*, 2005; van Buchem *et al.*, 2010).

Lower Miocene mixed carbonate-siliciclastic strata are well exposed in the northern and southern margins of the Falcón Basin (San Luis and Churuguara formations (fms., respectively) (Fig. 1). These mixed carbonate-siliciclastic systems are studied herein intending to continue the legacy of the surface geologists from the Creole Petroleum Corporation that in the early 50's and during about 10 years studied the geology of the Falcón Basin, and of many authors that conformed the Stratigraphical Lexicon of Venezuela since 1956 (Petróleos de Venezuela, 2011), which incorporates the up-to-date geological knowledge of the sedimentary basins of Venezuela.

This study is based on field data and focuses on the sedimentary evolution of the northern and southern Falcón Basin during the Early Miocene. It utilizes platform-to-basin depositional models derived from facies distribution and stratal architecture. The analysis is further supported by a palaeogeographic reconstruction, larger foraminifera biostratigraphy, the development of a long-term sequence

stratigraphic framework, and an evaluation of the accommodation history. The second goal of the study is to compare the Lower Miocene carbonates exposed in the northern and southern margins of the Falcón Basin with the Oligocene-Miocene carbonates of the Perla gas field located in the Gulf of Venezuela. This geological synthesis offers updated and original insights into the factors that controlled the evolution of the southern Caribbean basins during Early Miocene times, while also advancing understanding of the recent, poorly constrained tectonosedimentary evolution of the South American-Caribbean boundary.

GEOLOGICAL SETTING

The Falcón Basin

During the Cenozoic, the oblique convergence between the northern South American continental margin and the Caribbean volcanic arc generated different zones of extension and compression within the Caribbean plate. In the Oligocene-Early Miocene times, an East-West rifting (Fault Family 1, Fig. 1) occurred northward of the Venezuelan metamorphic fold-thrust belt (Lara Nappes) and southward of the Caribbean volcanic arc (Aruba, Curaçao and Bonaire islands) (Fig. 1), behind a North-South trending subduction zone which involved the South American and Caribbean plates (Escalona and Mann, 2011; Gorney *et al.*, 2007). Within this geodynamic framework, the Falcón Basin (NW Venezuela) started to open towards the East as a back-arc rift basin overlying Caribbean forearc terranes (Audemard, 1995; Escalona and Mann, 2011; Gorney *et al.*, 2007; Porras, 2000). The main subsidence period of the Falcón Basin spanned from the late Rupelian to the Burdigalian (Albert-Villanueva, 2016; Escalona and Mann, 2011; Macellari, 1995; Wheeler, 1963). From the Langhian on, the eastward tectonic inversion of the Falcón Basin caused an eastward and northward migration of depocenters and the formation of an East-West trending fold belt referred as the “Falcón Anticlinorium”, which implied the subaerial exposure of the Cenozoic synrift succession (Figs. 2, 3) (Albert-Villanueva *et al.*, 2017; Baquero *et al.*, 2009; Boesi and Goddard, 1991; Escalona and Mann, 2011; Gorney *et al.*, 2007; Macellari, 1995).

This upper Rupelian-Burdigalian synrift succession is up to 3,300m thick in the central basin and about 1,000m in the margins, spans about 15 Myr (absolute age interval for the late Rupelian to Burdigalian period) according to Vandenberghe *et al.* (2012) and Hilgen *et al.* (2012), and can be subdivided into 10 lithostratigraphic units with the rank of formations (Figs. 2; 3; 4) (Wheeler, 1963). Macellari (1987) subdivided the sedimentary record filling up the Falcón Basin into 2 large-scale Transgressive-Regressive (T-R) sequences (C1 and C2, Fig. 4).

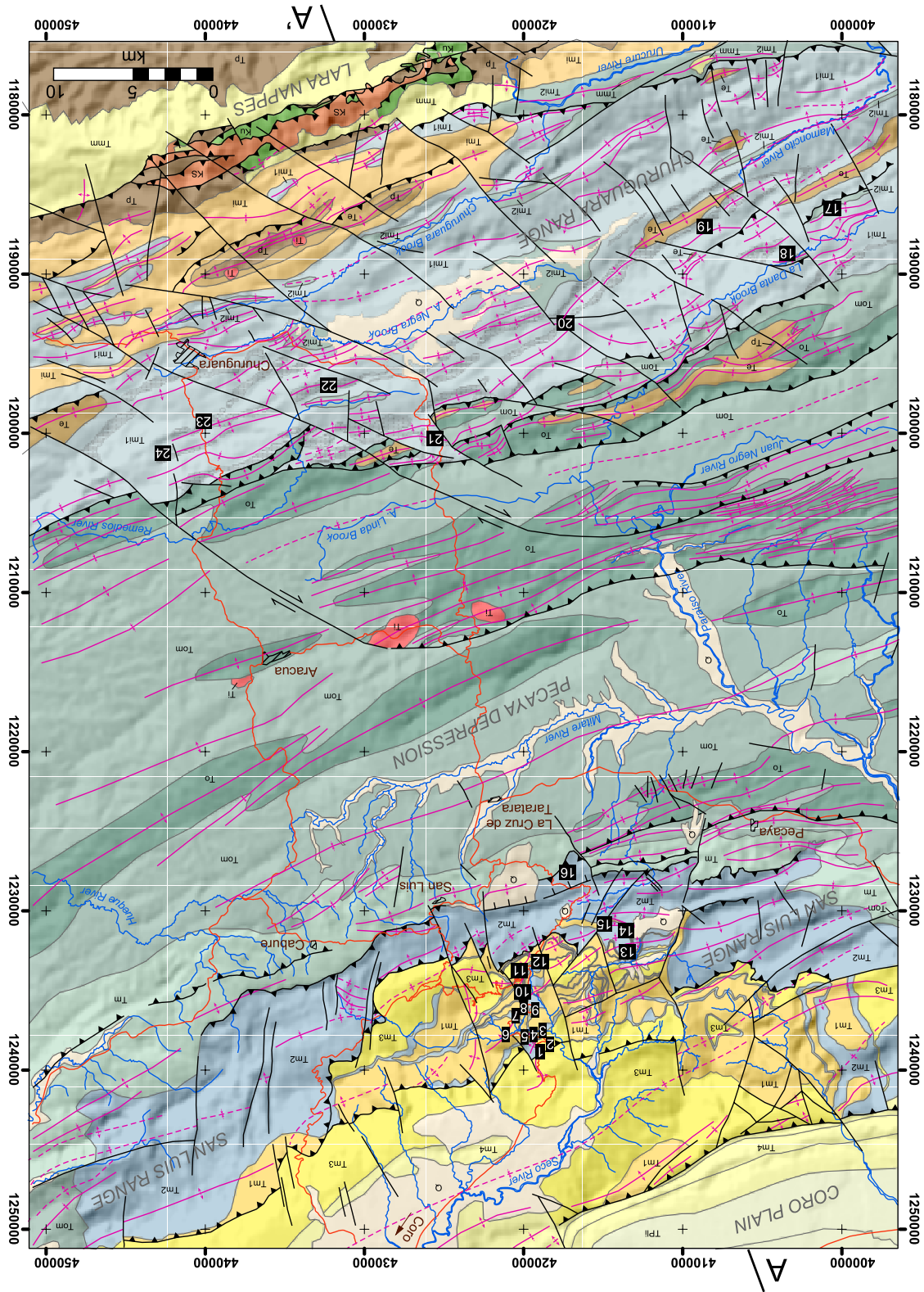


FIGURE 2. Geological map of the studied area projected in a UTM grid (Zone 19N) (modified from [Albert-Villanueva et al., 2017](#)). The location of the map is indicated in the [Figure 1](#) with a white dot-lined square. The legend of the geological units is represented in [Figure 3](#). A-A' indicates the location of the geological cross-section displayed in [Figure 3](#). Black-squared numbers indicate the position of the studied sections. KS= Cretaceous igneous-metamorphic rocks, Ku= Cretaceous sedimentary rocks, Ti= Cenozoic intrusive rocks, Tp= Paleocene sedimentary rocks, Te= Eocene sedimentary rocks, To= Oligocene sedimentary rocks, Tom= Oligocene-Miocene sedimentary rocks, Tm= Miocene sedimentary rocks, Tmi= Lower Miocene sedimentary rocks, Tmm= middle Miocene sedimentary rocks, TPl= Pliocene sedimentary rocks.

The San Luis and Churuguara mixed carbonate-siliciclastic sedimentary units studied herein are of Early Miocene age and were deposited in semigrabens at the northern and southern margins of the Falcón Basin, respectively (Fig. 1) (Albert-Villanueva et al., 2017). During this period, the sedimentation in the central basin was dominated by turbidites (Pedregoso Formation, Fm.) and pelagic shales (Pecaya and Agua Clara fms.) (Fig. 1). The sedimentary successions analyzed unconformably overlie the Bartonian-Priabonian siliciclastic deposits of the Jarillal Fm. (Figs. 2; 3; 4), which has been interpreted by Escalona and Mann (2011) as deposited into a forearc sag basin, prior to the formation of the Falcón Basin.

The two areas studied are located in the San Luis and Churuguara ranges (Fig. 2), which correspond to the northern and southern flanks of the Falcón Anticlinorium, respectively (Fig. 3) (Baquero et al., 2009; Boesi and Goddard, 1991; Macellari, 1995). In the northern Falcón Anticlinorium, Hodson (1926) and Senn (1935) first defined the San Luis Fm. as a series of limestones with foraminifera and corals interbedded with shales and sandstones. These authors indicated the unconformable character of the formation upon the upper Eocene series and locally, beneath the Miocene deposits (Figs. 3; 4). In addition, Senn (1935) attributed the San Luis Fm. to the middle Oligocene on account of the occurrences of *Spiroclypeus* spp. and *Miogypsina hawkinsi*. Wheeler (1963) subdivided the sedimentary succession giving rise

to the San Luis Range into 3 lithostratigraphic units (Figs. 2; 3; 4), and defined the San Luis Fm. as a blue to gray massive reefal limestones with larger foraminifera, coralline algae and corals. Wheeler (1963) interpreted the San Luis Fm. as a reef-rimmed carbonate platform.

To the North, these platform carbonates occur interfingered with sandstones and shales of the Patieitos and Guarabal fms. (Fig. 3) which were interpreted by Wheeler (1963) as the lateral-equivalent back-reef siliciclastic deposits of the San Luis Fm. to the South, the San Luis carbonates backthrust the Pedregoso turbidites (Figs. 2; 3). Based on larger foraminifera and coral associations, Wheeler (1963) extended the age of the San Luis Fm. from the middle Oligocene to the Early Miocene. Later, Díaz de Gamero (1977) ascribed the San Luis Fm. to the Early Miocene based on planktonic foraminifera associations from turbiditic series of the Pedregoso Fm., which are considered a southern lateral equivalent of the San Luis Fm. (Figs. 3; 4).

On the other hand, based on the finding of *Rotalia mecatepecensis* and *Rotalia* cf. *mexicana* in strata belonging to the San Luis Fm., González de Juana et al. (1980) assigned the lower part of the formation to the middle Oligocene. Johnson et al. (2009) studied the coral faunas found in the San Luis, Pedregoso, Castillo and Agua Clara fms. (Figs. 2; 3; 4) identifying Oligocene, Miocene and, Oligo-Miocene biotas. Based on these associations,

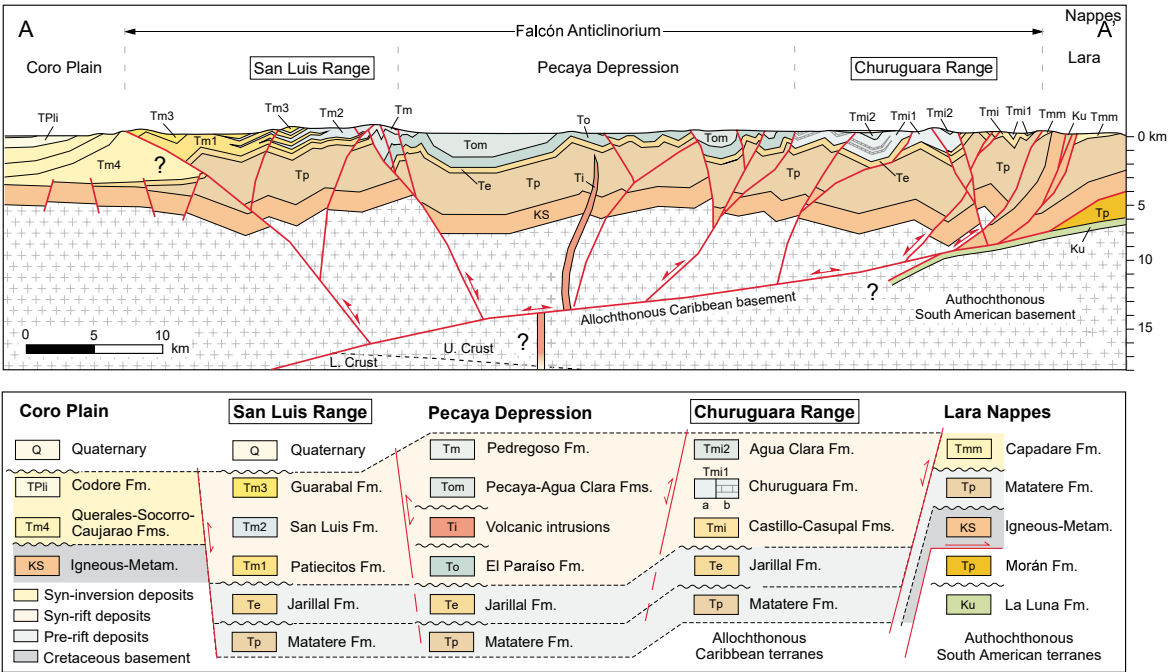


FIGURE 3. Above: A-A' geological cross-section indicated in Figure 2 (modified from Albert-Villanueva et al., 2017). Below: Legend of the different lithostratigraphic units represented in Figures 2 and 3, with their lateral and vertical stratal relationships. Tm1l a= Churuguara siliciclastics, Tm1l b= Churuguara carbonates. See Figure 2 caption for key.

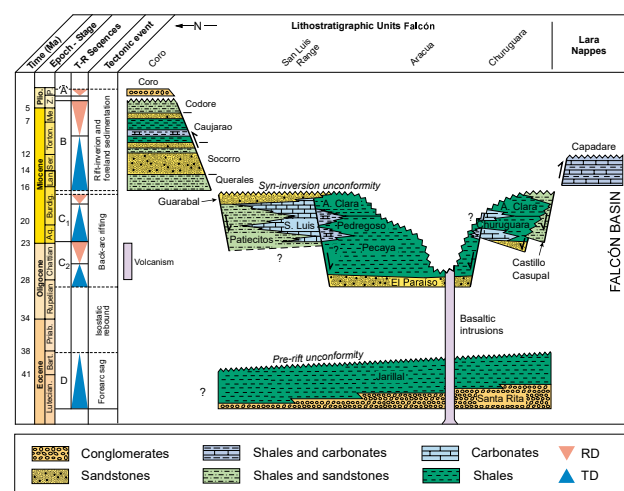


FIGURE 4. Stratigraphic framework and age constraints for the Cenozoic in the Falcón Basin, showing the T-R Sequences defined by Macellari (1989) and the main tectonic events. The absolute ages for the Cenozoic are based on Vandenberghe *et al.* (2012) and Hilgen *et al.* (2012). TD= Transgressive Deposits, RD= Regressive Deposits.

Johnson *et al.* (2009) interpreted the San Luis Fm. to be of late Oligocene age. Albert-Villanueva *et al.* (2017, 2019) dated the San Luis Fm. as Early Miocene based on larger foraminifera occurrences.

In the western part of the San Luis Range, the marine shales of the Agua Clara Fm. (Fig. 4) interfinger and overlie the San Luis Fm. (Senn, 1935). Based on the analysis of planktonic foraminifera assemblages, Díaz de Gamero (1977, 1989) established the age of the base of the Agua Clara Fm. within the *Catapsydrax dissimilis* Zone, which is of Early Miocene age (Bolli *et al.*, 1994). In the central part of the San Luis Range, Wheeler (1963) correlated a series of siliciclastic deposits overlying the San Luis Fm. with the Agua Clara Fm., restricting the age of the top of the San Luis Fm. to the Early Miocene.

In the southern Falcón Anticlinorium, Liddle (1946) and Wheeler (1963) first defined the Churuguara Fm. as a lithostratigraphic unit composed by an alternation of dark-gray shales, skeletal sandy limestones to calcareous sandstones, massive reefal limestones and glauconite-rich sandstones. The same authors identified the conformable character of the formation upon the Eocene strata of the Jarillal Fm. and beneath the Lower Miocene deposits of the Agua Clara Fm. (Figs. 3; 4). Based on planktonic and larger foraminifera associations, Wheeler (1963) attributed the lower and middle parts of the Churuguara Fm. to the early-middle Oligocene, whereas the upper part was ascribed to the Early Miocene on account of the occurrences of *Textularia falconensis* and age-diagnostic mollusc assemblages.

The Churuguara mixed carbonate-siliciclastic unit locally interfingers with the Pecaya and lower Agua Clara pelagic-shales to the North (Fig. 2) and with the Castillo and Casupal marginal siliciclastics to the South (Figs. 2; 3). Díaz de Gamero (1977) regarded this mixed carbonate-siliciclastic unit as a lateral equivalent of El Paraíso, Pecaya and lower Agua Clara fms. in the central basin area (Figs. 2; 3; 4), which aged from early Oligocene to Early Miocene based on planktonic foraminifera assemblages. Based on larger foraminifera associations, Albert-Villanueva *et al.* (2017, 2019) assigned the Churuguara Fm. to the Early Miocene.

The Perla gas field

The Perla gas field lies approximately below 60 meters of water depth in the Gulf of Venezuela, and is located westwards of the Paraguana Peninsula and eastwards of the Guajira Peninsula. To the Southwest is bounded by the Urumaco Trough (Fig. 1). These SE striking normal faults (Fault Family 2; Fig. 1) are associated with the right-lateral strike-slip motion of the Caribbean plate during the Oligocene-Miocene times, synchronously to the opening of the Falcón Basin towards the South (Escalona and Mann, 2011; Macellari, 1995). The Perla reservoir carbonates are of Chattian-Burdigalian age, and unconformably overlie granodioritic fault-block basement and synrift siliciclastic sandstones (Castillo *et al.*, 2017; Pomar *et al.*, 2015).

Benkovics *et al.* (2012) and Pomar *et al.* (2015) described this carbonate reservoir as composed by three transgressive units bounded by flooding surfaces. Pomar *et al.* (2015) interpreted these carbonates dominated by rhodoliths and larger foraminifera as distally steepened ramps. These reservoir carbonates are topped by a drowning unconformity and sealed by Agua Clara equivalent black shales (Benkovics *et al.*, 2012; Borromeo *et al.*, 2011; Pinto *et al.*, 2011). More recently, Valencia and Laya (2020) studied the porosity system and diagenesis of this reservoir.

MATERIALS AND METHODS

Panoramic photomosaics of the outcrops and orthophotomaps were used for mapping of facies, the establishment of depositional and architectural models, the sequence stratigraphic analysis and the correlation of sequences along the San Luis and the Churuguara ranges. Furthermore, 24 stratigraphic sections ranging from 26 to 1,537m-thick were measured along the northern and southern Falcón Basin (Figs. 2; 3; 4). A detailed sedimentological analysis was performed for each section. Microfacies were analyzed on 408 thin sections produced from rock samples collected in the field. In addition, microfossil assemblages were studied to interpret

depositional environments and for biostratigraphic purposes. The biostratigraphic analysis was based on larger foraminifera associations and was correlated to planktonic and larger foraminiferal biostratigraphic frameworks and zones in Díaz de Gamero (1977, 1989), Butterlin (1981), Bolli *et al.* (1994), BouDagher-Fadel (2008), BouDagher-Fadel and Price (2010a, b) and BouDagher-Fadel *et al.* (2010).

The sequence stratigraphic analyses were defined in terms of T-R sequences (see Catuneanu *et al.*, 2009; Embry and Johannessen, 1992). The advantage of using T-R sequences in front of other sequence models is the good exposure of the key surfaces used to furnish the chrono-stratigraphic framework. These surfaces mark large-scale changes in facies evolution (from shallowing-to deepening-upwards or vice versa) and include subaerial unconformities, maximum regressive surfaces, transgressive ravinement surfaces and maximum flooding surfaces (see Catuneanu *et al.*, 2009).

To establish the accommodation changes, quantitative subsidence analyses were carried out on three selected representative sections using PetroMod software, based on standard back-stripping methods (Bond and Kominz, 1984; Sclater and Christie, 1980; Watts, 1981). The variables used in these methods are lithology, absolute age (based on Vandenbergh *et al.*, 2012 and Hilgen *et al.*, 2012) and palaeobathymetry that was estimated from sedimentological and palaeontological data. Decompaction was calculated in function of lithological density values and porosity/depth relationships (Schmoker and Halley, 1982; Sclater and Christie, 1980). No eustatic corrections were performed. The total accommodation was obtained from the total subsidence (decompacted) corrected with estimated palaeo-water depth values.

FACIES ASSOCIATIONS AND BIOTIC INVENTORY

Eleven siliciclastic and fourteen carbonate facies and subfacies can be distinguished in the San Luis and Churuguara ranges (Figs. 2; 3). Siliciclastic lithofacies constitute the Patiecitos Fm., the Guarabal Fm. and most of the Churuguara Fm., and represents approximately 76% of the studied sections, whereas the carbonate lithofacies form the San Luis Fm. and part of the Churuguara Fm. (Fig. 4), correspond to the remaining 24% of the studied sections. The classification of the different siliciclastic and carbonate facies assemblages characterized is either descriptive or interpretative to facilitate comprehension of the resulting depositional models. The identification of the depositional environments and processes was based on the analysis of lithology, sedimentary structures, grain size, palaeocurrent data and fossil occurrences. The different

carbonate microfacies were defined by fabric characteristics and dominating biotic components. The distinctive features of these facies are summarized and illustrated in Figures I II, and described in the Appendix.

Fossil assemblages

A total of 338 thin sections have been studied for fossil identification purposes: 237 from the northern San Luis sections and 101 from the southern Churuguara carbonate sections. Skeletal components in the San Luis and Churuguara limestones are dominated by benthic foraminifera and coralline algae. Notably, coralline algae often appear as small fragments within the matrix, constituting approximately 5 to 20% of the total skeletal fraction (Fig. II). The lack of preservation of sporangial conceptacles in most of the studied samples, makes classifications practically unfeasible even at the family or subfamily level. Due to their greater abundance and better preservation, taxonomic studies have focused on benthic foraminifera assemblages.

Benthic foraminifera

The biostratigraphic study was based on random sections of larger foraminifera contained in rock thin sections. The small number of centered sections prevents a solid species determination, especially in miogypsinids, in which a statistical biometric study is required.

Identified benthic foraminifera include *Miarchaias* sp., *Miosorites americanus*, *Annulosorites spiralis*, *Heterostegina antillea*, *Operculinoides panamensis*, *Miogypsina* cf. *mexicana*, *Miogypsina* cf. *gunteri*, *Miogypsina* cf. *globulina*, *Miogypsina* cf. *panamensis*, *Miogypsina* cf. *cushmani*, *Miogypsina* sp., *Eulepidina undosa*, *Lepidocyclina canellei*, *Lepidocyclina* sp., *Amphistegina* sp., *Neorotalia* sp., *Planorbulinella* sp., *Sphaerogypsina* sp., *Spiroloculina* sp., *Biloculina* sp., *Triloculina* sp., other miliolids, rotalids, peneroplids, textularids, lagenids, victoriellids, cibicidids and bolivinids (Fig. 5).

BIOSTRATIGRAPHY

The distribution of the age-diagnostic species in San Luis and Churuguara sections are shown in Figure 6. The studied carbonate sections of both San Luis and Churuguara formations are characterized by the occurrence of larger foraminifera species ranging in age from Oligocene to Early Miocene, including *Eulepidina undosa*, *Lepidocyclina canellei*, *Heterostegina antillea*, *Operculinoides bullbrooki* and *Miarchaias* sp. (Butterlin, 1981; Cole, 1961a, 1964; Robinson, 2004; Robinson

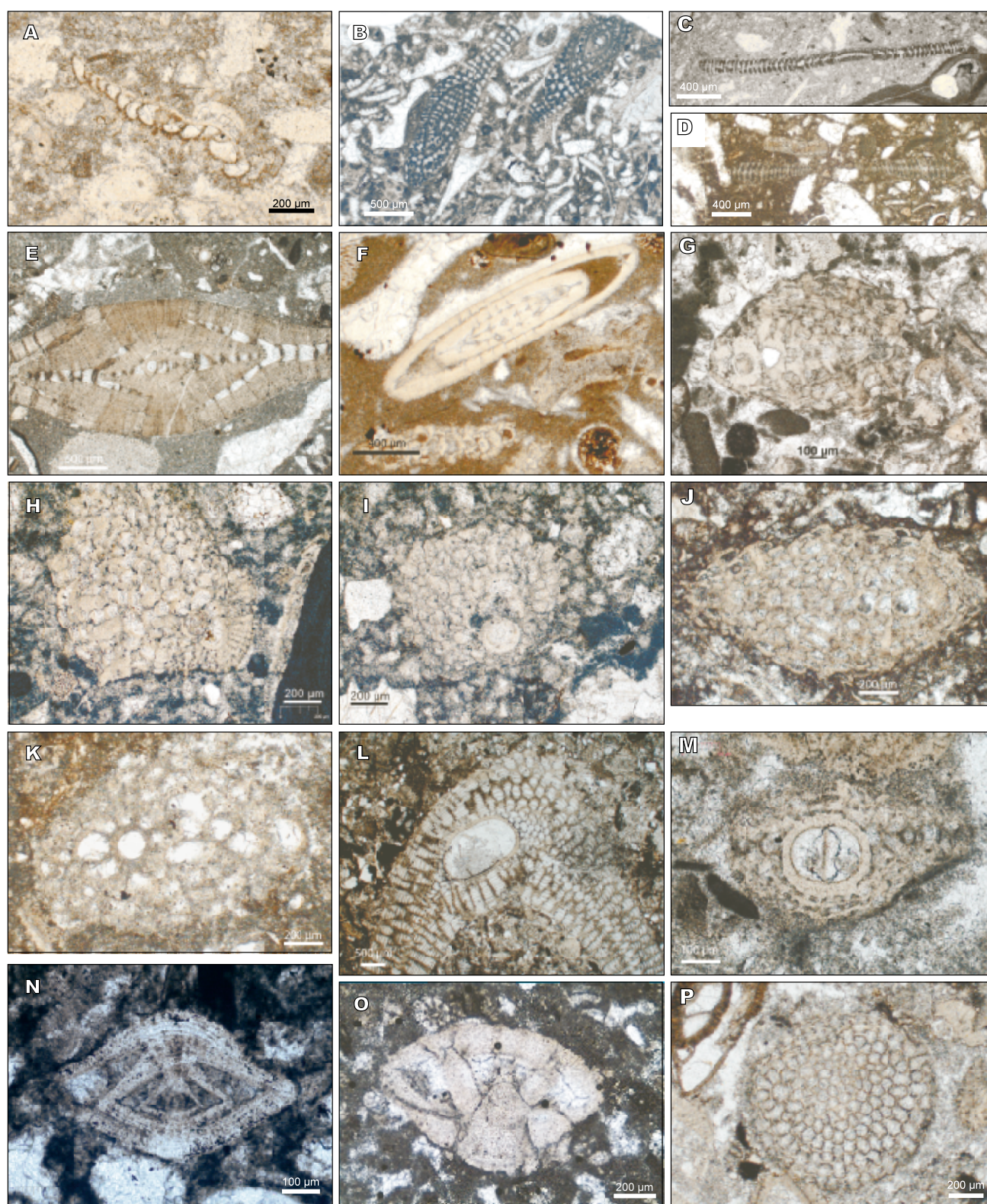


FIGURE 5. Representative early Miocene larger foraminifera from the Falcón Basin. A) *Planorbulina* sp. B) *Miarchaias* sp. C) *Miosorites americanus*. D) *Annulosorites spiralis*. E) *Heterostegina antillea*. F) *Operculinoides panamensis*. G) *Miogypsina* cf. *mexicana*. H) *Miogypsina* cf. *gunteri*. I) *Miogypsina* cf. *globulina*. J) *Miogypsina* cf. *panamensis*. K) *Miogypsina* cf. *cushmani*. L) *Eulepidina undosa*. M) *Lepidocyclina canellei*. N) *Amphistegina* sp. O) *Neorotalia* sp. P) *Sphaerogypsina* sp.

and Wright, 1993; Senn, 1935), associated with taxa of exclusive Miocene age, such as *Miosorites americanus*, *Annulosorites spiralis* and *Miolepidocyclina mexicana/panamensis* (Banerjee et al., 2000; BouDagher-Fadel, 2008; Butterlin, 1981; Hottinger, 2001; Robinson, 2004; Seiglie, 1982; Seiglie et al., 1977; Serra-Kiel et al., 2007) (see Figs. 5; 6). This association restricts the age of both San Luis and Churuguara carbonate successions to the Early Miocene (Fig. 6). According to BouDagher-Fadel et al. (2010) the Aquitanian is marked by the first appearance of *L. canellei* in samples from Brazil.

The analysis of the distribution of miogypsinids permitted a more accurate dating of both mixed carbonate-siliciclastic successions (see Figs. 5G–K; 6). Miogypsinids evolved from a rotalid genus and follow an evolutive trend reducing the number of spiral chambers (“nepionic reduction”), becoming biserial (two spirals) and developing lateral chamberlets. However, such trends are followed parallelly in the different bioprovinces. For example, the development of lateral chamberlets took place in the latest Rupelian in the American province, in the late Chattian in the Mediterranean, and in the Aquitanian in the Far East (BouDagher-Fadel and Price, 2010a). The reduction in spiral chamber development occurred at different times and rates across different regions, as noted by Drooger (1954), who observed the significantly earlier appearance of equivalent species in the Western Hemisphere compared to Europe.. The use of the same species names for species with similar features (e.g. same number of spiral chambers) from different bioprovinces, as well as the biostratigraphical correlations between bioprovinces based on these similar species can be misleading. We could add to this the confusion with the Oligocene/Miocene boundary in America that affected the biostratigraphical interpretations of larger foraminifera (e.g. Eames, 1953, 1954).

All the miogypsinids in the studied samples have lateral chamberlets, suggesting a Miocene age (e.g. BouDagher-Fadel and Price, 2010a). The lower parts of the San Luis and Churuguara formations are characterized by *M. antillea* and other undetermined species of miogypsinids with rather few lateral chamberlets, without pillars, and with the initial chambers in an excentric position. *Miogypsina antillea* occurs in the Early Miocene (Butterlin, 1963; Cole, 1961b; Cole and Applin, 1961; Drooger 1952), although some authors (Butterlin, 1981; Mello e Sousa et al., 2003) extend its range up to Middle Miocene. In the upper part of the studied carbonate successions (San Luis and Churuguara formations) there is a change in the miogypsinid assemblage, with the appearance of *M. cf. globulina*, *M. cf. cushmani* and *M. cf. mexicana/venezuelana*. According to Butterlin (1981), *Miogypsina globulina* indicates the lower Burdigalian, while according to BouDagher-Fadel and Price (2010a) has a long

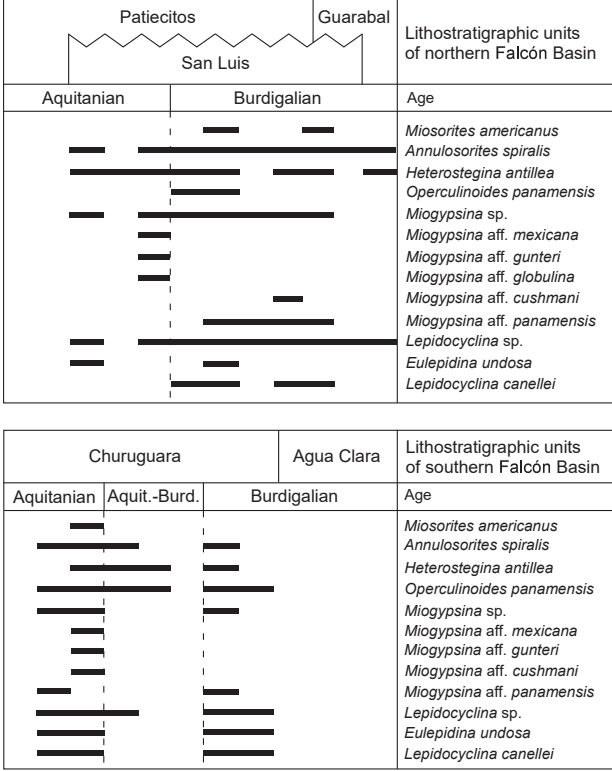


FIGURE 6. Lithostratigraphic units, ages and distribution of biostratigraphic-key larger foraminifera species recorded in northern (left) and southern (right) margins of the Falcón Basin (modified from Albert-Villanueva, 2019).

biostratigraphical range from the upper Rupelian to the Burdigalian. *Miogypsina mexicana* has been assigned to different genera (*Miogypsinita* in Butterlin, 1981; *Miolepidocyclina* in BouDagher-Fadel and Price, 2010a) because the initial chambers are not in excentric position. According to BouDagher-Fadel and Price (2010a), the uppermost occurrence of *Miolepidocyclina mexicana* is in the Aquitanian. The association of *M. mexicana*, *M. venezuelana*, and *M. cf. cushmani* would correspond to the Middle Miocene (Langhian) according to Butterlin (1981). The co-occurrence of these miogypsinid species with *Operculinoides bullbrooki*, and *Lepidocyclina canellei* in the lower part of San Luis and Churuguara successions would rather indicate a Lower Miocene age. Based on these data on larger foraminifera, we interpret the lower part of San Luis and Churuguara fms. as Aquitanian and the upper part as Burdigalian in age, which is in accordance with the biostratigraphic interpretation based on planktonic foraminifera by Díaz de Gamero (1977, 1989).

Comments on some species of larger foraminifera

Miosorites americanus (Cushman 1918) and *Annulosorites spiralis* (Hottinger 2001) are known from the Miocene of the Caribbean region (Banerjee et al., 2000;

Hottinger, 2001; Robinson, 2004; Serra-Kiel et al., 2007), often reported under other generic names (e.g. “*Sorites*” in Caudri, 1996; “*Orbitolites*” in Cushman, 1919). These soritids were reported (but not figured) from the Agua Clara Fm. as “*Amphisorus?* sp.” (Gravell, 1933) and “*Amphisorus americanus*” (Wheeler, 1963). The latter author interpreted a Lower Miocene age for this formation.

Lepidocyclina canellei shows a great variability in size and shape, including the presence or absence of pillars. It is characterized by a thick-walled isolepidine embryo 150–300 µm in size with the two embryonic chambers bounded by a flat wall. According to Cole (1961a), *L. giraudi*, *L. miraflorensis*, *L. asterodisca*, and *L. waylandvaughani*, are all junior synonyms of *L. canellei*. Although it is a dominant species in the Miocene, its range is considered as middle or early Oligocene to Early Miocene (e.g. Caudri, 1996; Vaughan, 1933). According to Boudagher-Fadel et al. (2010), the first appearance of *L. canellei* in sections from Brazil marks the Aquitanian.

Eulepidina undosa is a common index larger foraminifera of the Oligocene in the Caribbean (e.g. Butterlin, 1981; Robinson and Wright, 1993). Initially defined as two different species by Cushman (1919), *Lepidocyclina* (*Eulepidina*) *undosa* and *L. (E.) favosa*, they are nowadays considered ecophenotypes of the same species (Caudri, 1996; Cole, 1952; Frost and Langenheim, 1974; Vaughan, 1928), the latter being a junior synonym of the former (Cole and Applin, 1961), and with a third co-occurring species also defined by Cushman (1919, 1920), *Lepidocyclina gigas*, now interpreted as the microspheric form (Frost and Langenheim, 1974). The “undosa type”, flatter and with a smaller embryo, is related to reef facies, while the “favosa type” dominates in inter-reef or back-reef facies, although there is a complete gradation between the two types (Frost and Langenheim, 1974). Its biostratigraphical range comprises the Oligocene and the Early Miocene (Boudagher-Fadel and Price, 2010b; Butterlin, 1981, 1984; Cole and Applin, 1961; Eames et al., 1968; Frost and Langenheim, 1974; Mello e Sousa et al., 2003; Robinson, 2004; Robinson and Wright, 1993; Robinson et al., 2018).

According to Cole (1964) and Robinson and Wright (1993), only one species of *Heterostegina*, *H. antillea* occurred in the Caribbean region during the Oligocene-Miocene. The other reported species from this time interval (*H. israelskyi* Gravell and Hanna, 1937, *H. texana* Gravell and Hanna, 1937, *H. panamensis* Gravell, 1933) differ only in test shape and size, and would be ecophenotypes. The stratigraphical range of *H. antillea* spans from the late Oligocene to the earliest Miocene (Butterlin, 1981; Caudri, 1996; Frost and Langenheim 1974; Mello e Sousa et al. 2003; Robinson and Wright, 1993).

The American Eocene-Miocene nummulitids have been assigned to different genera (*Camerina*, *Nummulites*, *Operculinoides*, *Operculinella*, *Paleonummulites*). The specimens occurring in the studied sections are mostly characterized by flat tests and a moderately operculinoid-like spiral, which are assignable to *Operculinoides panamensis/bullbrookii*. The lack of oriented and centered sections prevents precise determination. This group consistently shows large variability in size and shape, which is interpreted as related to the depositional environment (e.g. Cole, 1958). However, according to Frost and Langenheim (1974), this variability is always present and is not related to environmental conditions. Cole (1958) concluded that there are only two species of *Operculinoides* in the Oligocene (*O. panamensis* and *O. dia*) and only one species, *O. cojimarensis*, in the Miocene. *Operculinoides panamensis* has been synonymized with *O. dia*, which is considered to occur in the Early Miocene (e.g. Butterlin, 1981). According to Caudri (1996), *O. bullbrookii* is easily distinguished from *O. panamensis* and also occurs in rocks of Early Miocene age (based on planktonic foraminifera).

DEPOSITIONAL MODELS

The interpreted 11 siliciclastic and 14 carbonate facies and subfacies (see Figs. I; II; Appendix), together with their spatial distribution in the studied areas, have been integrated into three overall depositional models representing the northern and southern Falcón Basin during the Early Miocene. The growth of carbonate platforms in this region was favoured by the presence of shallow-marine shelf areas associated with normal fault blocks in the basin margins (Albert-Villanueva et al., 2017) and controlled by factors such as sediment supply, rate of carbonate production and changes in accommodation (Bosence, 2005; Williams et al., 2011).

Northern Falcón

The Lower Miocene sedimentation in the northern Falcón Basin was dominated by marginal delta systems (Patiecitos and Guarabal fms.) interfingering and passing southward into coralline algae and benthic foraminifera-bearing platform carbonates (San Luis Fm.) (Fig. 7A). The southern limit of the San Luis Fm. was characterized by a synsedimentary normal fault system that generated olistoliths deposited within the Pedregoso turbidite succession (Fig. 7B). In the Cerro de los Ahumados section, Northwest of Pecaya (Fig. 7C), an excellent dip-oriented and non-deformed exposure of the San Luis Fm., preserves large-scale depositional clinobeds. In this regard, continuous, subparallel, relative thick strata characterize the upper and middle parts of a carbonate platform. The subparallel strata pass laterally into large scale clinobeds

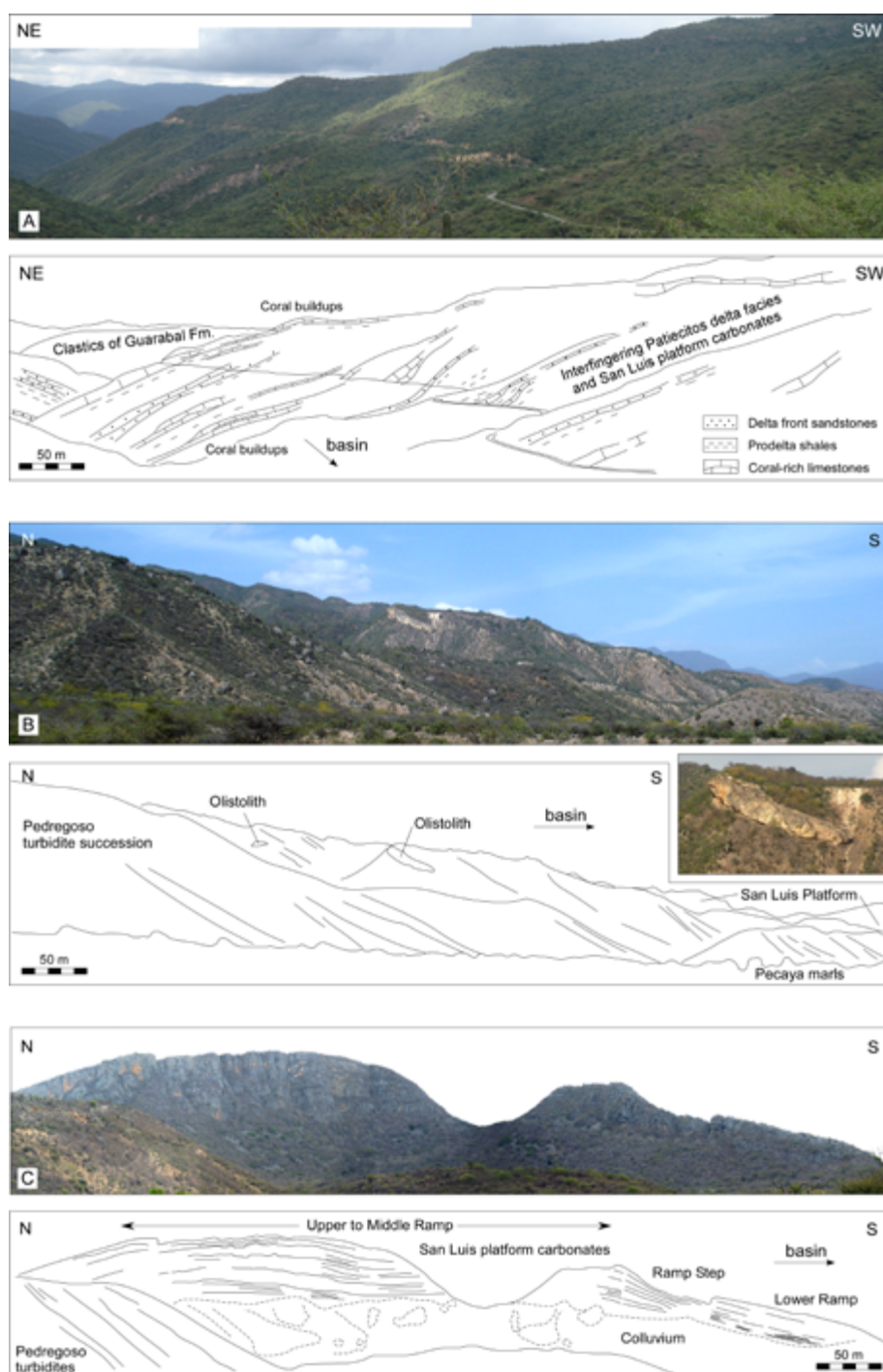


FIGURE 7. Outcrop-scale views and line-drawing interpretations of the San Luis platform carbonates (northern Falcón Basin), their lateral boundaries and depositional geometries. A) Outcrop picture of a mixed carbonate-siliciclastic succession dominated by deltaic deposits and interfingering with coral mounds. This succession marks the northern limit of the San Luis carbonate system, which pinches out into the Patieitos-Guarabal marginal siliciclastic strata. The picture was taken on the road Lara-Falcón Troncal 4, in the northern flank of the San Luis Range. B) Field view of Lower Miocene turbidite deposits of Pedregoso Fm. with olistostrome intervals that limited the San Luis Fm. towards the South. The transition from the San Luis platform carbonates to the basinal-equivalent Pedregoso turbidite succession is not preserved due to the presence of a reverse fault system. However, the occurrence of San Luis-like olistoliths within the Pedregoso turbidite system suggest the synsedimentary destruction of the San Luis carbonate platform margin by a normal fault system bounding the carbonate platform towards the South. The photo was taken few kilometers southwards of the Cerro de los Ahumados (Northwest of Pecaya). C) Dip-oriented section of the San Luis carbonate platform exhibiting a distally-steepened ramp profile. Upper and middle ramp deposits are characterized by subparallel bedded, laterally continuous tabular strata, with absence of barrier deposits. Middle ramp strata thin and show an abrupt increase in dip basinwards, indicating the presence of a distal ramp step. Lower ramp deposits are tabular, thin, and display both parallel and cross bedding. No significant deformation is observed in this outcropping sedimentary succession. The photo was taken at the Cerro de los Ahumados, near the southwestern edge of the San Luis platform, Northwest of Pecaya.

related to a steep-like structure and basinwards into a thinner and tabular package with internal subparallel to cross beddings. Shoals or a barrier reef were not recognized along the depositional profile. According to these observations, the depositional profile along the San Luis Range during the Early Miocene corresponded to a distally-steepened ramp (sensu Read, 1982). Similar Oligocene-Miocene carbonate ramps dominated by coralline algae and benthic foraminifera have been described worldwide, including Mediterranean, Middle East (Arabian and Iranian plates), Atlantic, Indo-Pacific and Caribbean regions (Bassi and Nebelsick, 2010; Bover-Arnal et al., 2017; Brandano and Corda, 2002; Brandano et al., 2009; Corda and Palmiotto, 2015; O'Connell, 2012; Pomar et al., 2015; Shabafrooz et al., 2015; van Buchem et al. 2010).

The different facies recognized are organized in belts along a palaeobathymetric gradient on the mixed carbonate-siliciclastic distally-steepened ramp (Fig. 8). According to the stratal architecture, biotic associations and their palaeontological constraints, four differentiated ramp settings were distinguished: i) upper ramp with the

influence of marginal delta system, characterized by the presence of biota such as *Miarchaias* sp., *Miosorites americanus*, *Annulosorites spiralis* (Fig. 5B–D), green algae, and corals, ii) proximal middle ramp with rhodoliths (Fig. IIRF), branching coralline algae, *Miogypsina*, *Amphistegina*, nummulitids, and less abundant *Eulepidina* and *Lepidocyclus* (Fig. 5E–P), representing the transitional zone to iii) a distal middle ramp setting dominated by coralline algae detritus (Fig. IICADF), *Amphistegina*, *Miogypsina*, nummulitids, *Eulepidina* and *Lepidocyclus* (Fig. 5E–P), that passes basinwards into iv) lower ramp strata rich in *Lepidocyclus* and *Eulepidina* debris (Figs. 7L; 5N) and planktonic foraminifera (Fig. IIPFF).

Delta front

The near-shore zone comprises the Delta Front Subfacies (Figs. IDFS; 8). The presence of thick trough cross-bedded, matrix-clean, lithic sandstones and microconglomerates, mixed with abraded and reworked molluscs and other skeletal grains, indicate the presence of a coastal belt dominated by submarine bars and dunes, deposited under

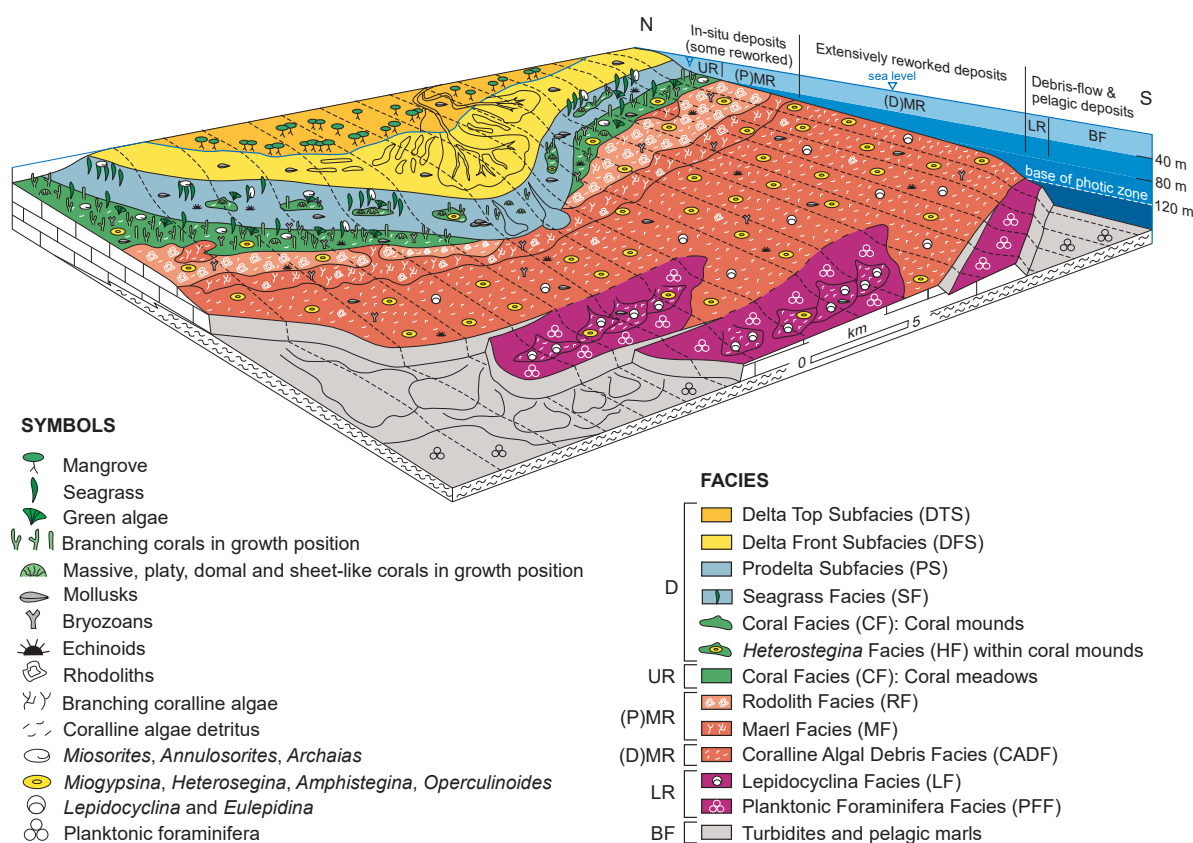


FIGURE 8. Depositional model for the Lower Miocene mixed carbonate-siliciclastic ramp system from the northern Falcón Basin showing the lateral distribution of the different facies domains and their main biogenic components. The facies boundaries are marked by changes in sedimentary conditions (e.g. photic conditions, siliciclastic input, energy, depositional profile). The facies boundaries can be transitional or sharp depending on the gradual or abrupt nature of the changes in sedimentary conditions. The deltaic facies correspond to the Patientes Formation, the platform carbonates to the San Luis Formation and the basin turbidites and marls to the Pedregoso Formation. D= Delta, UR= Upper Ramp, (P)MR= Proximal Middle Ramp, (D)MR= Distal Middle Ramp, LR= Lower Ramp, BF= Basin Floor.

the influence of fair-weather waves and littoral currents.

Prodelta

Prodelta Subfacies belt (Figs. IPS; 8) occurs below the Fair-Weather Wave Base (FWWB), adjacent to the coastal sand-shelf (Figs. IDFS; 8). The predominance of gray-blue shale with molluscs, sporadic platy corals in growth position and minor fine-grained sandstone interbeds indicate a quiet marine sedimentary environment, characterized by processes of continental-derived fine clastic deposition by vertical suspension fallout. The thin alternations of shale, silt and sandstone beds, as well as the occurrence of channel-filling and slumped strata indicate sediment remobilization processes likely driven by episodic bottom storm waves or currents, slope instability processes, tides and sea-level changes.

Benthic (free, sedentary or sessile organisms) and epiphytic carbonate-producing biota thrived below the FWWB, in a prodelta setting, which included the Coral Facies (Fig. IICF), the Seagrass Facies (Fig. IISF) and the *Heterostegina* Facies (Fig. IIHF). These carbonate-dominated lithofacies are organized in buildups encased in the siliciclastic blue shale of the Prodelta Subfacies (Figs. IDF, 7A; 8). Buildups are made up of amalgamated coral bioherms and biostromes (Fig. IICBS) constituting a rigid framework interfingering with detrital coral-bearing strata (Fig. IIDCS), seagrass deposits (Fig. IISF), bivalve-rich layers and minor *Heterostegina*-dominated facies (Fig. IIHF). The siliciclastic content is variable within the carbonate beds, keeping a clear relationship with the biotic associations observed. In this respect, mixstone coral facies (*sensu* Insalaco, 1998) and interbedded Seagrass facies are characterized by a micritic matrix poor in siliciclastics together with skeletal components indicative of tropical-subtropical well-lit marine environment. Such biota characteristic of an upper photic zone (*sensu* Hottinger, 1997) include *Miosorites americanus*, *Annulosorites spiralis*, *Miarchaias* sp., *Panorbulina* sp., *Sphaerogypsina* sp. (Fig. 5), peneroplids, victoriellids, miliolids, textularids, green algae (*Halimeda* sp.) (Fig. IISF) and abundant scleractinian colonies (Fig. IICF). On the other hand, *Heterostegina* facies and biostromes of branching *Porites* include a silty to sandy matrix and tropical marine fauna which thrived in the deeper part of the upper photic environment. This biotic association thriving in a mesophotic zone includes *Heterostegina antillea* (Fig. 5E) and subordinated *Operculinoides panamensis* (Fig. 5F), *Lepidocyclus* sp., *Eulepidina* sp., *Amphistegina* sp., and coralline algae fragments (Bevington-Penney and Racey, 2004; Hallock and Pomar, 2008; Hottinger, 1997).

The occurrence of packstones, floatstones and boundstones rich in euphotic biota within a micritic matrix (poor in terrigenous), alternating with rudstones dominated by mesophotic biotic assemblages embedded in a siliciclastic-rich matrix, suggests changes in the photic conditions driven by variations in clastic discharges along the prodelta setting, where buildups grew up. In this regard, episodes of low clastic influx and well illumination permitted the proliferation of a high diversity of coral growth forms (mixstone-domestone facies) and associated seagrass facies (see *e.g.* Novak *et al.*, 2013). Whereas episodes of higher-water turbidity and lower light penetration caused the demise of coral buildups and the proliferation of few genera of nummulitids, lepidocyclusinids and coralline algae (see *e.g.* Lokier *et al.*, 2009). Beds dominated by monospecific thin branching *Porites* in growth position within a shaly-clayey matrix indicate episodes of decay of coral diversity and proliferation of few species that can thrive and catch-up in turbid waters, characterized by high sedimentation rates (Guzmán and Guevara, 1998; Johnson *et al.*, 2009). In addition, larger foraminifera, carpets of branching *Porites* and bivalve beds played an important role as hard substrates, which allowed coral colonization and bioherm growth (Novak *et al.*, 2013). These variations of sedimentary influx (and hence in the photic conditions affecting the carbonate-producing communities) within the prodelta setting can be explained by lateral migration of delta-mouth bar and associated delta lobes, changes in river discharges and other possible deltaic or eustatic cycles.

Upper ramp

Upper ramp deposits are located basinwards, in front of the prodelta-shale facies belt, and are characterized by a drastic reduction of siliciclastic influx and a predominance of carbonate sedimentation (Fig. 8). Planar to wavy-bedded successions of pillarstones of sparsely branching and columnar scleractinians (Fig. IICBS) interbedded with rudstones of reworked corals (Fig. IIDCS) constitute the dominant facies type in the upper ramp. This facies contains abundant skeletal components dominant in the upper photic zone of a tropical shallow ramp setting (Hottinger, 1997) including *Miosorites americanus*, *Annulosorites spiralis*, *Miarchaias* sp., miliolids, rovaliids, *Amphistegina*, *Miogypsina* (Fig. 5), textularids and green algae fragments. Soritids, archaiasinids and miliolids live actually on the surface of marine plants and algae between 0 and 40m of water depth, in tropical to subtropical restricted or inner platform settings (Hottinger, 1997, 2001; Langer and Hottinger, 2000; Reiss and Hottinger, 1984). Miogypsina lived in tropical shallow-marine environments of normal salinity, less than 50m deep, associated with coral thickets or seagrass banks (Frost *et al.*, 1983; Geel, 2000). Mixed coral-seagrass meadows are common in Early Miocene inner ramp settings (Bover-Arnal *et al.*, 2017; Brandano

et al., 2009; Pomar *et al.*, 2015; Shabafrooz *et al.*, 2015). From the geometrical reconstruction of the marginal delta slope and palaeobathymetric constrains based on the dominant foraminiferal associations, there is evidence that upper ramp coral carpets thrived in water depths between 20 to 40m (Fig. 8).

Proximal middle ramp

Proximal middle ramp deposits occur seaward of the coral-bearing facies belt and consist of massive, unsorted and bioturbated levels of alternating rhodolith and branching red algae floatstone/rudstone with a bioclastic packstone matrix (Figs. IIRF; MF; 8). Skeletal matrix is dominated by coralline algae detritus and thin-shelled hyaline perforated larger foraminifera that thrived in the deeper part of the upper photic zone, between 40 and 80m water depth (Hottinger, 1997), such as *Miogypsina*, *Amphistegina*, *Heterostegina*, *Operculinoides*, *Eulepidina* and *Lepidocyclina* (Fig. 5E–O). Matrix also contain less abundant reworked tests of foraminifera adapted to shallow upper photic zone (*e.g.* soritids, archaiasinids) (Fig. 5B–D), probably transported and resedimented from near-shore environments by storm waves or currents.

The abundance of rhodoliths in addition with high bioerosion, skeletal abrasion and fragmentation (Fig. IIRF; MF) are indicative of low sedimentation rates that implied a long-term residence of biogenic components over the sea bed (Aguirre *et al.*, 2017; Bover-Arnal *et al.*, 2017). Moreover, syndepositional taphonomic features of skeletal components are also good indicators of sediment transportation rates (Beavington-Penney, 2004; Bover-Arnal *et al.*, 2017; Peebles and Lewis, 1991). In this regard, skeletal fragments exhibit different rates of abrasion and fragmentation (Fig. IIRF; MF). According to Beavington-Penney (2004) low to moderate damages in outer tests of *Nummulites* indicate moderate to extensive transport or wave re-working, whereas high fragmentation levels may reflect transport within turbidity currents or predation by large bioeroders. Additionally, experimental analysis over modern foraminifera sediments from Jamaica by Kotler *et al.* (1992) demonstrated that different foraminifera species display varying susceptibilities to mechanical abrasion. Larger foraminifera examined (including nummulitids) can appear well preserved or moderately to highly abraded and fragmented in Rhodolith and Maerl facies assemblages. These taphonomic features are thus in accordance with variable regimes of sediment remobilization in the proximal middle ramp setting. In the same way, coralline algae occur as rhodoliths (Fig. IIRF), crusts, well-preserved branches (Fig. IIMF), or sand sized detritus exhibiting different degrees of abrasion and fragmentation (Fig. IIRF; MF). Furthermore, the rhodoliths studied are commonly nucleated around coral fragments (Fig. IIRF) and deposited near the

coral-rich facies belt (Fig. 8). All these observations, added to the predominance of massive and nodular beddings, with no sedimentary structures and the absence of other sedimentological features indicative of high energetic regimes, suggest low to moderate transportation rates. Notwithstanding, the minor occurrence of amalgamated channel structures, basinwards dipping clinobeds and parallel, cross and slumped beddings indicate the presence of local allochthonous rhodolith accumulations, probably generated by processes of downslope transport.

Distal middle ramp

In the distal middle ramp setting, the facies change seaward to poorly-sorted, highly-fragmented and abraded coralline algal and larger foraminifera packstone (Figs. IICADF; 8). Coralline algal debris facies is volumetrically the most important lithofacies occurring in the San Luis carbonate ramp. Larger foraminifera include different species of *Amphistegina*, *Miogypsina*, *Heterostegina*, *Operculinoides*, *Eulepidina* and *Lepidocyclina* (Fig. 5E–O) which thrived in the lower part of the upper photic zone (*c.* 40–80m) in tropical shallow seas during the Early Miocene (Hottinger, 1997). In accordance with Beavington Penney (2004), the high degree of abrasion and fragmentation of the nummulitid foraminifera examined (Fig. IICADF), indicates the presence of extensively reworked substrates under turbidite currents and/or predation activity by large bioeroders.

The occurrence of structureless beds lacking hydrodynamic sedimentary features, such as laminations, trough cross-bedding or marked textural variations, along with taphonomic attributes indicating extensive remobilization of skeletal components, appears to be contradictory. In this respect, hydrodynamic studies by Jorjy *et al.* (2006) demonstrated that skeletal grains with different sizes can have the same hydrodynamic behavior as long as the density of grains are low and strait ranged. For this reason, sedimentary structures are rarely observed in heterometric carbonates composed by low-density grains (*e.g.* porous larger foraminifera). The amount of micropeloidal micrite within the highly reworked skeletal fabric and the absence of sedimentary structures could be in accordance with low-energy environment with recurrent higher-energy events (*e.g.* turbidite currents).

Lower Ramp

Middle ramp strata pass seawards, after a ramp step, into lower ramp deposits (Fig. 7C; 8), which are represented by alternations of plane- to wavy-stratified limestones with larger foraminifera (Fig. IILF) and planktonic foraminifera packstones to wackestones (Fig. IIPFF). Skeletal grains are dominated by highly-abraded and fragmented tests of

low-light adapted larger foraminifera (*e.g. Eulepidina*, *Lepidocyclina*, *Operculinoides*) (Fig. 5F, L, M) mixed with abundant pelagic fauna including globigerinids. Large and flat tests of *Eulepidina*, *Lepidocyclina* and *Operculinoides* are associated to the lower photic zone (c. 80-120m; Hottinger, 1997). On the other hand, the abundance of pelagic fauna, the micropeloidal micrite in the matrix, the occurrence of hardgrounds and common glauconite-rich intervals indicate a low sedimentary regime in a pelagic environment. In addition, abrasion and fragmentation attributes of nummulitid tests examined could be also in accordance with moderate or extensive transport driven by turbiditic currents from lower photic zone to deeper settings (see Beavington Penney, 2004).

The lateral transition from lower ramp strata to basin floor deposits is not preserved, nowadays obliterated by South-dipping reverse fault system (Figs. 2; 3). Hanging-wall deposits of this reverse fault system are the turbidites of the Pedregoso Fm., which is equivalent in age with the San Luis platform carbonates, situated in the foot-wall block (Figs. 2; 3; 7B, C). These carbonate turbidites are integrated by alternations of olistostromes, coral breccias and reworked skeletal limestones with abundant intraclasts interbedded within black shale deposits. This gravity-flow succession also exhibits minor siliciclastic episodes. The sedimentary features observed indicate the presence of normal faults that were active during the Early Miocene and bounded the southern margin of the San Luis carbonate platform from the basinwards turbidite system.

Southern Falcón

The Early Miocene sedimentary environment in the southern Falcón basin was dominated by widespread siliciclastic sedimentation with two episodes of local carbonate deposition, both corresponding to the Churuguara Fm. These two local carbonate horizons include echinoid-rich calcarenites passing upwards to larger foraminifera and red algae-bearing limestones that occur as two detached tabular lithosomes interbedded within a thick succession of siliciclastic marine deposits. Carbonate banks thin and pass southward and eastward to pelagic shales and turbidites, whereas towards the West they interfinger with shallow-marine siliciclastics. The Churuguara carbonate systems are exposed as isolated outcrops, ranging from ten to hundred meters in thickness, segmented by recent karstic erosion (Fig. 9). NE-SW trending fractures belonging to Oca Ancón fault system plus contributed to deform, fragment and displace the original carbonate platform bodies. These lateral and associated inverse faults also constitute the northern limit of the Churuguara platform carbonates, bringing them into contact with basal the El Paraiso deltaic deposits and the overlaying Pecaya-Agua Clara pelagic shales deposited in the central Falcón Basin (Figs. 2; 3).

The lateral relationships between Churuguara limestones and their age-equivalent pelagic shales, deposited towards the North in the central area of the basin, were not observed in the field due to the occurrence of the aforementioned fault system. Consequently, the depositional profile of the Churuguara carbonate systems was not recognized in the field due to the absence of continuous outcrops at the scale of a platform or platform-to-basin profile. Notwithstanding, most facies associations are constituted by grain-dominated skeletal limestones organized in continuous, relatively thick subparallel strata with occasional small-scale scleractinian biostromes ranging in sizes from metric to decametric scales (Fig. 9). Additionally, well developed or prominent reefs or shoal barriers were not recognized along the studied outcrops. These observations are consistent with a carbonate ramp model in a broad sense. Similar Oligocene-Miocene larger foraminifera and coralline algae isolated carbonate banks have been described in sedimentary basins around the world (*e.g. Bover-Arnal et al. 2017; Brandano et al., 2017; Pomar et al., 2015; Riera et al., 2022; Tournadour et al., 2020; Vaziri-Moghaddam et al., 2010*).

The distinct facies are arranged in belts, reflecting a depth zonation across the depositional profile (Fig. 10). Based on the stratal framework, faunal occurrences and their palaeobiological constraints, four differentiated ramp settings were distinguished: i) transitional facies constituted by lagoons or estuary systems bordered by nummulitid shoals, transitioning upwards to an eastward prograding delta system; ii) upper ramp dominated by echinoids passing vertically into soritids, archaiaenids, green algae and coral-bearing limestones; iii) middle ramp characterized by extensively reworked larger foraminifera, coralline algae, and minor rhodolith pavements and iv) lower ramp characterized by lepidocyclinid debris.

Aquitania carbonate ramp

Estuary: The lowermost strata of the western Churuguara Fm. are confined in two East-West trending palaeovalleys or semigrabens referred as La Danta and Churuguara Sub-basins (Figs. 1; 10). These deposits were characterized by receiving sediments from both, fluvial inputs from the West and marine inputs from the East. Additionally, the sedimentary facies reflect the dual influence of coastal marine and fluvial processes. These distinctive features constitute the geological definition of estuary deposits (*sensu Dalrymple, 1992*).

Internal estuary facies are characterized by bayhead deltas, consisting of medium to coarse-grained delta front deposits interbedded within prodelta or lagoon shales, displaying an overall coarsening upwards trend (Fig. IBDS). Well sorting, high mineralogical maturity dominated by quartz grains and chert clasts, low amounts of matrix

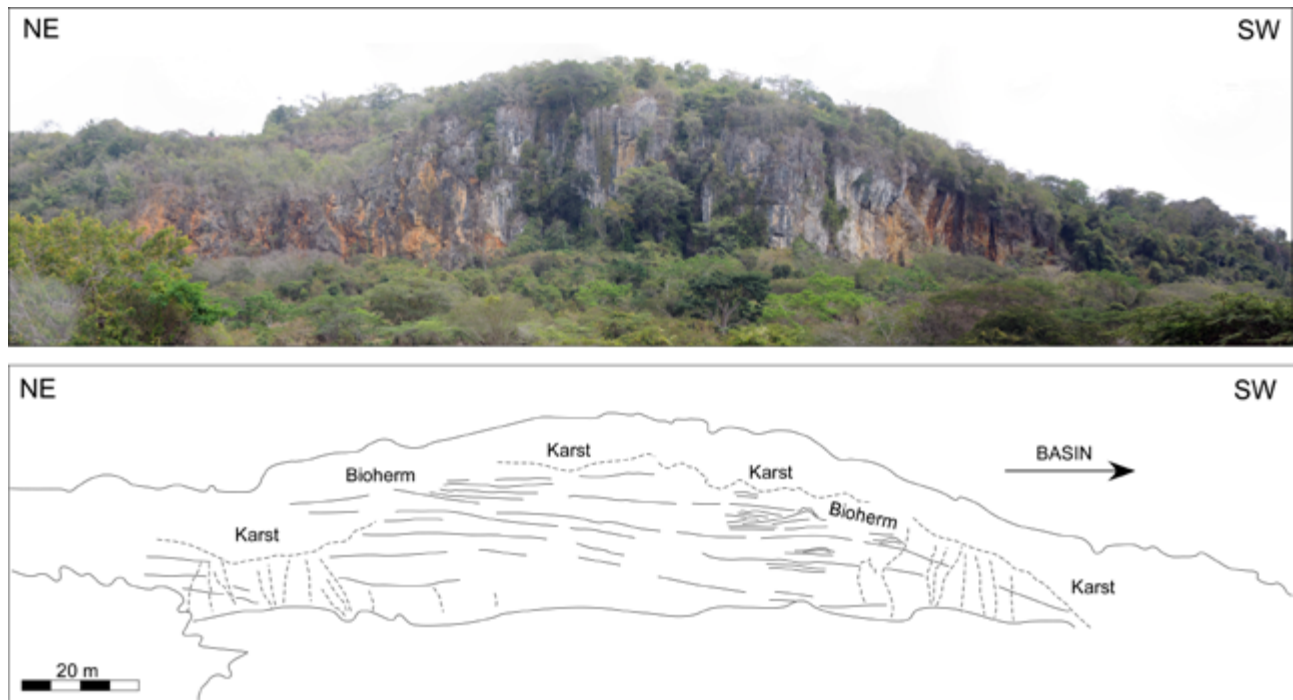


FIGURE 9. An outcrop-scale view and line-drawing interpretation of the Churuguara platform carbonates (southern Falcón Basin) characterized by isolated karstic dome-like mogotes or residual hills. These distinctive landforms were formed by the region's intense fracturing and faulting patterns, the limited thickness of the Churuguara carbonate banks, and the effects of tropical weathering. However, the remaining outcrops along the southern margin of the Falcón Basin preserve small snapshots of the original carbonate platform morphology. The integration of individual outcrop observations, correlated through stratigraphical and palaeontological criteria, geological mapping, orthophotos, and satellite imagery, was employed to identify the carbonate platform morphology on a large scale. The stratal architecture is characterized by subparallel beds that are roughly uniform in thickness, with no abrupt lateral changes, breaks, or significant thickness variations. Small-scale coral bioherms were recognized along the depositional profile, although they do not constitute well-developed or prominent reef or shoal barriers. These observations are consistent with a carbonate ramp architectural model. The photograph was taken along the New Road from Coro to Churuguara, approximately 7-8km North of Churuguara city (refer to Fig. 2 for the location of the first carbonate bar on the hanging wall of the reverse fault, just North of Section 19).

and tractive sedimentary structures are characteristic of energetic environments with persistent or long-term processes of sediment removal. Conversely, evidence of erosional, channel-like, and lenticular strata, large scale cross bedding and well-developed clinoforms indicate an amalgamation of submarine distributary channels and mouth bars, likely situated in a delta front setting. Subordinated small-scale sigmoidal and flaser beddings, along with local bidirectional ripples suggest a low pervasive wave or tidal overprint, predominantly influenced by riverine processes and relatively protected from coastal marine reworking. The scarce presence of marine fauna, and low bioturbation coupled with interbedded fine levels of coal and vegetal rests, lends support to the prevailing continental influence, with high terrigenous inputs and minor marine reworking.

Bayhead deltas transition seawards, to the East, into internal lagoons or sediment sinks dominated by massive dark grey clays and minor sandstone interbeds (Fig. ILS). This central region is primarily influenced by low-energy processes, characterized by the deposition of suspended

mud. Predominantly calm deposition conditions are occasionally disrupted by sporadic high-energy events, possibly associated with intermittent storms, as evidenced by the occurrence of fine laminated sandstone and siltstone interbeds. The presence of hummocky cross stratifications, along with wave, combined-flow, and current ripples, indicates both bottom currents and oscillatory wave movements, potentially triggered by storms. Additionally, current ripples may result from increased fluvial discharges, causing turbidite flows that extend into the central lagoon. Gingras *et al.* (2012) indicated that Miocene or more recent strata characterized by low faunal diversity, along with horizons dominated by *Gyrolithes*, *Skolithos*, and *Planolites*, are characteristic of brackish-coastal marine environments. In this regard, the low variability of ichnofacies and skeletal fragments, such as small bivalves and sporadic gastropods, along with the presence of *Gyrolithes*, indicates the prevalence, or intermittent, episodes of high salinity. These conditions may be associated with the disconnection of the internal lagoon from the sea, low (or intermittent) freshwater discharges from the continent, or both.

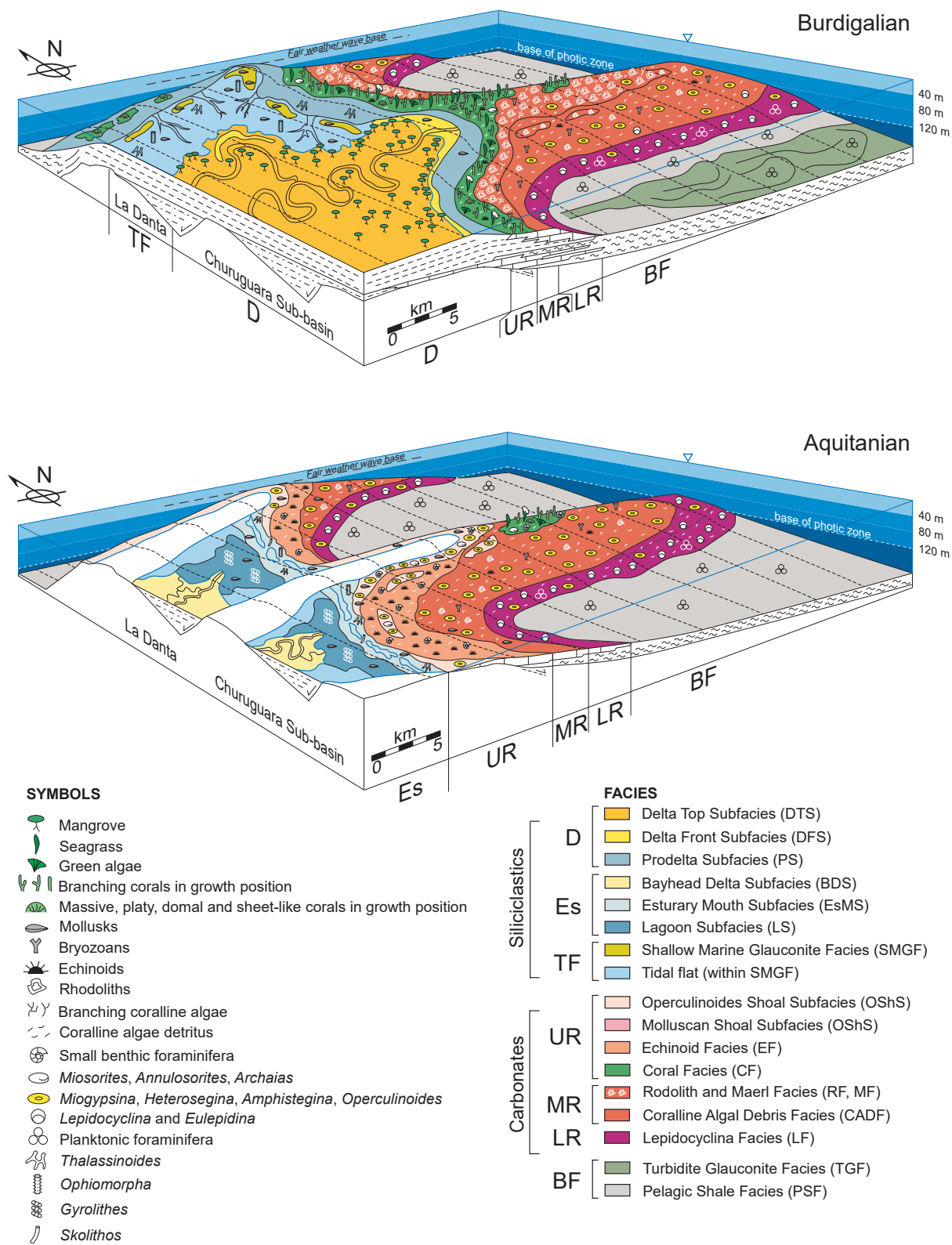


FIGURE 10. Depositional models for the Aquitanian and Burdigalian isolated carbonate ramp systems in the southern Falcón Basin showing the lateral distribution of the different facies belts, their main biogenic components and most representative ichnofossils. The facies boundaries are marked by changes in sedimentary conditions (e.g. photic conditions, siliciclastic input, energy, depositional profile). The facies boundaries can be either transitional or sharp, depending on whether the changes in sedimentary conditions are progressive or abrupt. All facies represented belong to the Churuguara Fm., defined as an intercalation of platform carbonates, shales and sandstones. D= Delta, Es= Estuary, TF= Tidal Flat, UR= Upper Ramp, MR= Middle Ramp, LR= Lower Ramp, BF= Basin Floor.

Internal lagoon facies occur rimmed shoreward by marine reworked sandstones intermixed with abraded skeletal fragments comprising the estuary mouth facies suite. These successions are typically coarsening and thickening upwards, fine-to-coarse grained, cross-bedded and planar laminated, with abundant burrows and shell beds (Fig. IESMS). This sedimentary pattern indicates increasing energy conditions upwards. Additionally, these facies are dominated by shallow marine ichnofossils usually associated with tidally influenced settings, such as *Planolites*, *Ophiomorpha* and *Thalassinoides* (Gingras *et al.*, 2012). Other sedimentary features include channel-like deposits with herringbone, bidirectional current ripples, as well as the occurrence of reworked marine fauna dominated by mollusc fragments and lesser amounts of echinoids, serpulids, foraminifera and red algae. These characteristics are consistent with coastal barrier sands enclosing the estuary mouth, which were locally dissected by tidal-inlets and associated tidal deltas.

Upper ramp: Seawards of estuary mouth deposits, foreshore sands and clays occur interfingering with carbonate banks dominated by *Operculinoides*, fragments of bivalves and gastropods (Figs. IIOSHS; 5F). These nummulitid accumulations vary between 0.2 to 2m in thickness and usually are arranged in thinning upwards sets. Sedimentological features indicative of high energy are common, and include erosive bases with pebble lags, cross and wavy beds, siliciclastic calcarenites with tractive structures, a high degree of bioclastic abrasion and fragmentation, and bioclastic imbrication. In this deposits geopetal structures were also observed. According to Hottinger (1997), the major occurrence of *Nummulites* (eq. *Operculinoides*) is offshore, close to the limit between the upper and the lower photic zone, at water depths from 40 to 80m. On the other hand, Beavington-Penney (2004) studied the effects of transport-induced abrasion on the test of selected nummulitids by exposing them under simulated reworking conditions using a mobile traction carpet. The nummulitids observed in the Churuguara deposits exhibit a high degree of breakage, with the outer test wall damaged or partially missing, presence of holes with irregular margins penetrating through the outer wall, and 'pits' or micro-indentations covering the test surface (Fig. IIOSHS). According to the Beavington-Penney's experiments, the taphonomic features observed indicate extensive transport ratios and long-term wave reworking. Additionally, the co-occurrence of genera associated to shallow euphotic waters like soritids (Figs. 5C, D), archaiaasinids (Fig. 5B), miliolids, and *Halimeda* sp. are consistent with littoral bars or banks formed by allochthonous nummulitids intermixed with shallower skeletal fragments transported landward and reworked by waves. Higher content of micrite or calcisiltite in the matrix indicate transitions to deeper settings (in back- or fore-bank contexts), probably below the FWB.

Similar Eocene examples of shoal nummulitic banks are described in deposits from Spain (Trempe Basin), Tunisia, Libia, Egypt, Italy and Oman (e.g. Aigner, 1983; Arni, 1965; Bassi *et al.*, 2013; Jorjy *et al.*, 2006; Racey, 2001; Serra-Kiel *et al.*, 2003).

Operculinoides shoal banks transition basinwards, towards the East and South, into upper to middle ramp limestones. These deposits are mostly represented by echinoid calcarenites (Fig. IIEF) and local patches of branching corals and seagrass meadows (Fig. IICF). Echinoid limestones are found to the West, within the engulfed marine portion located offshore of estuarine bays. In contrast, coral and seagrass carpets are likely to be found eastward, thriving in open sea shallow waters. These habitats were favoured by the presence of palaeo-highs formed by the submerged portion of the half-graben shoulder.

Upper to middle ramp fine-grained grainstones to packstones contain well-preserved, likely in-situ, irregular echinoids (Fig. IIEF). The morphological features of the identified echinoderms, including a wedged profile, heart shape, bilateral symmetry, anus displaced towards the posterior margin of the test, reduced petaloid ambulacra, and presence of small pore pairs for tube feet on the top of the test, are characteristics of deep infaunal sea-urchins. These spine-coated organisms inhabit soft substrates by burrowing in sublittoral environments with moderate to low energy levels (Kroh, 2001; Kroh and Nebelsick, 2003; Marcosu and Nebelsick, 2019). The skeletal content comprises about or higher than 50% echinoid plate and spine fragments, followed by coralline algae, gastropod and bivalve detritus, smaller benthic foraminifera, planktonic foraminifera, and sporadic fragments of recrystallized larger foraminifera. The strong diagenetic overprint, low preservation, as well as the high degree of fragmentation of skeletal remains, do not permit the identification of most carbonate fragments. However, high amounts of red algae detritus and sporadic larger foraminifera indicate depths within the photic zone, whereas planktonic foraminifera are indicative of open marine conditions. The influence of marginal siliciclastic systems, the abundance of mollusc detritus, and smaller benthic foraminifera indicate shallow marine environments. The high degree of fragmentation of skeletal fragments added the presence of meter scale cross beds suggest extensive reworking conditions, provably by storm waves or currents.

Local accumulations of poorly reworked shallow marine *Heterostegina*-bearing deposits (Fig. IIHF) occur in distal parts of isolated coral mounds (Fig. IICF), within a proximal middle ramp setting. According to Beavington Penney and Racey (2004), living *Heterostegina* species from Hawaii are restricted to water depths from 30 to 73m.

Accordingly, Langer and Hottinger (2000) ascribe different species of *Heterostegina* within the lower part of the upper photic zone in tropical to subtropical areas, on both hard and soft substrates, and often forming accumulations on coral reef slopes.

Middle ramp: The middle ramp strata consist of extensively reworked deposits dominated by coralline algae and larger foraminifera (Fig. IICADF). These foraminifera include symbiont species adapted to oligophotic waters of tropical seas, such as *Miogypsina*, *Heterostegina*, *Operculinoides*, *Eulepidina* and *Lepidocyclus* (Fig. 5G–K, E, F, L, M) (BouDagher-Fadel, 2008; Hallock, 1985, 1999; Hottinger, 1997), accompanied by abraded skeletal fragments originating from the shallowest upper photic zone, such as corals, and epiphytic porcelaneous foraminifera. This assemblage suggests deposition in shallow marine waters, below the FWFB, and within the lowermost upper photic zone (c. 40–80m; Hottinger, 1997). These sedimentary settings are characterized by the reworking of potential bottom currents or storm-generated waves, which likely contribute to the redistribution of sediments from upper ramp settings.

Lower ramp: Lower ramp deposits are dominated by *Lepidocyclus*- and *Eulepidina*-rich debris with hemipelagic fauna, comparable to those described in the San Luis distally steepened ramp, located in the northern part of the Falcón Basin (see the above section on the Northern Falcón). Interbedded with these deposits are likely in-situ occurrences of large, thin *Lepidocyclus* and *Eulepidina*, and small *Operculinoides*-bearing strata (Fig. IILF), characterized by undamaged to poorly eroded specimens within a micritic micropeloidal matrix. These deposits were situated in the deepest part of the photic zone (c. 80–120m; Hottinger, 1997), below the storm wave base level, and were locally disturbed or remobilized by bottom turbidite currents, which subsequently remobilized and transported them basinwards.

Burdigalian carbonate ramp

Upper ramp: Transitional and litoral deposits of the western portion of Churuguara Fm. (southern Falcón Basin) evolve vertically from estuary and nummulitid shoals to an alternation of an East-draining delta system and open-coast tidal flat deposits which transition basinwards into skeletal carbonate ramps. Upper ramp stratified coral boundstones, rudstones and floatstones dominated by branching *Porites* contain abundant skeletal fragments representative of shallow marine environments of tropical to subtropical seas (Fig. IICF). *Miarchaias*, *Miosorites*, *Annulosorites* (Fig. 5B, C, D), miliolids and peneropliids are porecelaneous epiphytes usually associated with seagrass meadows, whereas *Sphareogypsina* sp. (Fig.

5P) and gypsinids are encrusting foraminifera thriving in upper photic depths usually related with coral-bearing deposits (Bover-Arnal *et al.*, 2017; Brandano *et al.*, 2009; Hottinger, 1997, 2001). *Miogypsina*, *Heterostegina*, and *Amphistegina* (Fig. 5G–K, E, N, O) are dominant in the deepest part of upper photic zone (c. 40–80m; Hottinger, 1997). The abundance of branching scleractinian remains in stratified deposits, along with the co-occurrence of shallow euphotic larger foraminifera intermixed with deeper photic genera, indicates the development of shallow marine meadows dominated by branching corals and seagrass communities. These environments likely existed at water depths near the transition between the shallow and deep upper photic zones (40m *sensu* Hottinger, 1997), and were influenced by reworking processes that facilitated the remobilization of middle ramp larger foraminifera (e.g. *Miogypsina*, *Heterostegina*) (Fig. 5G–K, E) from middle to upper ramp settings. Equivalent present day mesophotic coral communities have been found in tropical and subtropical regions at water depths between 30 to 150m below the sea (Diaz *et al.*, 2023; Lesser *et al.*, 2009; Pyle *et al.*, 2016).

Middle ramp: Although coralline red algae can thrive in water depths ranging from euphotic to oligophotic environments, their primary occurrence in tropical seas is associated with mesophotic to oligophotic conditions, typically at depths between 20 and 80m (Adey *et al.*, 1982; Bosence, 1991; Nalin *et al.*, 2008). This is because, in the euphotic zone, red algae communities must often compete with organisms from the chlorozoan association (e.g. corals, seagrass, calcareous green algae) (Less and Buller, 1972). Coralline algae only massively colonize the shallower photic zone when environmental conditions are unsuitable for the growth of corals and calcareous green algae (Carannante *et al.*, 1988; Nalin *et al.*, 2008; Pomar *et al.*, 2004). In this regard, middle ramp deposits of the Burdigalian Churuguara ramp are dominated by rhodalgal pavements with rhodoliths and larger foraminifera (Fig. IICADF RF). In proximal middle ramp settings, coralline algae assemblages are accompanied by skeletal fragments associated with coral or seagrass facies, which are characteristic of the shallower upper photic zone (c. <40m; Hottinger, 1997). These skeletal association include porcelaneous and hyaline epiphytic foraminifera (e.g. peneropliids, soritids, miliolids), *Orbulina*, *Amphistegina* (Fig. 5P, N, O), and geniculate corallines. The shallow euphotic bioclasts are intermixed with lesser amounts of oligophotic larger foraminifera such as *Operculinoides*, *Heterostegina*, *Eulepidina*, and *Lepidocyclus* (c. 40–80m, Hottinger, 1997) (Fig. 5E, L, M). Towards distal parts of the middle ramp, the proportion of oligophotic symbiont larger foraminifera increases, while the occurrence of skeletal fragments associated with shallower photic areas decreases or even disappears.

Lower ramp: Lower ramp deposits of the Burdigalian carbonate bank are equivalent in facies, sedimentological features, and skeletal components to those described for the Aquitanian distal ramp settings characterized by parautochthonous to allochthonous lower photic foralgal and pelagic limestones. However, the lepidocyclinids identified in the distal parts of the Burdigalian Churuguara ramp are remarkably thicker and more robust than those occurring in the Aquitanian lower ramp, which are notably thinner and more delicate (Fig. IILF). Hallock (1988, 1999) noted a marked vertical diversification in nummulitids and amphisteginids linked to adaptations to light conditions, with thicker and more robust forms adapted to shallower depths and thinner, flatter forms thriving in deeper water conditions. Accordingly, Boltovskoy *et al.* (1991) indicate that a decrease in light results in a reduction of thickness in the test of larger foraminifera. In this regard, the variations in thickness observed in *Lepidocyclina* and *Eulepidina* specimens of the Churuguara Fm. could suggest a greater depth for the Aquitanian lower ramp compared to the Burdigalian equivalent deposits.

In general terms, the Churuguara carbonate ramps are characterized by sedimentological and taphonomic evidence of intense reworking, including high abrasion and fragmentation of skeletal components, alternations of grainstone and packstone textures, and occasional tractional sedimentary structures specially in proximal areas. These features indicate extensive sediment remobilization between proximal and distal settings, leading to a degree of facies homogenization. In this respect, the Churuguara carbonate ramps were characterized by shallow, low gradient slopes, ranging from 20 to 120m in depth and characterized by extensive sediment redistribution. Nevertheless, some

selection of euphotic and oligophotic biotas highlights bathymetric subdivisions between upper, middle and lower ramp settings (Fig 10).

LOWER MIOCENE SEDIMENTARY EVOLUTION AND SEQUENCE STRATIGRAPHY OF THE FALCÓN BASIN

Lower Miocene mixed-carbonate siliciclastic systems, rich in corals, coralline algae and larger foraminifera examined in the Falcón Basin, unconformably overlay middle Eocene pelagic shales and marls from the Jarillal Fm. (Albert-Villanueva *et al.*, 2017; Guevara, 1967; Hunter, 1974, 1978; Macellari, 1995; Wheeler, 1963) (Fig. 4). This basal unconformity has regional significance and is well-exposed in the central and southern parts of the basin (Figs. 2; 11), while in northern Falcón Basin, it is evidenced by seismic and exploration well data (Macellari 1987, 1995). The studied Lower Miocene mixed carbonate-siliciclastic strata were deposited in the latest and most extensive stage of South Caribbean back-arc rifting, characterized by the development of marginal semigrabens bordering the main central depocenter of the basin (Figs. 1; 4) (Albert-Villanueva, 2016). These deposits record a major Aquitanian-Burdigalian T-R cycle with regional importance, coinciding with the Lower Miocene tectonic-induced sedimentary cycle C1, as defined by Macellari (1987, 1995) in the southwestern Caribbean basins (Fig. 4). According to the same author, sedimentary cycle C1 exhibits a transgressive character. This large-scale sedimentary behaviour has also been observed in the studied sections, characterized by a general retrogradational trend of marine facies and the progressive onlapping and spilling out of marginal sedimentary facies beyond the basin limits (Fig. 4). From the late Burdigalian

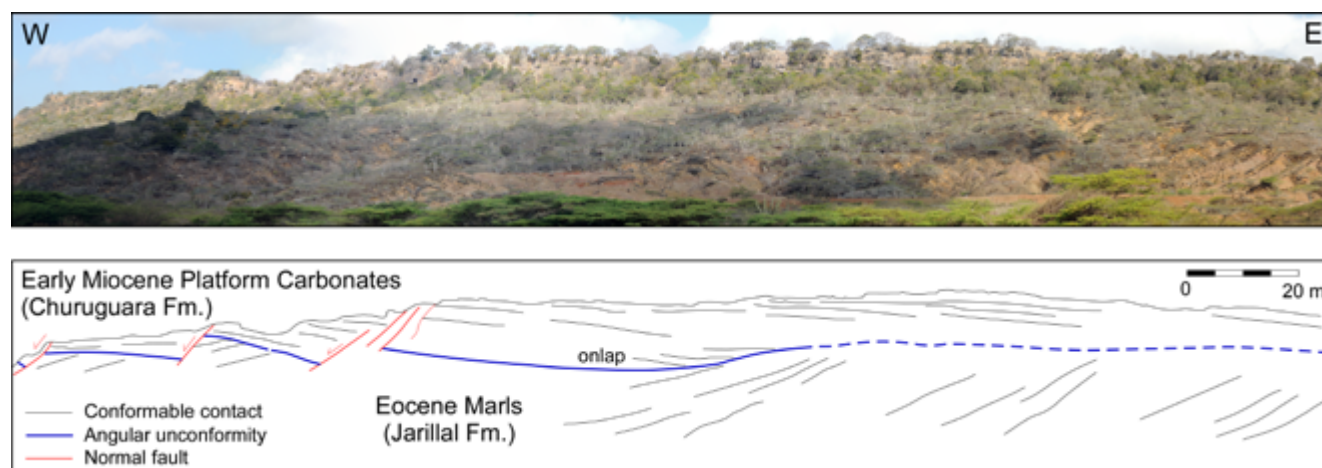


FIGURE 11. An outcrop-scale view and line-drawing interpretation of the unconformable contact between the basal platform carbonates of the Churuguara Fm. and the underlying Eocene marls of the Jarillal Fm. The unconformity exhibits an angular character, resulting from tilting associated with the regional uplift of the previous South Caribbean fore-arc sag basin. The platform carbonates were deposited during the Early Miocene in the context of an East-West trending back-arc rifting in the South Caribbean, which formed the Falcón Basin. The normal faults observed are post-Miocene. The image was taken at La Cienega, located approximately 40km Southwest of Churuguara. (refer to Fig. 2, section 19 for location).

onwards, a shift in stacking pattern occurred, characterized by a general regression, punctuated by the progradation of marginal siliciclastic facies towards the central parts of the basin (Figs. 4; 12; 13; 14).

Six 10 to 100 meter-scale lower rank T-R depositional sequences were identified in both the northern and southern margins of the Falcón Basin, resulting from higher-frequency relative sea-level fluctuations. Depositional sequences were primarily determined by changes in the stratal stacking pattern, and are bounded by well-developed transgressive surfaces (Figs. 12; 14).

Stratigraphic surfaces that mark a change of stratal stacking pattern from transgression to regression, defined as maximum flooding surfaces (Frazier, 1974; Galloway, 1989; Posamentier and Vail., 1988; Van Wagoner et al., 1988), were not recognized as such in the studied sections. Therefore, this shift in the stratal stacking pattern was characterized as a Maximum Flooding Zone (MFZ) (*sensu* Siggerud and Steel, 1999). It was tentatively placed within the stratigraphic interval that marks the transition from a deepening-upwards to a shallowing-upwards succession, or more precisely, within zones characterized by condensed deep marine facies, such as glauconite-enriched pelagic strata.

Northern Falcón

In the northern margin of the Falcón Basin, 16 stratigraphic sections of Aquitanian-Burdigalian mixed carbonate-siliciclastic strata, ranging from 25 to 310m in thickness, were measured along a dip-oriented profile from North to South (Figs. 2; 12). These sections are perpendicular to the palaeo-coastline, spanning along 13.2km from proximal to distal settings and displaying a total thickness of 810m. A 2D sequence stratigraphic and facies distribution model was generated by the correlation of different stratigraphic logs (Fig. 12). Stratal correlation was achieved by directly tracing across the various studied outcrops, utilizing landscape outcrop photographs, satellite images, and orthophotos to track correlative units. Where direct correlation proved challenging, indirect methods, including the matching of lithostratigraphic units, biostratigraphic domains, and facies associations, were employed.

Sequence 1

The six transgressive-regressive units recognized in the northern Falcón Basin comprise a suite of interfingering southward-prograding delta systems belonging to the Patieitos and Guarabal fms. and retrograding coral-bearing

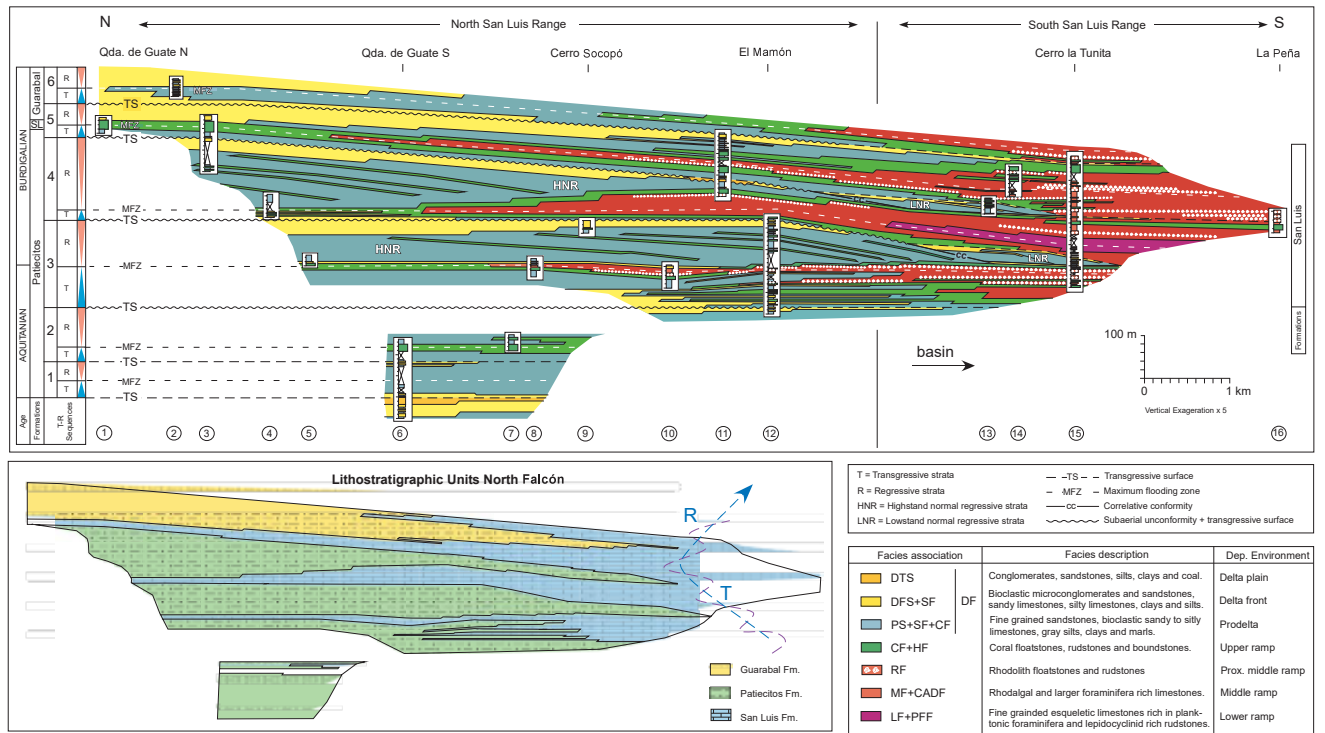


FIGURE 12. Dip-oriented stratigraphic correlation and facies distribution of the mixed carbonate-siliciclastic deposits (San Luis Fm.) of the North Falcón Basin. The six Lower Miocene transgressive-regressive sequences include the southwards prograding delta systems of the Patieitos and Guarabal fms. interbedded with retrograding platform carbonates of the San Luis Fm. Overall delta wedges show a backstepping stacking pattern as a consequence of a long-term transgressive cycle. From the upper Burdigalian on, a shift in the staking pattern is marked by a general progradation of siliciclastic wedges. Higher and lower rank variations of accommodation are indicated by blue and pink dashed lines, respectively. The datum is represented by the transgressive surface at the bottom of Sequence 3.

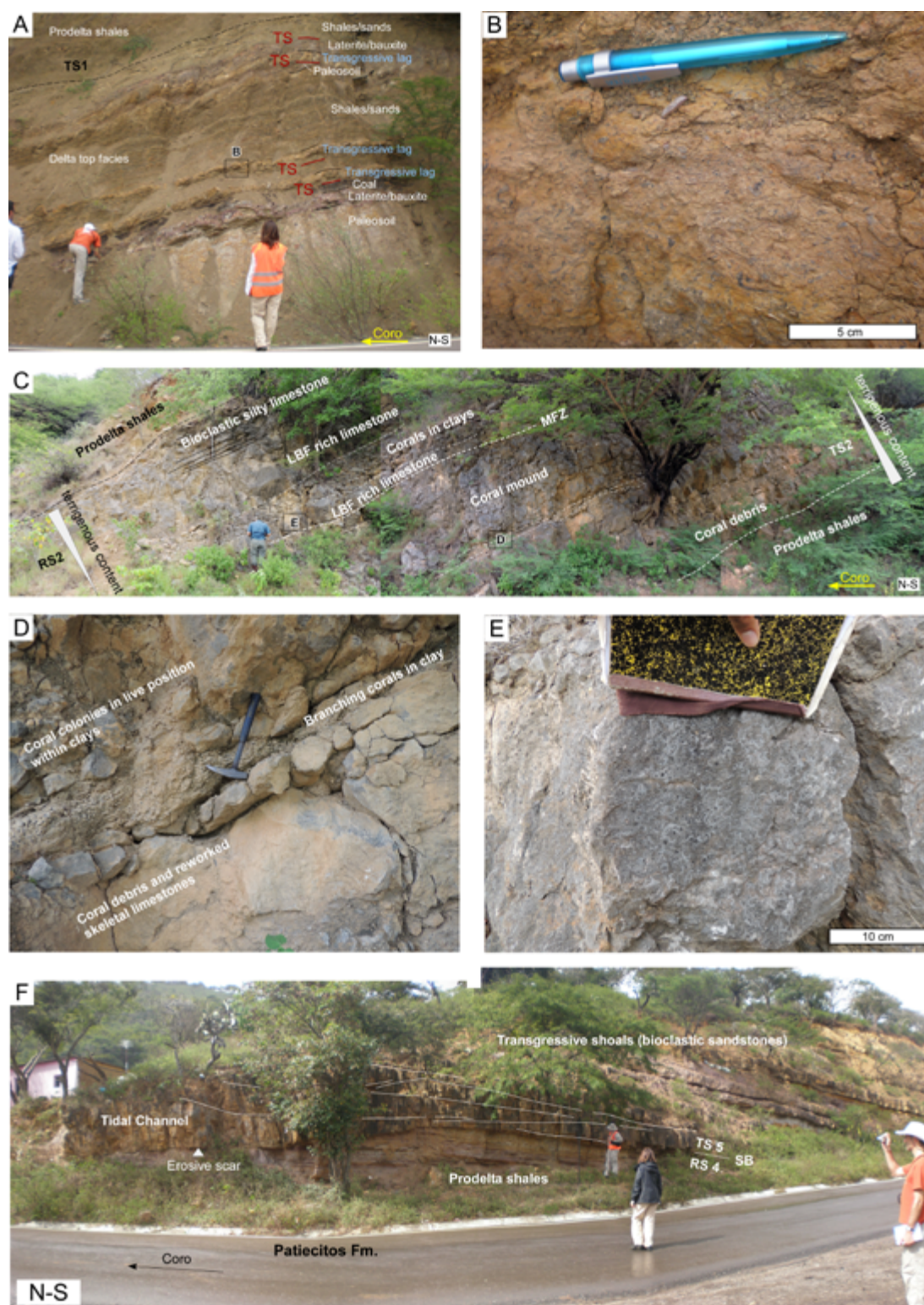


FIGURE 13. Different outcrop photographs from the northern flank of the San Luis Range (see Fig. 1 for location) illustrating the stratal relationships between the retrograding coral-bearing facies of the San Luis Fm., which interfinger with the prograding deltaic deposits of the Patieitos Fm. A) Delta top facies interfingering with transgressive lags consisting of sandy limestones rich in bivalves. B) A detailed view of a transgressive shoal facies rich in reworked bivalves. C) Coral mound unit encased within prodelta shales. Line drawings illustrate different episodes of sedimentation including a lower unit constituted by coral debris, which is overlain by a patch reef dominated by scleractinians in growth position, followed by a stratified succession of sandy and clayey limestones rich in larger benthic foraminifera. D) A close-up view of the biostromal unit constituted by thin branching corals embedded within a clay-rich matrix giving rise to coral carpets indicated in Figure 13C. E) Close-up view of the heterostegina-rich facies indicated in Figure 13C. F) Erosive channel affecting the normal regressive unit of Sequence 4 filled with transgressive tidally-reworked sandstones.

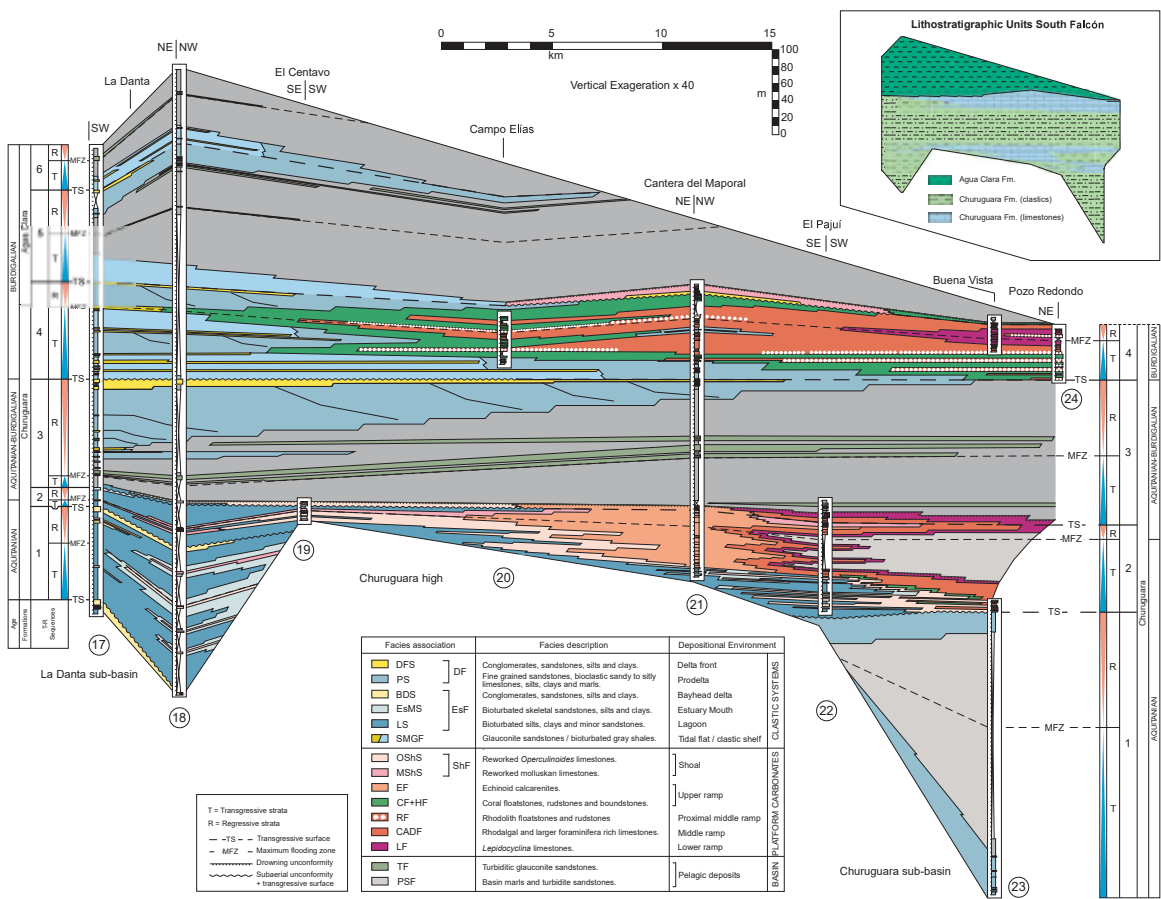


FIGURE 14. Strike-oriented stratigraphic correlation and facies distribution of the Lower Miocene isolated carbonate-banks (Churuguara Fm.) interbedded with siliciclastic deposits of the southern Falcón Basin. Transgressive sequences consist of retrograding carbonate ramps topped by drowning unconformities, which are overlain by pelagic marls. Regressive strata are prograding coastal siliciclastics (deltas and tidal flats) passing basinwards to platform carbonates or pelagic marls interbedded with glauconite-rich turbidites. The datum is represented by the transgressive surface in the top of Sequence 3.

and foralgal limestones of San Luis Fm. The lowermost transgressive unit of Sequence 1 (Fig. 12) crops out in the northern flank of Cerro Galicia, in the central San Luis Range (Figs. 2; 12 section 6), and is marked by a transitional change from continental prograding delta top deposits (Fig. 12TS) of coastal swamps, identified by alternations of pseudogleys, laterites/bauxites, coal layers, distal sandstone crevasse-splays, and shales, interfingering with transgressive lags constituted by silty to sandy limestone beds rich in reworked gastropods and bivalves (*i.e. Ostrea* sp.) (Fig. 13A, B). These higher-frequency transgressive pulses indicate a change of pattern from deltaic progradation to retrogradation of coastline facies over the delta top deposits. In this case, the sequence boundary is marked by a maximum regressive zone characterized by the presence of multiple lower-rank composite surfaces integrated by subaerial unconformities with bauxite, laterite and/or palaeosol intervals overprinted by transgressive ravinement surfaces. These composite boundary surfaces are overlain by cm to dm thick transgressive lag deposits (Fig. 13A, B). For

convenience, we placed the sequence boundary at the bottom of the first transgressive lag or reworked limestone shell bed, indicated as a Transgressive Surface (TS) (Fig. 13B). The late transgressive stage of Sequence 1 corresponds to a deepening upwards succession of shallow marine prodelta shales and distal sandstone interbeds becoming less frequent towards the MFZ (Fig. 13PS). Regressive strata of Sequence 1 are constituted by a thickening and coarsening upwards succession of prodelta clays interbedded and transitioning upwards into delta front sand bars (Fig. 13DFS). The T-R sequence 1 is composed exclusively of siliciclastic delta facies of the Patiecitos Fm. constituting the lowermost strata cropping out in the northern Falcón Basin. The age of those deposits has not been determined due the lack of age diagnostic larger foraminifera.

Sequence 2

Above the uppermost siliciclastic shoals of Sequence 1, a retrograding unit belonging to the transgressive part of

Sequence 2 occurs (Fig. 12). This unit consists of shales and prodelta marls, overlain by foredelta transgressive nodular limestones primarily composed of encrusted and reworked coral debris, rhodoliths, coralline algae detritus, and bivalves (Figs. IIDCS; 13C). These deposits are interbedded with coral biostromes, predominantly composed of branching *Porites* sp., with a siliciclastic matrix (Fig. 13C, D). These monospecific coral carpets thrived in distal prodelta environments, and they are interpreted as higher-frequency regressive pulses within a higher-rank transgressive context. Transgressive reworked deposits transition vertically into well-developed and diverse scleractinian communities, forming meter-scale coral mixstones *sensu* Insalaco (1998), associated with larger foraminifera, bivalves, and echinoderms in an upper ramp setting or as isolated coral mound facies embedded in the distal prodelta deposits (Fig. IDE, C). The onset of regression is marked by tabular and nodular sandy limestones with larger foraminifera, coralline algae, and bivalves (Figs. IIHF; 13C, E), attributed to an event of increased terrigenous input, which caused significant water turbidity, the demise of coral communities, and the proliferation of oligophotic fauna in a distal prodelta to proximal upper ramp setting. In other cases, the increase in siliciclastic input led to a reduction in coral diversity, with sparse sheetstones as cluster-reefs or sheet-like pillarstones of branching *Porites* embedded within prodelta shales and sands (see Insalaco, 1998). Novak *et al.* (2013) studied analogous Burdigalian coral populations within deltaic deposits in Indonesia, observing a decline in coral communities and a proliferation of larger foraminifera linked to increased terrigenous input. Despite carbonate-producing organisms have low tolerance to turbid waters rich in suspended sediments, there are several examples of organic adaptations and extremophile specimens that actually grow in areas of terrigenous sedimentation. Today's examples include the extensive coral reef growing in the Amazon River mouth (Moura *et al.*, 2016), or on the delta front of Mahakam Delta in Indonesia (Syahrir *et al.*, 2018). Other examples of coral facies in terrigenous are well documented in the Cenozoic stratigraphic record from Spain, Indonesia and Caribbean regions (*e.g.* Braga *et al.*, 2012; Morsilli *et al.*, 2012; Novak *et al.*, 2013; Santisteban and Taberner, 1988).

The lowermost outcropping platform carbonates from the San Luis Fm. constitute the MFZ of Sequence 2 and contain a larger foraminifera association represented by *E. undosa*, *H. antillea*, *Amphistegina* sp., and *A. spiralis*, dating back to the Early Miocene (Aquitania-Burdigalian) (Figs. 5; 6). The regressive unit of Sequence 2 is characterized by widespread delta progradation, as indicated by a decametre scale succession of prodelta marls overlain by delta front amalgamated mouth bars (Fig. 12). Prodelta to delta front deposits display coarsening upwards trends, which are culminated by delta plain successions

of mud flat shales interbedded with thin shell beds and recurrent events of subaerial exposition like palaeosols or pseudogleys.

A vertical evolution of deltaic successions is observed between sequences 1 and 2, reflecting a transition from continental to increasingly marine conditions. This shift is especially marked in the delta top deposits, changing up from a fluvial-dominated regime characterized by interdistributary bay shales with coal beds and vegetal remains, crevasse splays, and fluvial channels to open marine tidal flat deposits dominated by marine bioturbated shales with thin intercalations of bivalve- and gastropod-rich rippled sandstones. The vertical transition from river-deltas being relegated upwards to tide-deltas is associated to a transgressive context.

Sequence 3

The Sequence 3 begins with transgressive sedimentation, characterized by stepped retrogradation of deltaic facies and widespread proliferation of coral communities. The rise in relative sea level was periodically overtaken by sediment supply, resulting in multiple backstepped transgressive surfaces (see other examples in Cattaneo and Steel, 2003; Swift *et al.*, 1991), followed by episodes of extensive coral development. These multiple transgressive events are separated by higher frequency regressive pulses resulting from lateral lobe migrations, increased sediment influx from the continent, or higher-frequency sea-level fluctuations. The increase of sedimentary input reduced the size of coral colonies, limited their span, and ultimately led to their decline. Notably, significant development of scleractinian bioconstructions occurred in deltaic environments during transgressive phases, rather than during regressive stages.

The transgressive deposits of Sequence 3 evolve upwards and basinwards from siliciclastic to carbonate settings (Fig. 12), passing from retrograding delta facies rich in corals to upper and middle ramp rhodalgic limestones interbedded within coral biostromes. Rhodoliths mainly occur encrusting fragments of branching corals and larger foraminifera (Fig. IIRF), resulting from the transgressive reworking of previous coral meadows. Several examples of Cenozoic to recent rhodolith-bearing limestones deposited during transgressive periods are reported in Mediterranean, Caribbean, and Pacific analogues (Bassi and Nebelsick, 2010; Bover-Arnal *et al.*, 2017; Gläser and Betzler, 2002; Nalin *et al.*, 2008; Pomar *et al.*, 2015).

The MFZ of Sequence 3 is marked by the deposition of a carbonate unit overlying an extensive transgressive ravinement surface. This transgressive carbonate unit onlaps prodelta slope and delta shelf deposits, extending more than 10km towards the northern margin of the basin.

Even under maximum flooding conditions, the water depth remained very shallow, as evidenced by the occurrence of highly abraded, reworked, encrusted, and bioeroded skeletal grains transported landwards from middle ramp settings (*e.g.* nummulitids, miogypsinids, coralline algae), mixed with fossil fragments characteristic of nearshore environments (*e.g.* miosoritids, archaiasinids, tiny porcelaneous and hyaline foraminifera, fragments of corals, geniculate corallines, calcified green algae, molluscs, and echinoid fragments). Other sedimentological and textural evidence include a variable but persistent siliciclastic content, the predominance of grainstone textures, along with the presence of sedimentary structures of shallow marine reworking such as cross-bedding and erosive bases. The larger foraminifera association determined within the transgressive strata of Sequence 3 includes *M. cf. mexicana*, *M. cf. gunteri*, and *M. cf. globulina*, belonging to the Aquitanian (Figs. 5; 6).

Sequence 4

Overlying the maximum flooding carbonates of Sequence 3, regressive siliciclastic-influenced strata (Patieitos Fm.) of Sequence 3 were deposited, followed by transgressive platform carbonates (San Luis Fm.) of Sequence 4, and subsequently by regressive siliciclastics (Patieitos Fm.) of Sequence 4 (Fig. 12). Accordingly, the regressive units of sequences 3 and 4 comprise two deltaic successions ranging from 50 to 100m in thickness, characterized by prodelta marls interbedded with coral bioherms passing up into mouth bar sandstones. These siliciclastic units were deposited during Highstand Normal Regressions (HNR) *sensu* Catuneanu *et al.* (2009). Subsequent sea-level drops following these two highstands led to the erosion of delta front and prodelta facies and the deposition of falling-stage submarine fans (see Hunt and Tucker, 1992, 1995), which extended basinwards, interfingering with distal carbonate ramp facies. These forced regressive deposits consist of microconglomerates and sandstones, which often grade into pebbly and sandy skeletal limestones due to an increase in siliciclastic input resulted from the erosion of HNR deltaic facies, and their redeposition within upper ramp settings. Recurrent erosive surfaces, locally overprinted by paleosols with preserved root marks and ferruginous crusts (or laterites), are observed at the top of the HNR deltaic deposits of sequences 3 and 4. These features indicate episodes of subaerial exposure and erosion affecting the subaerially exposed delta front mouth bars and prodelta shale facies.

Sequence 5

A channel incision of 2-3m deep was identified in the HNR delta unit of Sequence 4 associated with the falling-stage systems tract. Succeeding coarsening and shallowing-

upwards delta deposits of 15-20m thick were identified in a basin position and interpreted as Lowstand Normal Regressive (LNR) strata after the onset of regressions of sequences 3 and 4, and downlapping the falling stage submarine fans (Fig. 12). The incised valley cutting through the HNR deposits of Sequence 4 is infilled by transgressive, cross-bedded, tidal sand bars from Sequence 5 (Fig. 13F). Above the erosive surface at the top of the HNR delta wedges lies a transgressive surface, followed by a succession of retrograding shoal skeletal sandstones and sandy limestones, interbedded with bioturbated lagoonal and inner-shelf clays. The skeletal shoal bars contain reworked mollusks, corals, coralline algae, and larger foraminifera, transported onshore from carbonate ramp settings. These bars mark the first transgressive pulses of Sequences 4 and 5. Vertically, the nearshore transgressive deposits transition into massive San Luis ramp carbonates, which interfinger and overlap the retrograding delta facies. Furthermore, the distal HNR delta wedges do not downlap directly above the MFZ. Instead, the prodelta marls transition basinwards into upper ramp facies characterized by coral meadows and middle to lower ramp facies with extensively reworked larger foraminifera and coralline algae.

Sequence 6

The last TR sequence (Sequence 6) recorded a widespread siliciclastic progradation towards the South, marking a major lithological shift following the most extensive development phase of the San Luis carbonate platform towards the North, associated with the MFZ of Sequence 5 (Fig. 12). In the northern sector of the Falcón Basin, the siliciclastic deposits below the MFZ of Sequence 5 correspond to the Patieitos Fm. and display a transgressive character, whereas the siliciclastic unit above it constitutes the Guaraval Fm. and represents a regional progradation.

The larger foraminifera collected in the San Luis carbonate successions in sequences 4, 5, and 6 include *M. cf. Panamensis* and *M. cf. Cushmani* (Aquitanian-Burdigalian complex miogypsinids). In these latter sequences, the Aquitanian miogypsinids present in sequences 2 and 3 disappear (see Figs. 5; 6; and this paper's section on biostratigraphy), thus leading to the dating of sequences 4, 5 and 6 as Burdigalian.

Southern Falcón

In the southern margin of the Falcón Basin, 9 stratigraphic sections of Lower Miocene marine siliciclastics and isolated carbonate banks, varying in thickness from 25 to 730m, were correlated for the sequence-stratigraphic and facies distribution model (Figs. 2; 14). The stratigraphic section represents a Southwest to Northeast oblique-oriented

profile, intersecting two depocentres aligned parallel to the basin's southern edge. These depocentres are formed by two semigrabens, which in turn created two palaeo-highs tilting towards the basin margin and slightly eastward, permitting the development of isolated carbonate banks (Fig. 1). This tectono-sedimentary context aligns with the fault-block carbonate platforms defined by Bosence (2005, 2012) in marine rift basins. The carbonate banks onlap the tilted blocks, transitioning from proximal to distal settings towards the South and East. The limestone units exhibit a Northeast-Southwest elongated shape, ranging between 40 and 50km in length, 5 to 10km in width, and approximately 75m in thickness each (Figs. 1; 9). The correlation criterion used is consistent with that applied in the northern basin margin.

Sequence stratigraphic and facies distribution model shows up to six T-R sequences characterized by episodes of siliciclastic sedimentation alternated with phases of widespread development of platform carbonates (Figs. 4; 14). Similar to observations in the northern portion of the basin, the stratal stacking pattern reflects a general transgressive cycle, punctuated by six smaller-scale T-R sequences. This is evidenced by the deepening-upwards sedimentary pattern, with early continental sedimentation confined to the marginal depocenters (La Danta and Churuguara sub-basins), which then evolves vertically into carbonate and pelagic sedimentation. Furthermore, the onlapping and transgressive nature of the carbonate platforms, followed by subsequent episodes of platform drowning, aligns with a broader transgressive trend.

Sequence 1

The lowermost strata of the Churuguara series unconformably onlap the Eocene Jarillal marls in the La Danta valley (Figs. 2; 14 section 17), and in outcrops eastward of Churuguara (Fig. 2, eastward of section 23). These strata belong to Sequence 1 and are confined to the initially opening semigrabens. In the La Danta sub-basin, they are characterized by a transgressive infilling of estuarine deposits (Fig. IEsF), while in the Churuguara sub-basin, they are marked by retrograding deltaic facies (Fig. IDf), followed by pelagic shales (Fig. IPSF). Simultaneously, the Churuguara high experienced erosion (Figs. 2; 11; 14 sections 19, 20, 21, 22). In the La Danta Sub-Basin, the earliest preserved sediments consist of tidal sand bars composed of quartzarenites exhibiting a shallowing-upwards trend. These were followed by a rapid flooding, resulting in the retrogradation of the mouth bar inland and the overlap of estuarine facies (Fig. IEsF). These drowned valley facies include lagoon shales (Fig. ILS) transitioning upwards and seawards into barrier shoreface sandstones (Fig. IEsMS). Although basal alluvial or fluvial deposits are typically found in an ideal transgressive estuarine

succession (e.g. Dalrymple *et al.*, 1992), they were not identified here. However, the transgressive estuarine strata are exceptionally well preserved, showing no evidence of erosion or reworking by shoreface or tidal processes during the transgression. This preservation likely indicates a rapid increase in accommodation/subsidence, combined with elevated sedimentary inputs relative to the rate of littoral erosion (Dalrymple *et al.*, 1992; Davis and Clifton, 1987; Demarest and Kraft, 1987). Transgressive pulses are characterized by deepening-upwards parasequences of retrogradational estuary mouth sandstones (Fig. IEsMS), followed up by shelf deposits comprised of operculinoid and bivalve-rich rudstones (Fig. IOShF). These shallow marine reworked deposits are interpreted as being transported from upper to middle ramp settings, and overlap transgressive ravinement surfaces. The MFZ of Sequence 1 corresponds to a widespread retrogradation of shoreface sandstones, followed by the accumulation of operculinoid-rich transgressive lag deposits. The onset of regression of Sequence 1 is marked by a change in the stacking pattern, evidenced by the progradation of coastal sand barriers and siliciclastic shoals seawards, culminating in a significant regression of bayhead delta sandstones (Fig. IBDS) that overlie internal lagoon deposits. Contemporaneous sedimentation in the southern Churuguara depocenter is characterized by a rapid retrogradation of continental facies and marine drowning, as indicated by a thick succession of pelagic shales and the absence of carbonate sedimentation. This difference is associated with a major and more rapid subsidence. The latest regression stage in the Churuguara sub-basin is marked by the progradation of deltaic facies.

Sequence 2

The top of Sequence 1 is defined by a generalized regression, marked by an erosive surface or subaerial unconformity characterized by palaeosols and oxidized horizons (Fig. 15A). This extensive regressive event constitutes the limit between sequences 1 and 2. The subaerial unconformity was overprinted by a transgressive ravinement surface, followed by the sedimentation of a deepening-upwards succession of retrograding lagoon and tidal flat shales. Subsequently, wave-reworked bioclastic shoal facies, rich in *Operculinoides*, were deposited (Fig. IOShF OSs). The passage from continental to marine facies is transitional, marked by multiple parasequences with alternations of prograding estuary mouth bar sandstones and retrograding carbonate shoals. These parasequences are limited by several composite surfaces of subaerial unconformities overprinted by transgressive ravinement surfaces (Fig. 15A). Oceanization continued upwards with the establishment of isolated coral patch reef facies over hard substrates of reworked shoal deposits, along with the emplacement of retrograding carbonate ramp strata dominated by echinoderm-rich calcarenites (Fig. IIEF).

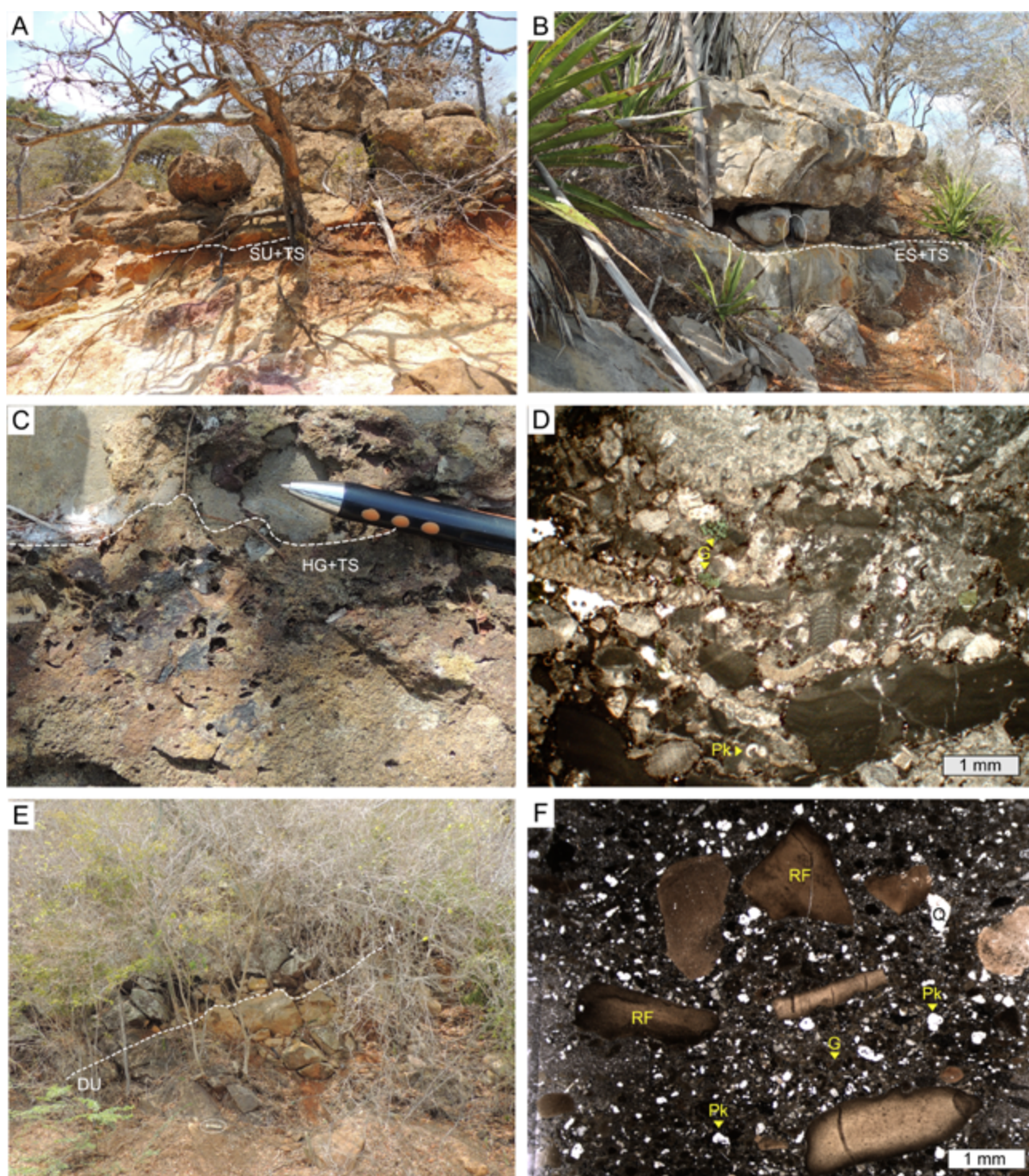


FIGURE 15. Outcrop exposures and microphotographs illustrating key sequence stratigraphic surfaces and transgressive deposits identified in the different stratigraphic sections studied. A) Subaerial unconformity marked by an erosive surface that partially erodes a palaeosol unit and is overlain by transgressive lag deposits of reworked *Operculinoides* and bivalves. B) Subaerial unconformity with local microkarst, overlain by a transgressive surface that separates a lower regressive succession of limestone rich in larger foraminifera and coralline algae-rich from an upper transgressive unit containing reworked bivalves and gastropods. C) Detail of harground surface with bioerosion, overlain by transgressive lag deposits. D) Condensed section associated with a maximum flooding zone, characterized by highly reworked oligophotic skeletal fragments, as well as glauconite and pelagic fauna. E) Drowning unconformity marking a change from carbonate to pelagic shale sedimentation. F) Transgressive pelagic microfacies located above the drowning unconformity, rich in mud-clasts, glauconite and planktonic foraminifera. G= glauconite, Pk= planktonic foraminifera, Q= quartz, RF= rock fragments constituted by mud clasts.

Echinoid calcarenites transition upwards and basinwards into middle and lower ramp coralline algal and larger foraminifera debris (Fig. IICADF, LF). In a distal setting, towards the NE, deepening-upwards oligophotic carbonate ramp parasequences are constituted by reworked coralline algae with nummulitids, heterosteginids, and miogypsinids (Fig. IICADF) passing up to lepidocyclinid rudstones with pelagic foraminifera and glauconite (Fig. IILF). The parasequences are topped by hardground surfaces (Fig. 15C), which are overlain by pelagic shales rich in glauconite (Fig. 15F). Drowning unconformities (Fig. 15E) correlate landwards, in hydrodynamic shallower settings, with condensed sections (Fig. 15D) and transgressive ravinement surfaces (Fig. 15A, B). Regressive strata of Sequence 2 represent a rapid and extensive progradation of transitional and shallow marine facies belts towards the basin. This rapid and vast regressive pulse is evidenced by the deposition of tidal flats and mollusc-rich shoals (Fig. IIMShS) over the carbonate ramp facies. Simultaneously, the carbonate ramp shifted basinwards, overlaying the transgressive marls. The larger foraminiferal association identified in the ramp carbonates of TR sequence 2 corresponds to the Aquitanian age, represented by *M. cf. mexicana*, *M. cf. gunteri*, and *M. cf. cushmani* (Figs. 5; 7).

Sequence 3

Sequence 3 marks a significant rise in relative sea level and a shift in sedimentation from ramp carbonates to fine-grained siliciclastics. The transgressive stage begins with retrograding carbonate ramp deposits, which are capped by a drowning unconformity (Fig. 15E) characterized by local hardground development (Fig. 15C), and are overlain by transgressive deeper pelagic marls rich in glauconite that contain mudstone intraclasts (Fig. 15F). Early regressive deposits of Sequence 3 consist of glauconite turbidites with abundant pelagic foraminifera (Figs. 10; 14; 16).

Although autochthonous glauconite accumulations have been reported in deep-oceanic environments, the formation of glauconite is generally assumed to occur under low sedimentation rates within continental shelf or carbonate platform environments (Amorosi, 1995, 1997; Odin and Fullagar, 1988; Velde, 2014). The sedimentological and maturity attributes of glauconite deposits are used to determine their autochthonous or allochthonous character (Amorosi, 1995). According to Amorosi (1997), allochthonous glauconitic sands can occur as thick beds, usually exhibiting high grain roundness and good sorting, with no linkage to phosphate and biogenic structures, along with other sedimentological evidence of transport. In this regard, the glauconite deposits of Sequence 3 consist of 5 to 10m-thick beds of well-sorted glauconite grains intermixed with slightly reworked skeletal grains (mostly planktonic foraminifera), displaying erosive

bases and sedimentological gradations. These facies are interpreted as allochthonous or detrital glauconite deposits transported from the epicontinental drowned shelf during early regression stages (Fig. 16). Regressive strata evolve upwards into a wide prograding siliciclastic deltaic wedge consisting of a coarsening upwards succession of delta front marls interbedded with thin, fine-grained sandstones transitioning vertically to distal shoreface bars with gastropods and bivalves and proximal mouth bars and beach sands (Figs. IPS; DFS; 14). The top of sequence 3 corresponds to a locally eroded subaerial unconformity, characterized by oxidized horizons linked to palaeosol development, overlain by a transgressive surface. The sequence boundary correlates basinwards with a correlative conformity (*sensu* Posamentier and Vail, 1988) marking the top of submerged deltaic shoreface and delta front.

Sequence 4

Sequence 4 begins with an early transgressive succession consisting of retrograding fine-grained siliciclastics and interbedded shallow marine glauconitic sands (Figs. ISMGF; 10; 14; 16). These facies were deposited in an inner shelf environment with very low siliciclastic inputs, predominantly associated with open marine tidal flats. The transgressive glauconitic sandstones exhibit abundant bioturbation, fragments of gastropods and bivalves, as well as cross laminations and ripple marks. The sedimentary features observed suggest that these deposits correspond to parautochthonous glauconitic subtidal or intertidal bars, and that glauconite was likely transported landwards from distal ramp settings (Fig. 16). In this case, the main source of sediments is not continental; instead, they originated from marine authigenic processes and were redeposited in shallower settings due to rising sea level. The significant amount of resedimented glauconite indicates prolonged periods of siliciclastic starvation, minimal carbonate production, and extended flooding of the continental platform. Tidal flat deposits transition upwards and basinwards into retrograding condensed carbonate successions (Fig. 15D) of branching coral carpets, rhodolith pavements and reworked larger foraminifera and coralline algae debris. These deposits made up upper to middle ramp carbonate parasequences, and are characterized by elevated degrees of fragmentation, bioerosion, and encrustation of skeletal grains, along with sporadic occurrences of phosphatized grains and glauconite. The occurrence of recurrent hardgrounds within the carbonate succession (Fig. 15C) indicates interruptions in carbonate production, likely caused by phases of downing. In the distal parts, middle ramp facies interfinger with retrograding units of reworked *Lepidocyclina*, *Operculinoides*, coralline algae, and planktonic foraminifera rudstones associated with oligophotic environments. These facies occur organized in coarsening-upwards sets of resedimented skeletal

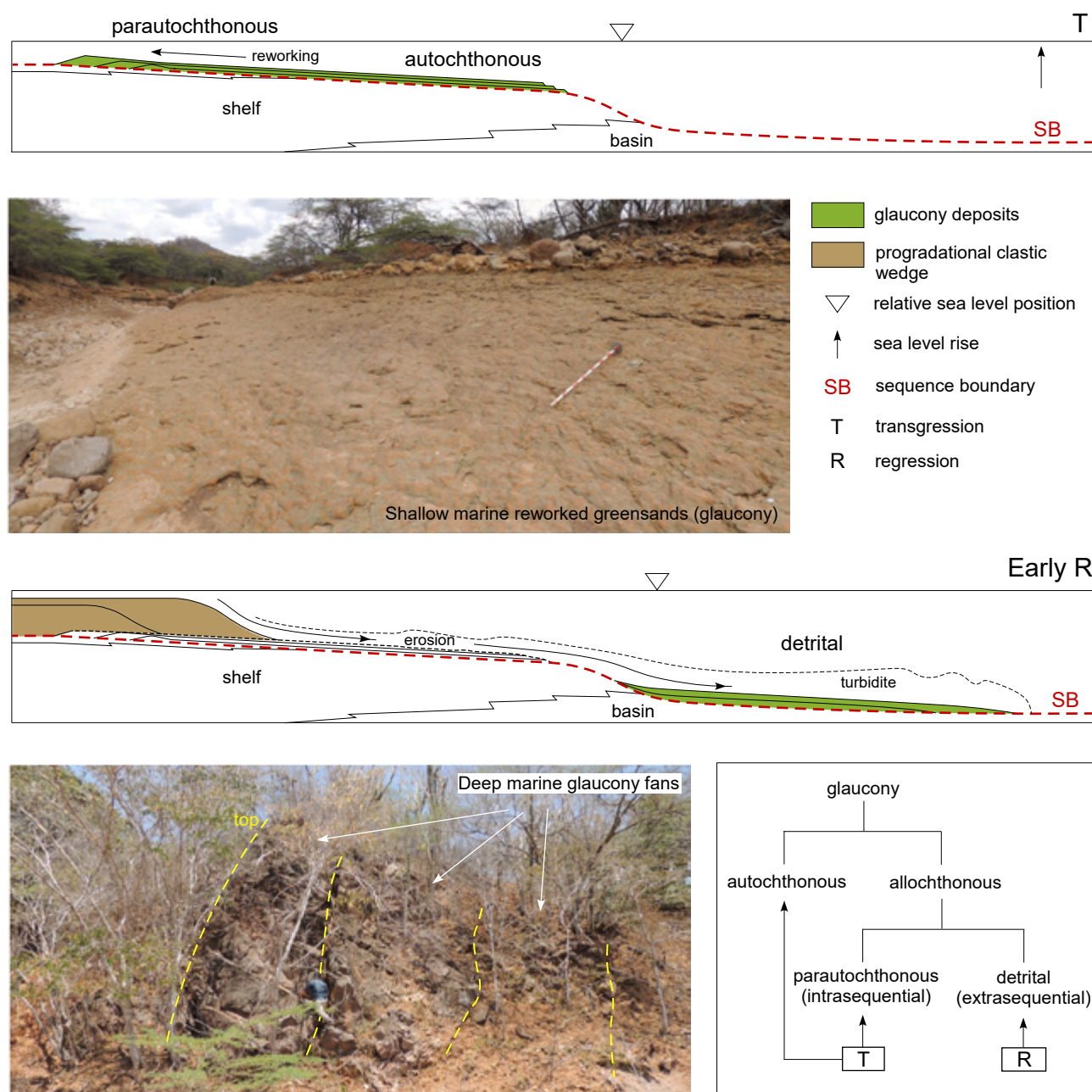


FIGURE 16. Conceptual sequence stratigraphic model of autochthonous and allochthonous glauconite deposits of the Churuguara Fm. (southern Falcón Basin) based on the relative sea-level position. The sequence stratigraphic model deduced for the Churuguara siliciclastic systems is consistent with that proposed by Amorosi (1991). Upper images: Outcrop view of shallow marine glauconitic sandstones showing an exposed bedding surface with interference ripple marks. The associated microfacies include shallow marine skeletal grains, detrital grains of quartz and feldspars, parautochthonous glauconite grains, and a clay-rich matrix. Lower images: Outcrop view of glauconite turbidite deposits, with the associated microfacies made up of detrital glauconite grains intermixed with pelagic foraminifera and a clay to marl matrix. The white scale bar is 1mm. The Jakob bar is 1.5m.

fragments, interpreted as fore-ramp debris. The regressive unit of Sequence 4 is recognized by a quick progradation of the delta front wedge passing seawards to upper ramp facies, characterized by a widespread proliferation of branching coral meadows. The larger foraminifera association identified in the carbonate ramp deposits of Sequence 4 are

dated to the Burdigalian, based on the sole occurrence of *M. cf. panamensis* and the absence of Aquitanian fauna (see Figs. 5; 6 and the above section on biostratigraphy). The abundance of phosphatic hardgrounds is consistent with the global phosphogenesis cycles of the Burdigalian-Langhian (Follmi *et al.*, 2008). This high nutrient

availability is also linked to the onset of the Monterey Event in the Burdigalian-Langhian period of the central Mediterranean area. This event is usually associated with increased phosphatic deposition during the Mid-Miocene Climatic Optimum, between 17 and 13.5 million years ago (Brandano *et al.*, 2016).

Sequences 5 and 6

Transgressive lag facies deposited above the transgressive surface that bounds sequences 4 and 5 marks a second drowning event affecting the Burdigalian carbonate ramp of the Churuguara Fm. The subsequent T-R sequences 5 and 6 represent a second phase of deeper marine sedimentation with alternating transgressive successions of pelagic shales that transition landwards into glauconite-rich continental tidal flats. This is followed by regressive deposits characterized by prograding deltas that evolve basinwards to detrital glauconitic turbidites (Figs. 10; 14; 16).

QUANTITATIVE SUBSIDENCE ANALYSIS

The tectonic evolution of the northern and southern Falcón Basin was controlled by marginal subsident blocks adjacent to a central graben, limited by ENE-WSW normal faults (see Fig. 1), which were reactivated as thrust faults in the Middle Miocene (see Figs. 2; 3; Albert-Villanueva *et al.*, 2017). The accommodation history was investigated by comparing quantitative subsidence models located at both basin margins: one situated in the northern San Luis marginal platform and two in the southern La Danta and Churuguara depocenters. The 1D subsidence curves are illustrated in Figure 17. Input data for subsidence models were derived from the high-resolution stratigraphic logs depicted in the sequence stratigraphic and facies distribution panels (see Figs. 12; 14). Petrophysical and geochemical parameters, which define the lithological properties attributed to the geological strata, are predefined within the PetroMod database. Eroded thicknesses were estimated by subtracting input stratigraphic sections from maximum stratigraphic thickness values obtained from various sources, including measured sections in the field, stratigraphic depths reported in the literature (Díaz de Gamero, 1977; González de Juana *et al.*, 1980), and isopach maps of sedimentary widths in the Falcón Basin (Macellari, 1987, 1995). Age constraints for depositional and erosional events were established using the larger foraminifera biostratigraphy presented in this study (see Fig. 6), combined with planktonic foraminifera associations described for the lithostratigraphic formations in the Falcón Basin (Díaz de Gamero, 1977, 1989).

The tectonic evolution of the northern Falcón Basin is characterized by a subsidence period spanning from

the latest Chattian to the end of the Burdigalian, and an inversion phase extending beyond the Langhian. The initial extensive episode exhibits a step-like subsidence pattern characterized by repeated short periods of accelerated and decelerated subsidence, culminating in a final accelerated subsidence pulse during the latest Burdigalian. Total subsidence is estimated to be about 880m over a period of approximately 8Myr (with an average rate of 110m/Myr), driven exclusively by tectonic processes. The subsequent Langhian uplift abruptly halted the tectonic extension, and caused the inversion of previously extensional faults. No evidence of thermal subsidence was recognized.

The tectonism in the southern part of the basin follows a similar pattern to that observed in the North, characterized by a brief, rapid phase of accelerated tectonic subsidence from the late Chattian to the end of the Burdigalian, which was abruptly interrupted by a generalized tectonic inversion starting in the Langhian. Total subsidence is approximately 1475m in the La Danta sub-basin and 1700m in the Churuguara sub-basin, occurring over a period of 7 to 8Myr. The total accumulated accommodation and subsidence rate are significantly greater in the South compared to the North, with the southern rates nearly doubling those in the North, averaging 210m/Myr. This discrepancy is attributed to a North-dipping, low-angle detachment level (Albert-Villanueva *et al.*, 2017; Baquero *et al.*, 2009), which generated an asymmetrical rift characterized by synthetic, southwards tilted rollovers or rotational blocks in the southern La Danta and Churuguara sub-basins (Fig. 1). These blocks experienced greater displacement due to the combined effects of rotation and vertical subsidence. In contrast, the northern region is dominated by antithetic fault blocks primarily affected by vertical net displacements (San Luis platform; Fig. 1), with minimal rotation, resulting in lower total accommodation values (Albert-Villanueva *et al.*, 2017).

ONSHORE-OFFSHORE COMPARISON OF OLIGOCENE-LOWER MIOCENE PLATFORM CARBONATES

The sedimentary evolution of the onshore tectonically-inverted Falcón Basin, and the offshore Perla carbonate reservoir (Gulf of Venezuela) during the Oligocene-Early Miocene, resulted from the interaction of various local, regional, and global factors influencing sedimentation rates (including siliciclastic inputs, carbonate production, and sediment redistribution), accommodation, depositional geometry of carbonate and siliciclastic bodies, and the location of major depocenters. These factors include biological evolution and ecological needs of carbonate producers, climatic fluctuations and their environmental impacts, eustatic variations, palaeogeography, and tectonic context (Fig. 18).

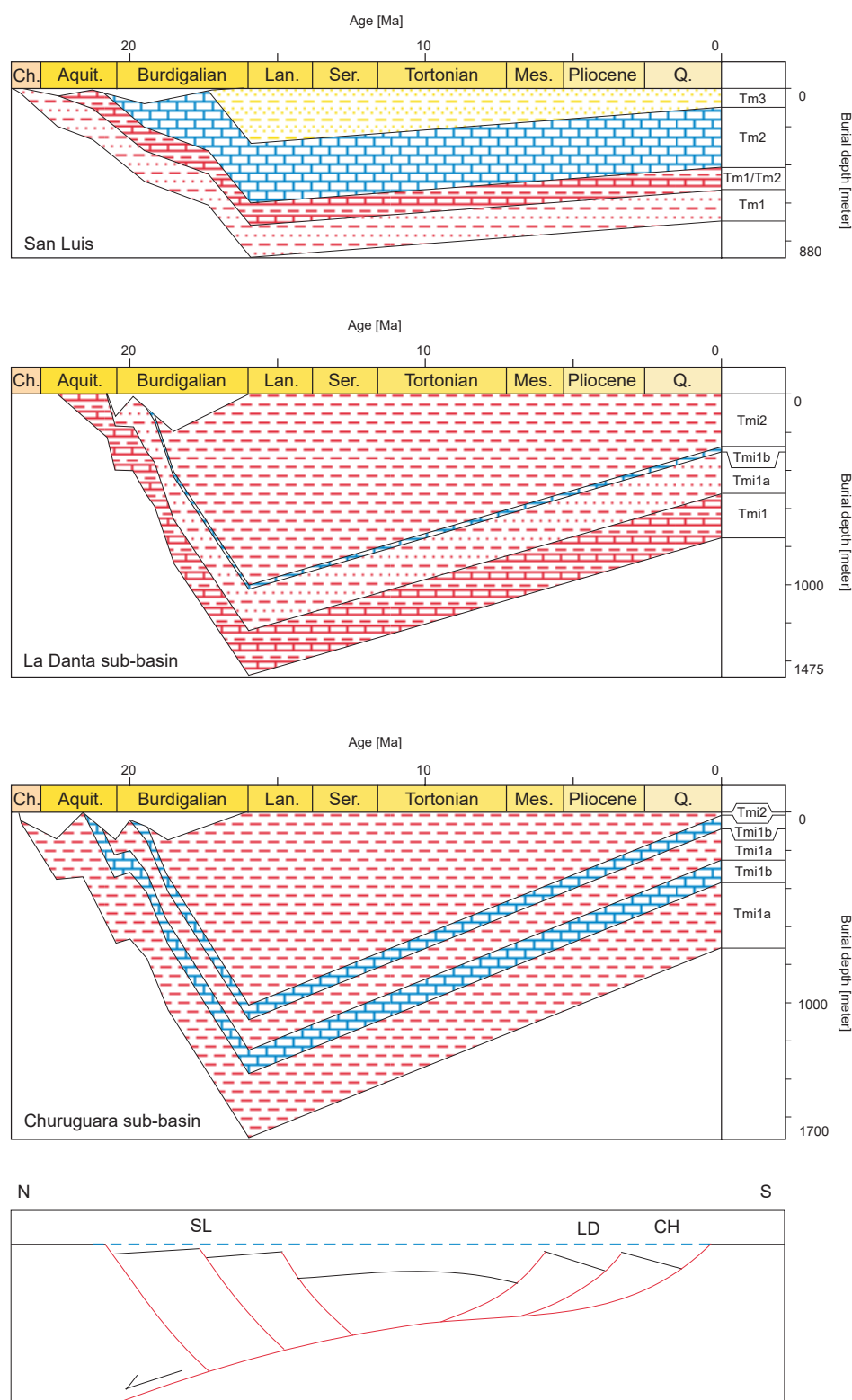


FIGURE 17. Simplified 1D subsidence models of northern and southern Falcón Basin, illustrating the incremental total accommodation in the different studied sections and their location in a N-S restituted cross-section (see Fig. 1 for map location). The total subsidence curves have been decompacted and palaeobathymetrically corrected. Absolute ages are sourced from [Gradstein *et al.* \(2012\)](#). Lithological units indicated include: Tm1 = Patiecitos Fm. (shales and sandstones), Tm2= San Luis Fm. (carbonates), Tm3= Guarabal Fm. (sandstones and shales), Tmi1= Churuguara Fm. (shales, sandstones and carbonates), Tmi1a= Carbonates of Churuguara Fm., Tmi1b= Siliciclastics of Churuguara Fm. (shales and sandstones), Tmi2= Agua Clara Fm (shales). See [Figures 2, 3, 4](#) for more detailed geological and stratigraphical information. SL= San Luis, LD= La Danta, CH= Churuguara.

According to Pomar *et al.* (2015), the carbonate successions of the Perla field are characterized by high-quality reservoir attributes, primarily due to the presence of poorly cemented rudstone-sized carbonate components resulting in elevated inter- and intragranular primary porosity, along with secondary moldic and matrix-dissolution microporosity (Pomar *et al.*, 2015). On the other hand, Valencia and Laya (2020) identified deep burial dissolution as the main diagenetic process responsible for creating pervasive microporosity in the Perla Limestone, supplemented by subordinated moldic and vuggy pores. However, the onshore equivalent carbonates of the San Luis and Churuguara fms. within the Falcón Basin are highly recrystallized and cemented. These onshore counterparts of the Perla reservoir exhibit a very low preservation of original porosity, occluded by shallow diagenetic processes during burial, tectonic inversion and exhumation.

Pomar *et al.* (2015) present a sequence stratigraphic model of the Perla field carbonate succession based on the analysis of well core samples and seismic data. In this study, the authors identified 13 high-frequency TR sequences grouped into 3 larger-scale transgressive-dominated cycles, which were deposited between the upper Chattian and Burdigalian stages (Fig. 18). The authors note that the low resolution of biostratigraphic data impedes precise determination of sequence periodicity. However, using the absolute ages determined by Pinto *et al.* (2014) at 3 levels of the Perla-1X well, the temporal extent of these sequences can be roughly estimated. The particular configuration of the basement, arranged in step-like semigrabens, and the equilibrium conditions between the increasing accommodation and the carbonate production rate, permitted the development of thick transgressive backstepping carbonate wedges (Fig. 19) dominated by low dense and highly-porous rhodoliths and larger foraminifera facies deposited in middle to outer ramp settings.

Similar to the Perla carbonate successions, the time span of the six TR sequences identified in the northern and southern Falcón Basin is shorter than the age resolution determined by larger foraminifera biostratigraphy. Despite this, the precise location of the Aquitanian-Burdigalian limit within the carbonate successions, based on the distribution of age diagnostic miogypsinid species, and the age boundaries of marls and siliciclastic units overlying the studied carbonate successions, based on planktonic foraminifera biostratigraphy by Diaz de Gamero (1977, 1989), permitted to estimate the duration of these sea-level fluctuations (Fig. 19). In this regard, the duration of TR sequences in the northern and southern Falcón Basin ranges from 0.5 to 2.5Myr, corresponding to the third-order sedimentary cycles described by Vail *et al.* (1991).

The Early Miocene was characterized by high-frequency sea-level fluctuations within the Falcón Basin

and marginal parts of Urumaco trough (Perla Carbonates) (Figs. 1; 19). This high frequency has been also observed in global eustatic sequencing (Abreu and Anderson, 1998; Haq *et al.*, 1987), and is associated with a period of high climatic variability between the late Oligocene and the climatic optimum of the Middle Miocene, characterized by relatively warm episodes interrupted by brief glacial periods (*i.e.* Miocene Aquitanian (MAi) and Miocene Burdigalian (MBi) events; Fig. 19) (Abreu and Anderson, 1998; Zachos *et al.*, 2001). The third-order TR sequences recognized in the Perla, San Luis, and Churuguara successions are likely decoupled by differences in accommodation rates, driven by differential tectonic subsidence at the three compared sites. However, two correlative and regional regressive events recorded in the Falcón Basin and the Perla Field coincide in time with the glaciations MAi-2 and MBi-1, indicating the influence of global eustasy at a regional level. More locally, the MAi-1 glaciation is correlated with a maximum regression in Perla and San Luis, MAi-3 coincides with a major regressive event in Perla and Churuguara, and the MBi-2 and MBi-3 icehouse events can be correlated with regional sequence boundaries in the Falcón Basin (San Luis and Churuguara fms.).

Regarding the accommodation history, a generally linear and rapid increase was recorded in the three sectors analyzed (Figs. 17; 18). This accelerated increase in accommodation is interpreted to have been primarily controlled by rapid subsidence in both the Falcón Basin (San Luis and Churuguara) and the Urumaco trough (Perla). This period of rapid subsidence coincides with the extensive regional episode (TR sequence C1 of Macellari 1987, 1995; Fig. 4) that affected the southwestern Caribbean margin during the Oligocene to Early Miocene.

The mixed carbonate-siliciclastic systems of San Luis and Churuguara are characterized by a general aggradational trend, while the Perla carbonates were interpreted by Pomar *et al.* (2015) as a retrogradational unit deposited during a second-order transgressive episode (Fig. 19). This would indicate that in Perla, the increase of accommodation clearly outpaced the sedimentation rate, whereas in San Luis and Churuguara, they were more balanced. A plausible explanation for this difference is that Perla experienced faster subsidence during the Early Miocene than San Luis and Churuguara. Alternatively, it could result from higher sedimentary rates in San Luis and Churuguara, driven by siliciclastic discharges, in contrast to Perla, where the terrigenous influx was much lower.

Similar to the case of the mixed carbonate-siliciclastic systems of San Luis and Churuguara, the Perla carbonate reservoir exhibits a distally steepened ramp depositional profile, formed in a broadly transgressive context and mainly consisting of mid- to outer ramp carbonates dominated

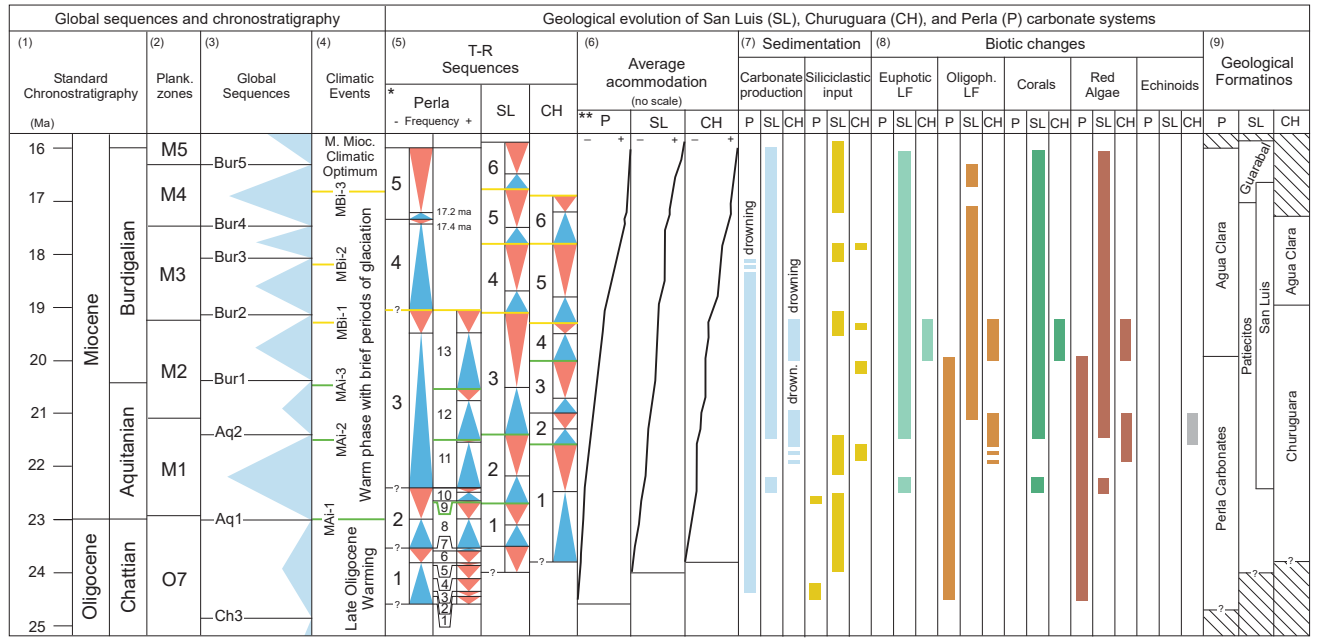


FIGURE 18. Synthetic chart comparing the chronostratigraphy of the Late Oligocene-Early Miocene, the main global climatic events, and the evolution of the carbonate systems of Perla (P), San Luis (SL) and Churuguara (CH). (1) Standard chronostratigraphy from [Gradstein et al. \(2012\)](#). (2) Tropical planktonic foraminifera zones ([Gradstein et al., 2012](#)). (3) High-frequency global eustatic curve by [Haq et al. \(1987\)](#), corrected with using the isotopic curve of [Abreu and Anderson \(1998\)](#). (4) Major global climatic events ([Abreu and Anderson, 1998](#); [Zachos et al., 2001](#)). (5) Third-order transgressive-regressive sequences (3-0.5Myr) observed in the studied sections. (6) Curves of cumulative accommodation variation for each studied zone. (7) Siliciclastic and carbonate sedimentary events across the different parts of studied basins. (8) Major biotic changes for the three studied zones. (9) Lithostratigraphy of each sector. Information regarding the Perla reservoir has been obtained from [Pinto et al. \(2014\)](#) and [Pomar et al. \(2015\)](#).

by red algae and larger foraminifera ([Pomar et al., 2015](#)). However, the thickness, spatial extent, and sedimentary architecture of the Perla reservoir differ significantly from the carbonate systems studied here due to variations in tectonic and palaeotopographic settings, accommodation and sedimentation rates, and interactions with marginal siliciclastic systems ([Fig. 19](#)). Accordingly, the sedimentary architecture of carbonate reservoirs in this region cannot be predicted using a generalized depositional model.

CONCLUSIONS

The mixed carbonate-siliciclastic systems studied were deposited in tropical seas during the Early Miocene, and exhibit very similar facies associations to age-equivalent deposits described in the Caribbean, Tethys and Indo-Pacific realms. They are characterized by carbonate ramps dominated by larger foraminifera and coralline algae.

The biostratigraphic study of larger foraminifera associations has dated the carbonate strata cropping out in the Falcón Basin to the Early Miocene, revising the previously assigned age of Oligocene-Early Miocene ([Johnson, 2009](#); [Macellari, 1995](#); [Pomar et al., 2015](#); [Wheeler, 1963](#)). Age determinations based on planktonic

foraminifera by [Díaz de Gamero \(1977\)](#) also placed these carbonate successions within the Early Miocene, in agreement with the present study. The key age-diagnostic larger foraminifera species, first appearing in the Caribbean Benthic Zone F1 (sensu [Butterlin, 1981](#)), are *Miosorites americanus* and *Annulosorites spiralis*. Additionally, the analysis of miogypsinids distinguishes two age-diagnostic associations respectively belonging to the Aquitanian and Burdigalian stages.

Autochthonous carbonate deposits are represented by coral colonies in growth position, usually forming coral mounds embedded within deltaic facies, or as sparse colonies or small bioherms in upper ramp settings. These scleractinian communities, instead of forming well-developed frameworks resistant to waves as seen in modern tropical seas, gave rise to meadows developed in prodelta environments and carbonate ramp settings situated below the fair-weather wave base.

The depositional geometries identified consist of distally steepened ramps or undifferentiated carbonate ramps, characterized by open marine conditions without barriers or bounding margins. This geometry is influenced by a carbonate factory, with sediments accumulating as rudstone to packstone textures, dominated by coralline algae and larger foraminifera,

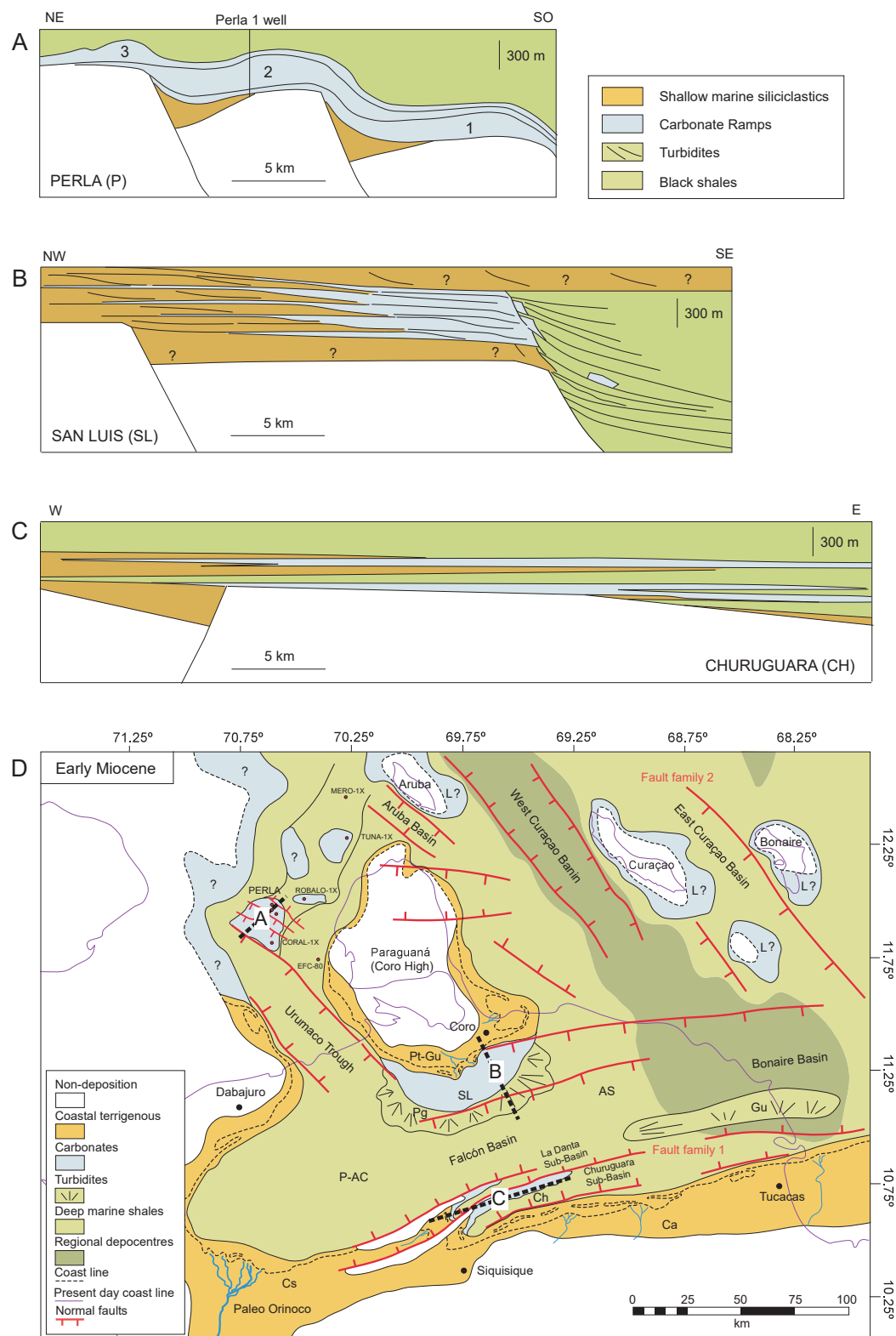


FIGURE 19. Comparison of the depositional geometries of Lower Miocene carbonates from A) Perla, and mixed carbonate-siliciclastic deposits from B) San Luis and C) Churuguara. The depositional architecture of the Perla carbonates, which unconformably overlie a granitic basement and synrift siliciclastic deposits, is based on interpretations derived from seismic and borehole data provided by Benkovics *et al.* (2012). The depositional architecture of the San Luis and Churuguara platform carbonates is based on conceptual models derived from reconstructions and correlations of outcrop line drawings and sequence stratigraphic interpretations. D) Early Miocene palaeogeography of the ENE-WSW trending Falcon back-arc basin and related NW-SE trending Caribbean pull-apart basins, including the locations of the three cross-sections corresponding to the Perla, San Luis, and Churuguara depositional systems. A) and B) sections are dip-oriented, while C) is strike-oriented.

set within a micritic matrix. Both inter- and intragranular porosity are generally low, often filled with micrite or cement. The platform's architectural configuration allowed for the sediment remobilization and partial homogenization, being transported from proximal to distal ramp settings during regressive phases, and from distal environments towards onshore areas during transgressions. Although the lateral facies variations are transitional, some depth-related zonation of skeletal components is still preserved.

The sedimentary record preserved on the northern and southern margins of the Falcón Basin exhibits a high-frequency stratigraphic cyclicity related to relative sea-level variations. This cyclicity is a response to the combined effects of eustatic fluctuations and tectonic activity in the region during the Early Miocene. The T-R sequences appear to be decoupled in the two studied sectors of the basin, potentially associated to differences in subsidence rates. Furthermore, the duration of the relative sea-level changes in the studied sections is shorter than the age constraints determined by the larger foraminifera biostratigraphy. Thus, T-R sequences 1 to 3 in the southern carbonate successions, along with T-R sequences 1 and 2 and the transgressive part of Sequence 3 from the northern carbonate series, are ascribed to the Aquitanian. On the other hand, the regressive part of Sequence 3 in San Luis, along with sequences 4 to 6 in both Churuguara and San Luis, belong to the Burdigalian.

Synrift-type subsidence was the main mechanism for generating accommodation during the Oligocene-Early Miocene in the Falcón Basin and its associated sub-basins. On the basin margins, a period of accelerated subsidence occurred between the Aquitanian and Burdigalian. From the Middle Miocene onwards, a change in tectonic regime resulted in the inversion of the Falcón Basin, with no thermal postrift subsidence phase recorded. While tectonic subsidence likely played a significant role in controlling relative sea-level variations, it did not completely obscure the global eustatic signal. Despite the limited resolution of the biostratigraphic data, a correlation exists between the global eustatic sequences reported in the literature and the cyclic relative sea level patterns recognized in the San Luis, Churuguara, and Perla successions.

Except for localized echinoid proliferation during the Aquitanian and the regional shift in myogypsinid species marking the Aquitanian-Burdigalian boundary, no significant biotic changes were observed in the carbonate-producing biota of this region in the Caribbean during the Early Miocene. The transition from the Chattian climatic optimum and the Early Miocene epoch of high climatic fluctuation, characterized by warm conditions interrupted by brief glacial intervals, is reflected in the Falcón Basin through short periods of increased terrigenous input driven by regional regressive pulses. The MAi-2 and MBI-1

glaciations coincide with two regional major regressions recorded in Perla, San Luis and Churuguara. In the Falcón Basin, these regressions are evidenced by the presence of incised erosive scars ranging in depth from 2 to 7m.

Although the carbonate-producing communities and platform profiles, represented by distally steepened ramps, are equivalent in onshore and offshore areas, notable differences in facies belts and sedimentary architecture caused by tectonic and palaeogeographic differences make the studied carbonate successions onshore of the Gulf of Venezuela non-analogous to the offshore Perla reservoir.

In this regard, the carbonate deposits of the Perla reservoir are dominated by unusually thick successions of rhodolith- and lepidocyclinid-rich limestones deposited in a middle to outer ramp settings. These carbonate deposits are interpreted to have been driven by long-term transgressive events that generated three backstepped carbonate wedges, situated away from siliciclastic sources. In the northern Falcón Basin, prograding deltaic systems mixed with carbonate ramp deposits, leading to the proliferation of coral communities, which thrived in turbid waters. On the other hand, middle to lower ramp facies in San Luis and Churuguara are characterized by reworked and fragmented larger foraminifera and red algae. In the Falcón Basin, the transgressive Perla-like facies are quite limited, occurring primarily as thin transgressive lag deposits.

The southern Falcón Basin recorded two brief episodes of carbonate sedimentation, represented by two drowned-carbonate banks interbedded within pelagic marls and turbidites, associated with marginal basin palaeohighs during the Aquitanian and Burdigalian stages. The lowermost Aquitanian unit recorded a transgressive phase and is characterized by symbiont-bearing benthic foraminifera deposited as extensively reworked shoal lags. These deposits are overlain by well-cemented calcarenites rich in echinoids. The proliferation of echinoid-bearing facies is probably the result of local palaeoenvironmental factors. In contrast, the Burdigalian carbonate bank includes transgressive strata of middle to lower ramp Perla-like facies, where primary porosity is occluded. However, the limited lateral extent and reduced thickness of these carbonate ramps are not comparable to the contemporaneous Perla successions. The restricted dimensions of the basement highs constrained the development of Churuguara carbonate ramps, which were unable to keep pace with the increasing accommodation driven by the tectonic subsidence.

ACKNOWLEDGMENTS

We thank Repsol Exploración S.A., the Grup de Recerca Reconegut per la Generalitat de Catalunya 2021 SGR-Cat 00349

“Geologia Sedimentària”, and the I + D + i research project IBERINSULA (PID2020-113912GB-I00), funded by MCIN/AEI/10.13039/501100011033 and the European Regional Development Fund (ERDF) for financial support. We specially thank Dr. Carlos Macellari, the original promoter of this research initiative, and recognize the dedication and personal interest he invested in it. We also appreciate the field and scientific support provided by Dr. José Fernández Carmona, Dra. Olga Rey, Bibiana Rubio, Albert Asensio, David Mendi and Dr. Franck Audemard. A grateful acknowledgment is also extended to the UCV staff and students, as well as the INPARQUES workers and volunteers in Falcón who provided logistical support during fieldwork campaigns and laboratory sessions. Deep gratitude to Mrs. Josefina and Mr. Tito of the Posada Bosquetito for their warm hospitality and the gracious, familial care extended to us during our stays. A special mention is made in memory of Mr. Tito, who has passed away and had a deep appreciation for fine Cocuy, which we shared together on several occasions. We thank Dr. Julio Aguirre for reviewing several sections of a first draft of the manuscript. We also acknowledge the final revisions provided by Dr. Laura Tomasetti, Dr. Arnaud Gallois and an anonymous reviewer.

REFERENCES

- Abreu, V.S., Anderson, J.B., 1998. Glacial eustasy during the Cenozoic; sequence stratigraphic implications. *American Association of Petroleum Geologists (AAPG) Bulletin*, 82(7), 1385-1400.
- Adey, W.H., Townsend, R., Boykins, W., 1982. The crustose coralline algae of the Hawaiian Islands. *Smithsonian Contributions to the Marine Sciences*, 15, 1-74.
- Aguirre, J., Braga, J.C., Bassi, D., 2017. Rhodoliths and Rhodolith Beds in the Rock Record. In: Risomena-Rodriguez, M., Nelson, W., Aguirre, J. (eds.). *Rhodolith/Maërl Beds: A Global Perspective*. Coastal Research Library, 15, 105-138.
- Aigner, T., 1983. Facies and origin of nummulitic build-ups: an example from the Giza Pyramids Plateau (Middle Eocene, Egypt). *Neues Jahrbuch für Geologie und Paläontologie*, 166, 347-368.
- Albert-Villanueva, E., 2016. Facies y secuencias deposicionales mixtas carbonático-siliciclásticas del Mioceno inferior de la Cuenca de Falcón (noroeste de Venezuela) como modelo exploratorio en el Caribe. Ph.D. dissertation thesis. Barcelona, University of Barcelona, unpublished, 312pp.
- Albert-Villanueva, E., González, L., Bover-Arnal, T., Ferràndez-Cañadell, C., Esteban, M., Fernández-Carmona, J., Calvo, R., Salas, R., 2017. Geology of the Falcón Basin (NW Venezuela). *Journal of Maps*, 13(2), 491-501.
- Albert-Villanueva, E., Bover-Arnal, T., Ferràndez-Cañadell, C., Salas, R., 2019. Comment on “Tectonic and environmental factors controlling on the evolution of Oligo-Miocene shallow marine carbonate factories along a tropical SE Circum-Caribbean” by Silva-Tamayo *et al.* (2017). *Journal of South American Earth Sciences*, 91, 394-396.
- Alexander, J., 1989. Delta or coastal plain? With an example of the controversy from the Middle Jurassic of Yorkshire. In: Whateley, M.K.G., Pickering, K.T. (eds.). *Deltas. Sites and Traps for Fossil Fuels*. London, The Geological Society, 41 (Special Publications), 11-19.
- Amorosi, A., 1995. Glaucony and sequence stratigraphy: A conceptual framework of distribution in siliciclastic sequences. *Journal of Sedimentary Research*, 65(4b), 419-425.
- Amorosi, A., 1997. Detecting compositional, spatial, and temporal attributes of glaucony: a tool for provenance research. *Sedimentary Geology*, 109, 135-153.
- Arni, P., 1965. L'évolution des Nummulitinae en tant que facteur de modification des dépôts littoraux. Paris, Mémoires du Bureau de Recherches Géologiques et Minières (BRGM), 32, 7-20.
- Audemard, F., 1995. Evolution geodynamique de la facade nord Sud-Americaine: nouveaux apports de l'histoire geologique du bassin de Falcón, Venezuela. Port of Spain, Trinidad and Tobago, XIV Caribbean Geological Conference, 2, 327-340.
- Banerjee, A., Yemane, K., Johnson, A.H., 2000. Foraminiferal biostratigraphy of Late Oligocene-Miocene reefal carbonates in southwestern Puerto Rico. *Micropaleontology*, 46(4), 327-342.
- Baquero, M., Acosta, J., Kassabji, E., Zamora, J., Sousa, J.C., Rodríguez, J., Grobas, J., Melo, L., Schneider, F., 2009. Polyphase development of the Falcón Basin in northwestern Venezuela: implications for oil generation. In: James, K.H., Pindell, J.L. (eds.). *The Origin and Evolution of the Caribbean Plate*. London, The Geological Society, 328 (Special Publications), 587-612.
- Bassant, P., van Buchem, F., Strasser, A., Lomando, A., 2004. A comparison of two early Miocene carbonate margins: The Zhujiang carbonate platform (subsurface, South China Sea) and the Piring Platform (outcrop, southern Turkey). In: Grammer, G.M., “Mitch” Harris, P.M., Eberli, G.P. (eds.). *Integration of outcrop and modern analogs in reservoir modeling*. American Association of Petroleum Geologists Memoir, 80, 153-170.
- Bassant, P., Van Buchem, F.S.P., Strasser, A., Gorur, N., 2005. The stratigraphic architecture and evolution of the Burdigalian carbonate-siliciclastic sedimentary systems of the Mut Basin, Turkey. *Sedimentary Geology*, 173, 187-232.
- Bassi, D., Nebelsick, J.H., 2010. Components, facies and ramps: Redefining Upper Oligocene shallow water carbonates using coralline red algae and larger foraminifera (Venetian area, northeast Italy). *Palaeogeography, Palaeoclimatology, Palaeoecology*, 295, 258-280.
- Bassi, D., Nebelsick, J.H., Puga-Bernabéu, Á., Luciani, V., 2013. Middle Eocene Nummulites and their offshore re-deposition: a case study from the middle Eocene of the Venetian area, northeastern Italy. *Sedimentary Geology*, 297, 1-15.
- Beavington-Penney, S.J., 2004. Analysis of the Effects of Abrasion on the Test of Palaeonummulites venosus: Implications for the Origin of Nummulithoclastic Sediments. *Palaaios*, 19, 143-155.

- Beavington-Penney, S.J., Racey, A., 2004. Ecology of extant nummulitids and other larger benthic foraminifera: applications in palaeoenvironmental analysis. *Earth-Science Reviews*, 67, 219-265.
- Benkovics, L., Castillo, V., Colmenares, J., Asensio, A., Esteban, M., Cobos, C., Barletta, V., Simon, C., Leon, K., 2012. Descubrimiento del Campo Perla: Un nuevo campo gigante en el Mar Caribe. 11th Simposio Bolivariano-Exploración Petrolera en las Cuencas Subandinas, Nuevas Fronteras II. Cartagena (Colombia), 11th Simposio Bolivariano-Exploración Petrolera en las Cuencas Subandinas, Nuevas Fronteras II, Extended abstract, 7pp.
- Boesi, T., Goddard, D., 1991. A new geologic model related to the distribution of hydrocarbon source rocks in the Falcón basin, northwestern Venezuela. In: Biddle, K.T. (eds.). *Active Margin Basins*. American Association of Petroleum Geologists (AAPG) Memoir, 52, 35-49.
- Bolli, H.M., Beckman, J.P., Saunders, J.B., 1994. The Falcón Basin. In: Bolli, H.M., Beckman, J., Saunders, J.B. (eds.). *Benthic Foraminiferal Biostratigraphy of the South Caribbean Region*. New York, Cambridge University Press, 277-303.
- Boltovskoy, E., Scott D.B., Medioli, F.S., 1991. Morphological variations of benthic foraminiferal tests in response to changes in ecological parameters: a review. *Journal of Paleontology*, 65, 175-185.
- Bond, G.C., Kominz, M.A., 1984. Construction of tectonic subsidence curves for the early Paleozoic miogeoclinal, southern Canadian Rocky Mountains: Implications for subsidence mechanisms, age of break-up, and crustal thinning. *Geological Society of America Bulletin*, 95, 155-173.
- Borromeo, O., Mirgalia, S., Sartorio, D., Bolla, E.M., Andrea, O., Reali, S., Castellano, S., Villalobos, R., 2011. The Perla World-Class Giant Gas Field, Gulf of Venezuela: Depositional and Diagenetic Controls on Reservoir Quality in Early Miocene Carbonates. *American Association of Petroleum Geologists (AAPG), Search and Discovery Article*, 90135. Last accessed: October 3, 2016. Website: <http://www.searchanddiscovery.com/abstracts/html/2011/ice/abstracts/abstracts066.html>
- Bosence, D., 1991. Coralline algae: mineralization, taxonomy, and palaeoecology. In: Riding, R. (ed.). *Calcareous algae and stromatolites*. Berlin, Springer, 98-113.
- Bosence, D., 2005. A genetic classification of carbonate platforms based on their basinal and tectonic settings in the Cenozoic. *Sedimentary Geology*, 175, 49-72.
- Bosence, D., 2012. Carbonate dominated marine rifts. In: Roberts, D.G., Bally, A.W. (eds.). *Regional geology and tectonics: Phanerozoic rift systems and sedimentary basins*. Elsevier, 104-130.
- BouDagher-Fadel, M.K., 2008. The Cenozoic larger benthic foraminifera: The Neogene. In: Wignall, P.B. (ed.). *Evolution and Geological Significance of Larger Benthic Foraminifera*. Developments in Palaeontology and Stratigraphy (Elsevier), 21, 277-303.
- BouDagher-Fadel, M.K., Price, G.D., 2010a. American Miogypsinidae: An analysis of their phylogeny and biostratigraphy. *Micropaleontology*, 56(6), 567-586.
- BouDagher-Fadel, M.K., Price, G.D., 2010b. Evolution and paleogeographic distribution of the lepidocyclinids. *Journal of Foraminiferal Research*, 40(1), 79-108.
- BouDagher-Fadel, M.K., Price, G.D., Koutsoukos, E.A.M., 2010. Foraminiferal biostratigraphy and paleoenvironments of the Oligocene-Miocene carbonate succession in Campos Basin, southeastern Brazil. *Stratigraphy*, 7(4), 283-299.
- Bover-Arnal, T., Ferrández-Cañadell, C., Aguirre, J., Esteban, M., Fernández-Carmona, J., Albert-Villanueva, E., Salas, R., 2017. Late Chattian platform carbonates with benthic foraminifera and coralline algae from the SE Iberian Plate. *Palaos*, 32, 61-82.
- Braga, J.C., de Neira, A.D., Lasseur, E., Mediato, J., Aguirre, J., Abad, M., Hernaiz-Huerta, P.P., Monthel, J., Pérez-Valera, E., Lopera, E., 2012. Pliocene-Lower Pleistocene shallow-water mixed siliciclastics and carbonates (Yanigua and Los Haitises formations) in eastern Hispaniola (Dominican Republic). *Sedimentary Geology*, 265, 182-194.
- Brandano, M., Corda, L., 2002. Nutrients, sea level and tectonics: constraints for the facies architecture of a Miocene carbonate ramp in central Italy. *Terra Nova*, 14, 257-262.
- Brandano, M., Frezza, V., Tomassetti, L., Fedley, M., Matteucci, R., 2009. Facies analysis and palaeoenvironmental interpretation of the Late Oligocene Attard Member (Lower Coralline Limestone Formation), Malta. *Sedimentology*, 56, 1138-1158.
- Brandano, M., Cornacchia, I., Raffi, I., Tomassetti, L., Agostini, S., 2016. The Monterey Event within the Central Mediterranean area: The shallow-water record. *Sedimentology*, 64(1), 286-310.
- Brandano, M., Cornacchia, I., Tomassetti, L., 2017. Global versus regional influence on the carbonate factories of Oligo-Miocene carbonate platforms in the Mediterranean area. *Marine and Petroleum Geology*, 87, 188-202.
- Brasier, M.D., 1975. An outline history of seagrass communities. *Palaeontology*, 18(4), 681-702.
- Butterlin, J., 1963. A propos de l'Oligocène de la région des Caraïbes. *Bulletin de la Société géologique de France*, 7(4), 390-393.
- Butterlin, J., 1981. Claves para la determinación de macroforaminíferos de México y del Caribe, del Cretácico superior al Mioceno medio. Mexico City, Instituto Mexicano del Petróleo, 219pp.
- Butterlin, J., 1984. Remarques sur des especes de grands foraminifères du Tertiaire des Petites Antilles francaises et sur la phylogenie des especes americaines du genre *Lepidocyclina*. Pau et Bordeaux 1983, Benthos'83, 2nd symposium Benthic Foraminifera, 6, 105-115.
- Carannante, G., Esteban, M., Milliman, J.D., Simone, L., 1988. Carbonate lithofacies as palaeolatitude indicators: problems and limitations. *Sedimentary Geology*, 60, 333-346.
- Castillo, V., Benkovics, L., Cobos, C., Demuro, D., Franco, A., 2017. Perla Field: The Largest Discovery Ever in Latin America. In: Merrill, R.K., Sternbach, C.A. (eds.). *Giant fields of the decade 2000-2010*. American Association of Petroleum Geologists (AAPG) Memoir, 113, 141-152.

- Cattaneo, A., Steel, R.J., 2003. Transgressive deposits: a review of their variability. *Earth-Science Reviews*, 62, 187-228.
- Catuneanu, O., Abreu, V., Bhattacharya, J.P., Blum, M.D., Dalrymple, R.W., Eriksson, P.G., Fielding, C.R., Fisher, W.L., Galloway, W.E., Gibling, M.R., Giles, K.A., Holbrook, J.M., Jordan, R., Kendall, C.G.St.C., Macurda, B., Martinsen, O.J., Miall, A.D., Neal, J.E., Nummedal, D., Pomar, L., Posamentier, H.W., Pratt, B.R., Sarg, J.F., Shanley, K.W., Steel, R.J., Strasser, A., Tucker, M.E., Winker, C., 2009. Towards the standardization of sequence stratigraphy. *Earth-Science Reviews*, 92, 1-33.
- Caudri, C.M.B., 1996. The larger Foraminifera of Trinidad (West Indies). *Eclogae Geologicae Helvetiae*, 89(3), 1137-1309.
- Cole, W.S., 1952. Eocene and Oligocene larger foraminifera from the Panama Canal zone and vicinity. U.S. Geological Survey Professional Paper, 244, 1-41.
- Cole, W.S., 1958. Larger Foraminifera from Carriacou. *Bulletins American Paleontology*, 38(171), 219-233.
- Cole, W.S., 1961a. An analysis of certain taxonomic problems in the larger foraminifera. *Bulletins of American Paleontology*, 41(197), 373-407.
- Cole, W.S., 1961b. Some nomenclatural and stratigraphic problems involving larger foraminifera. *Contributions from the Cushman Foundation for Foraminiferal Research*, 12(4), 136-147.
- Cole, W.S., 1964. American mid-Tertiary miogypsinid foraminifera. Classification and zonation. *Cushman Foundation for Foraminiferal Research Contributions*, 15(4), 138-153.
- Cole, W.S., Applin, E.R., 1961. Stratigraphic and geographic distribution of larger foraminifera occurring in a well in Coffee County, Georgia. *Cushman Foundation for Foraminiferal Research Contributions*, 12(4), 127-135, pls. 6-7.
- Corde, L., Palmiotto, C., 2015. Rhodalgol-foramol facies in equatorial carbonates: Insights from Miocene tectonic islands of the central Atlantic. *Palaeogeography, Palaeoclimatology, Palaeoecology*, 428, 21-30.
- Curet, E.A., 1992. Stratigraphy and evolution of the Tertiary Aruba Basin. *Journal of Petroleum Geology*, 15(3), 283-304.
- Cushman, J.A., 1918. The larger fossil foraminifera of the Panama Canal Zone. *Bulletin United States National Museum*, 10, 89-102.
- Cushman, J.A., 1919. Fossil foraminifera from the West Indies. In: Vaughan, T.W. (ed.). *Contributions to the geology and paleontology of the West Indies*. Publications Carnegie Institution, 291, 21-71.
- Cushman, J.A., 1920. American species of *Orthophragmina* and *Lepidocyclina*. U.S. Geological Survey Professional Paper, 125, 39-105.
- Dalrymple, R.W., Zaitlin, B.A., Boyd, R., 1992. Estuarine Facies Models: Conceptual basis and stratigraphic implications. *Journal of Sedimentary Petrology*, 62(6), 1130-1146.
- Davis, R.A.Jr., Clifton, H.E., 1987. Sea-level change and the preservation potential of wave-dominated and tide-dominated coastal sequences. In: Nummedal, D., Pilkey, O.H., Howard, J.D. (eds.). *Sea-level Fluctuations and Coastal Evolution*. Society for Sedimentary Geology (SEPM) Special Publication, 41, 167-178.
- Demarset, J.M., Kraft, J.C., 1987. Stratigraphic record of Quaternary sea levels: implications for more ancient strata. In: Nummedal, D., Pilkey, O.H., Howard, J.D. (eds.). *Sea-level Fluctuations and Coastal Evolution*. Society for Sedimentary Geology (SEPM) Special Publication, 41, 223-239.
- Diaz, C., Foster, N.L., Attrill, M.J., Bolton, A., Ganderton, P., Howell, K.L., Robinson, E., Hosegood, P., 2023. Mesophotic coral bleaching associated with changes in thermocline depth. *Nature Communications*, 14(1), 6528.
- Drooger, C.W., 1952. Study of American Miogypsinidae. Doctoral Thesis. Utrecht, University of Utrecht, 80pp.
- Drooger, C.W., 1954. The Oligocene-Miocene boundary on both sides of the Atlantic. *Geological Magazine*, 91(6), 514-518.
- Díaz de Gamero, M.L., 1977. Estratigrafía y micropaleontología del Oligoceno y Mioceno inferior del centro de la Cuenca de Falcón, Venezuela. *GEOS Revista Venezolana de Ciencias de la Tierra*, 22, 2-54.
- Díaz de Gamero, M.L., 1989. El Mioceno temprano y medio de Falcón septentrional. *GEOS Revista Venezolana de Ciencias de la Tierra*, 29, 22-35.
- Eames, F.E., 1953. The Miocene/Oligocene boundary and the use of the term Aquitanian. *Geological Magazine*, 90(6), 388-392.
- Eames, F.E., 1954. The Caribbean "Oligocene". *Geological Magazine*, 91, 326-327.
- Eames, F.E., Clarke, W.J., Banner, F.T., Smout, A.H., Blow, W.H., 1968. Some larger foraminifera from the Tertiary of Central America. *Palaeontology*, 11(2), 283-305.
- Embry, A.F., Johannessen, E.P., 1992. T-R sequence stratigraphy, facies analysis and reservoir distribution in the uppermost Triassic-Lower Jurassic succession, Western Sverdrup Basin, Arctic Canada. In: Vorren, T.O., Bergsager, E., Dahl-Stamnes, O.A., Holter, E., Johansen, B., Lie, E., Lund, T.B. (eds.). *Arctic Geology and Petroleum Potential*. Norwegian Petroleum Society Special Publication, Elsevier, 2, 121-146.
- Escalona, A., Mann, P., 2011. Tectonics, basin subsidence mechanisms, and paleogeography of the Caribbean-South American plate boundary zone. *Marine and Petroleum Geology*, 28, 8-39.
- Follmi, K.B., Gerstch, B., Penevey, J.P., De Kaenel, E., Stille, P., 2008. Stratigraphy and sedimentology of phosphate-rich sediments in Malta and south-eastern Sicily (latest Oligocene to early Late Miocene). *Sedimentology*, 55, 1029-1051.
- Fournier, E., Borgomano, J., Montaggioni, L.F., 2005. Development patterns and controlling factors of Tertiary carbonate buildups: Insights from high-resolution 3D seismic and well data in the Malampaya gas field (Offshore Palawan, Philippines). *Sedimentary Geology*, 175, 189-215.
- Frazier, D.E., 1974. Depositional episodes: their relationship to the Quaternary stratigraphic framework in the northwestern portion of the Gulf Basin. University of Texas at Austin, Bureau of Economic Geology Geological Circular, 71(1), 28pp.
- Frost, S.H., Langenheim, R.L.Jr., 1974. Cenozoic Reef Biofacies, Tertiary Larger Foraminifera and Scleractinian Corals from

- Chiapas, Mexico. De Kalb (Illinois), Northern Illinois University Press, 388pp.
- Frost, S.H., Harbour, J.L., Beach, D.K., Realini, M.J., Harris, P.M., 1983. Oligocene reef tract development, southwestern Puerto Rico. *Sedimenta*, 9, 132pp.
- Galloway, W.E., 1989. Genetic stratigraphic sequences in basin analysis. I. Architecture and genesis of floodingsurface bounded depositional units. *American Association of Petroleum Geologists (AAPG) Bulletin*, 73, 125-142.
- Geel, T., 2000. Recognition of stratigraphic sequences in carbonate platform and slope deposits: empirical models based on microfacies analysis of Palaeogene deposits in southeastern Spain. *Palaeogeography, Palaeoclimatology, Palaeoecology*, 155, 211-238.
- Gingras, M.K., MacEachern, J.A., Dashtgard, S.E., Zonneveld, J.P., Schoengut, J., Ranger, M.J., Pemberton, S.G., 2012. Chapter 16 - Estuaries. In: Knaust, D., Bromley, R.G. (eds.). *Trace Fossils as Indicators of Sedimentary Environments*. Elsevier, 64, 463-505.
- Gläser, I., Betzler, C., 2002. Facies partitioning and sequence stratigraphy of cool-water, mixed carbonate-siliciclastic sediments (Upper Miocene Guadalquivir Domain, southern Spain). *International Journal of Earth Sciences*, 91, 1041-1053.
- González de Juana, C., 1938. Contribución al estudio de la cuenca sedimentaria Zulia-Falcón. *Boletín de Geología y Minería Ministerio de Fomento de Venezuela*, 2(2-4), 123-138.
- González de Juana, C., Iturralde de Arozena, J., Picard, X., 1980. Capítulo 6 Cenozoico – Sistema Terciario – Cuenca de Falcón. In: González de Juana, C., Iturralde de Arozena, J., Picard, X. (eds.). *Geología de Venezuela y de sus Cuencas Petrolíferas*. Caracas, Foninves, 1, 542-605.
- Gorney, D., Escalona, A., Mann, P., Magnani, M.B., 2007. Chronology of Cenozoic tectonic events in western Venezuela and the Leeward Antilles based on integration of offshore seismic reflection data and on-land geology. *American Association of Petroleum Geologists (AAPG) Bulletin*, 91(5), 653-684.
- Gravell, D.W., 1933. Tertiary larger foraminifera of Venezuela. *Smithsonian Miscellaneous Collections*, 89(11), 1-44.
- Gravell, D.W., Hanna, M.A., 1937. The *Lepidocyclina texana* horizon in the *Heterostegina* zone, upper Oligocene, of Texas and Louisiana. *Journal of Paleontology*, 11(6), 517-529.
- Guevara, E.H., 1967. Contributions of the AVGMP Maracaibo basin Eocene nomenclature committee VI. The Santa Rita, Jarillal, and La Victoria formations. *Asociación Venezolana de Geólogos Mineros y Petroleros, Boletín Informativo*, 10(2), 51-69.
- Guzmán, H.M., Guevara, C.A., 1998. Arrecifes coralinos de Bocas del Toro, Panamá: Distribución, estructura y estado de conservación de los arrecifes continentales de la Laguna de Chiriquí y la Bahía Almirante. *Revista de Biología Tropical*, 46, 601-622.
- Habibi, T., Bover-Arnal, T., 2018. Larger Foraminiferal Biostratigraphy and Facies Analysis of the Oligocene–Miocene Asmari Formation in the Western Fars Sub-basin, Zagros Mountains, Iran. *Acta Geologica Sinica*, 92(6), 2079-2097.
- Hallock, P., 1985. Why are larger foraminifera large? *Paleobiology*, 11, 195-208.
- Hallock, P., 1988. Diversification in algal symbiont-bearing Foraminifera: a response to oligotrophy? *Genève, Revue Paléobiologie*, 2 (Special Volume), 789-797.
- Hallock, P., 1999. Symbiont-bearing Foraminifera. In: Sen Gupta, B. (ed.). *Modern Foraminifera*. Amsterdam, Kluwer, 123-139.
- Hallock, P., Pomar, L., 2008. Cenozoic Evolution of Larger Benthic Foraminifers: Paleooceanographic Evidence for Changing Habitats. Ft. Lauderdale (Florida), *Proceedings of the 11th International Coral Reef Symposium*, 5pp.
- Haq, B.U., Hardenbol, J., Vail, P.R., 1987. Chronology of Fluctuating Sea Levels Since the Triassic. *Science*, 235(4793), 1156-1167.
- Hilgen, E.J., Lourens, L.J., Van Dam, J.A., Beu, A.G., Boyes, A.F., Cooper, R.A., Krijgsman, W., Ogg, J.G., Piller, W.E., Wilson, D.S., 2012. The Neogene Period. In: Gradstein, F.M., Ogg, J.G., Schmitz, M.D., Ogg, G.M. (eds.). *The Geologic Time Scale*. Elsevier, Boston, 923-978.
- Hodson, F., 1926. Venezuelan and Caribbean Turritellas. *Bulletins of American Paleontology*, 11(45), 173-220.
- Hottinger, L., 1997. Shallow benthic foraminiferal assemblages as signals for depth of their deposition and their limitations. *Bulletin de la Société Géologique de France*, 168(4), 491-505.
- Hottinger, L., 2001. Archaiasins and related porcelaneous larger foraminifera from the late Miocene of the Dominican Republic. *Journal of Paleontology*, 75(3), 475-512.
- Hunt, D., Tucker, M.E., 1992. Stranded parasequences and the forced regressive wedge systems tract: deposition during base-level fall. *Sedimentary Geology*, 81, 1-9.
- Hunt, D., Tucker, M.E., 1995. Stranded parasequences and the forced regressive wedge systems tract: deposition during base-level fall – reply. *Sedimentary Geology*, 95, 147-160.
- Hunter, V.E., 1974. The mid-Tertiary stratigraphic unit of the southern Caribbean area. In: Jung, P. (ed.). *Contributions dedicated to the geology and paleobiology in the Caribbean and adjacent Areas—The Kugler Volume*. Naturforschende Gesellschaft Basel, Verhandlungen, 84, 172-190.
- Hunter, V.E., 1978. Foraminiferal correlation of Tertiary mollusc horizons of the southern Caribbean area. *Geologie en Mijnbouw*, 57, 193-203.
- Insalaco, E., 1998. The descriptive nomenclature and classification of growth fabrics in fossil scleractinian reefs. *Sedimentary Geology*, 118, 159-186.
- Iturralde-Vinent, M.A., 1972. Principal Characteristics of Oligocene and Lower Miocene Stratigraphy of Cuba. *American Association of Petroleum Geologists (AAPG) Bulletin*, 56(12), 2369-2379.
- Janson, X., van Buchem, F.S.P., Dromart, G., Eichenseer, H.T., Dellamonica, X., Boichard, R., Bonnaffé, E., Eberli, G., 2010. Architecture and facies differentiation within a Middle Miocene carbonate platform, Ermenek, Mut Basin, southern

- Turkey. In: van Buchem, F.S.P., Gredes, K.D., Esteban, M. (eds.). *Mesozoic and Cenozoic Carbonate Systems of the Mediterranean and the Middle East: Stratigraphic and Diagenetic Reference Models*. London, The Geological Society, 329 (Special Publications), 265-290.
- Johnson, K.G., Sánchez-Villarga, M.R., Aguilera, O.A., 2009. The Oligocene-Miocene Transition on Coral Reefs in the Falcón Basin (NW Venezuela). *Palaaios*, 24(1), 59-69.
- Jones, B., Hunter, I.G., 1994. Evolution of an Isolated Carbonate Bank during Oligocene, Miocene and Pliocene Times, Cayman Brac, British West Indies. *Facies*, 30, 25-50.
- Jorry, S.J., Haster, C.A., Davaud, E., 2006. Hydrodynamic behaviour of Nummulites: implications for depositional models. *Facies*, 52, 221-235.
- Kotler, E., Martin, R.E., Liddell, W.D., 1992. Experimental analysis of abrasion and dissolution resistance of modern reef-dwelling Foraminifera: Implications for the preservation of biogenic carbonate. *Palaaios*, 7, 244-276.
- Kroh, A., 2001. Echinoids from the Danian (Lower Paleocene) Bruderndorf Formation of Austria. In: Piller, W.E., Rasser, M.W. (eds.). *Palaeogene of the Eastern Alps*. Österreichische Akademie der Wissenschaften, Schriftenreihe der Erdwissenschaftlichen Kommissionen, 14, 377-463.
- Kroh, A., Nebelsick, J.H., 2003. Echinoid assemblages as a tool for palaeoenvironmental reconstruction – an example from the Early Miocene of Egypt. *Palaeogeography, Palaeoclimatology, Palaeoecology*, 201, 157-177.
- Kuss, J., Boukhary, A., 2008. A new upper Oligocene marine record from northern Sinai (Egypt) and its paleogeographic context. *GeoArabia*, 13(1), 59-84.
- Langer, M.R., Hottinger, L., 2000. Biogeography of selected “larger” foraminifera. *Micropaleontology*, 46(1), 105-126.
- Lees, A., Buller, A.T., 1972. Modern temperate-water and warm-water shelf carbonate sediments contrasted. *Marine Geology*, 13, 67-73.
- Lesser, M.P., Slattery, M., Leichter, J.J., 2009. Ecology of mesophotic coral reefs. *Journal of Experimental Marine Biology and Ecology*, 375(1-2), 1-8.
- Liddle, R.A., 1946. Chapter 9 Cenozoic. In: Liddle, R.A. (ed.). *The geology of Venezuela and Trinidad*. New York, Paleontological Research Institution Ithaca, 298-546.
- Lokier, S.W., Wilson, M.E.J., Burton, L.M., 2009. Marine biota response to clastic sediment influx: a quantitative approach. *Palaeogeography, Palaeoclimatology, Palaeoecology*, 281, 25-42.
- Macellari, C., 1987. *Regional Geology and Oil Potential of the Guajira Peninsula, Northwestern Venezuela, and Aruba*. Earth Sciences and Resources Institute, Columbia (South Carolina), University of South Carolina, unpublished technical report, 294pp.
- Macellari, C., 1995. Cenozoic sedimentation and tectonics of the southwestern Caribbean pull-apart basin, Venezuela and Colombia. In: Tankard, A., Suarez, S., Welsink, H. (eds.). *Petroleum Basins of South America*. American Association of Petroleum Geologists (AAPG) Memoir, 62, 757-780.
- Mann, P., 1999. Caribbean sedimentary basins: classification and tectonic setting from Jurassic to present. In: Mann, P. (ed.). *Caribbean Basins. Sedimentary Basins of the World*, vol. 4. Amsterdam, Elsevier Science B.V., 3-31.
- Marcosu, A., Nebelsick, J.H., 2019. Paleoeology of sublittoral Miocene echinoids from Sardinia: A case study for substrate controls of faunal distributions. *Journal of Paleontology*, 93(4), 764-784.
- Martínez, M., Montero, J., Gutiérrez, J.V., González, C., 2007. *Geoquímica orgánica de las unidades sedimentarias de la Cuenca Central de Falcón*. Caracas, Memorias IX Congreso Geológico Venezolano, 1-10.
- Mello e Sousa, S.H., Fairchild, T.R., Tibana, P., 2003. Cenozoic biostratigraphy of larger foraminifera from the Foz do Amazonas basin, Brazil. *Micropaleontology*, 49, 253-266.
- Morsilli, M., Bosellini, F.R., Pomar, L., Hallock, P., Aurell, M., Papazzoni, C.A., 2012. Mesophotic coral buildups in a prodelta setting (late Eocene, southern Pyrenees, Spain): a mixed carbonate-siliciclastic system. *Sedimentology*, 59(3), 766-794.
- Moura, R.L., Amado-Filho, G.M., Moraes, F.C., Brasileiro, P.S., Salomon, P.S., Mahiques, M.M., Bastos, A.C., Almeida, M.G., Silva Jr., J.M., Araujo, B.E., Brito, F.P., Rangel, T.P., Oliveira, V.C.V., Bahia, R.G., Paranhos, R.P., Dias, R.J.S., Siegle, E., Figueiredo Jr., A.G., Pereira, R.C., Leal, C.V., Hajdu, E., Asp, N.E., Gregoracci, G.B., Neumann-Leitão, S., Yáger, P.L., Francini-Filho, R.B., Fróes, A., Campeão, M., Silva, B.S., Moreira, A.P.B., Oliveira, L., Soares, A.C., Araujo, L., Oliveira, N.L., Teixeira, J.B., Valle, R.A.B., Thompson, C.C., Rezende, C.E., Thompson, F.L., 2016. An extensive reef system at the Amazon River mouth. *Science Advances*, 2(4), e1501252.
- Muessig, K., 1984. Structure and Cenozoic tectonics of the Falcón basin, Venezuela and adjacent areas. In: Bonini, W.E., Hangraves, R.B., Shagam, R. (eds.). *The Caribbean-South American plate boundary and regional tectonics*. Geological Society of America Memoir, 162, 217-230.
- Mutti, M., Droxler, A.W., Cunningham, A.D., 2005. Evolution of the Northern Nicaragua Rise during the Oligocene-Miocene: Drowning by environmental factors. *Sedimentary Geology*, 175, 237-258.
- Nalin, R., Nelson, C.S., Basso, D., Massari, E., 2008. Rhodolith-bearing limestones as transgressive marker beds: fossil and modern examples from North Island, New Zealand. *Sedimentology*, 55(2), 249-274.
- Nebelsick, J.H., Rasser, M.W., Bassi, D., 2005. Facies dynamics in Eocene to Oligocene circumalpine carbonates. *Facies*, 51, 197-216.
- Novak, V., Santodomingo, N., Rösler, A., Di Martino, E., Braga, J.C., Taylor, P.D., Johnson, K.G., Renema, W., 2013. Environmental reconstruction of a late Burdigalian (Miocene) patch reef in deltaic deposits (East Kalimantan, Indonesia). *Palaeogeography, Palaeoclimatology, Palaeoecology*, 374, 110-122.
- Odin, G.S., Fullagar, P.D., 1988. Geological significance of the glaucony facies. In: Odin, G.S. (ed.). *Green marine clays. Oolitic Ironstone Facies, Verdine Facies, Glaucony Facies*

- and Celadonite-Bearing Rock Facies—A Comparative Study. Development in Sedimentology, Amsterdam, Elsevier, 45, 295-332.
- O'Connell, L.G., James, N.P., Bone, Y., 2012. The Miocene Nullarbor Limestone, southern Australia; deposition on a vast subtropical epeiric platform. Sedimentary Geology, 253-254, 1-16.
- Peebles, M.W., Lewis, D.L., 1991. Surface textures of benthic foraminifera from San Salvador, Bahamas. Journal of Foraminiferal Research, 21(4), 285-292.
- Petróleos de Venezuela, 2011. Código Estratigráfico de las Cuencas Petroleras de Venezuela. Petróleos de Venezuela. Last accessed: May–Jun 2017, no longer available. Website: <http://www.pdvsa.com/lexico/lexicoh.htm>
- Pettijohn, F.J., Potter, P.E., Siever, R., 1972. Sand and Sandstones. New York, Springer-Verlag, 618pp.
- Pinto, J., Ortega, S., Marin, Z., Berrios, I., Perez, A., Pirela, M., 2011. Controls on the newly-discovered gas accumulations in the Miocene “Perla” carbonate bank, Gulf of Venezuela: A preliminary assessment. I South American Oil and Gas Congress, SPE Western Venezuela Petroleum Section, Maracaibo, 36, 1-4.
- Pinto, D., Diaz, N., Tang, G., Arends, A., Ramírez, R., Pomar, L., Padrón, V., 2014. Interpretación de rampas carbonáticas asociadas a paleoislas durante el Oligoceno-Mioceno en el Golfo de Venezuela. Caso de estudio: Campo de Perla. Memorias del 1er Congreso Venezolano de Gas Natural, Petroleos de Venezuela S.A., 16(1), 18pp.
- Pomar, L., Brandano, M., Westphal, H., 2004. Environmental factors influencing skeletal grain sediment associations: a critical review of Miocene examples from the Western Mediterranean. Sedimentology, 51, 627-651.
- Pomar, L., Esteban, M., Martinez, W., Espino, D., Castillo de Ott, V., Benkovics, L., Castro Leyva, T., 2015. Oligocene-Miocene carbonates of the Perla field, offshore Venezuela: Depositional model and facies architecture. In: Bartolini, C., Mann, P. (eds.). Petroleum geology and potential of the Colombian Caribbean Margin. American Association of Petroleum Geologists (AAPG) Memoir, 108, 647-674.
- Porras, L., 2000. Evolución tectónica y estilos estructurales de la región costa afuera de las cuencas de Falcón y Bonaire. Simposio Bolivariano Exploración Petrolera en las Cuencas Subandinas, 279-292.
- Posamentier, H.W., Vail, P.R., 1988. Eustatic controls on clastic deposition. II. Sequence and systems tract models. In: Wilgus, C.K., Hastings, B.S., Kendall, C.G.St.C., Posamentier, H.W., Ross, C.A., Van Wagoner, J.C. (eds.). Sea Level Changes – An Integrated Approach. Society for Sedimentary Geology (SEPM) Special Publication, 42, 125-154.
- Pyle, R.L., Boland, R., Bolick, H., Bowen, B.W., Bradley, C.J., Kane, C., Kosaki, R.K., Langston, R., Longenecker, K., Montgomery, A., Parrish, F.A., 2016. A comprehensive investigation of mesophotic coral ecosystems in the Hawaiian Archipelago. PeerJ, 4, 1-45.
- Racey, A., 2001. A review of Eocene nummulite accumulations: structure, formation and reservoir potential. Journal of Petroleum Geology, 24(1), 79-100.
- Read, J.F., 1982. Carbonate platforms of passive (extensional) continental margins: types, characteristics and evolution. Tectonophysics, 81, 195-212.
- Reiss, Z., Hottinger, L., 1984. Benthic Foraminifera: Response to environment. In: Reiss, Z., Hottinger, L. (eds.). The Gulf of Aqaba. Ecological Studies (Analysis and Synthesis), 50, 203-284.
- Riera, R., Bourget, J., Allan, T., Håkansson, E., Wilson, M.E.J., 2022. Early Miocene carbonate ramp development in a warm ocean, North West Shelf, Australia. Sedimentology, 69, 219-253.
- Robinson, E., 2004. Zoning the White Limestone Group of Jamaica using larger foraminiferal genera: a review and proposal. Cainozoic Research, 3(1-2), 39-75.
- Robinson, E., Wright, R.M., 1993. Jamaican Paleogene larger foraminifera. In: Wright, R.M., Robinson, E. (eds.). Biostratigraphy of Jamaica. Geological Society of America, Memoir, 182, 283-345.
- Robinson, E., Paytan, A., Chien, C.-T., Broach, K., 2018. Dating the White Limestone of Jamaica using Sr isotope stratigraphy: a progress report. Caribbean Journal of Earth Science, 49, 11-21.
- Santisteban, G., Taberner, C., 1988. Sedimentary models of siliciclastic deposits and coral reefs interrelation. In: Doyle, L.J., Roberts, H.H. (eds.). Carbonate: Clastic Transitions. Developments in Sedimentology, Elsevier, 42, 35-76.
- Schmoker, J.W., Halley, R.B., 1982. Carbonate porosity versus depth: a predictable relation for south Florida. American Association of Petroleum Geologists (AAPG) Bulletin, 66, 2561-2570.
- Sclater, J.G., Christie, P.A.F., 1980. Continental stretching: an explanation of the postmid-Cretaceous subsidence of the central North Sea Basin. Journal of Geophysical Research, 85, 3711-3739.
- Scotese, C.R., 2012. Global Geology Project. Last accessed: May–June 2017. Website: <http://www.globalgeology.com/>
- Seiglie, G.A., 1982. A note of the homeomorphism of three soritid genera (Foraminiferida). Micropaleontology, 28(4), 431-434.
- Seiglie, G.A., Grove, K., Rivera, J.A., 1977. Revision of some Caribbean Archaiasinae, new genera, species and subspecies. Ecologiae geologicae Helvetiae, 70(3), 855-883.
- Senn, A., 1935. Die stratigraphische Verbreitung der Tertiären Orbitoiden, mit spezieller Berücksichtigung ihres Vorkommens in Nord-Venezuela und Nord-Marokko. Ecologiae Geologicae Helvetiae, 28, 51-373.
- Serra-Kiel, J., Mató, E., Saula, E., Travé, A., Ferràndez-Cañadell, C., Busquets, P., Samsó, J.M., Tosquella, J., Barnolas, A., Álvarez-Pérez, G., Franquès, J., Romero, J., 2003. An inventory of the marine and transitional Middle/Upper Eocene deposits of the Southeastern Pyrenean Foreland Basin (NE Spain). Geologica Acta, 1(2), 201-229.
- Serra-Kiel, J., Ferràndez-Cañadell, C., García Senz, J., Hernaiz Huerta, P.P., 2007. Cainozoic larger foraminifers from Dominican Republic. Boletín Geológico y Minero de España, 118, 359-384.

- Shabafrooz, R., Mahboubi, A., Vaziri-Moghaddam, H., Ghabeishavi, A., Moussavi-Harami, R., 2015. Depositional architecture and sequence stratigraphy of the Oligo–Miocene Asmari platform; Southeastern Izeh Zone, Zagros Basin, Iran. *Facies*, 61, 423.
- Sharaf, E., (Toni) Simo, J.A., Carroll, A.R., Shields, M., 2005. Stratigraphic evolution of Oligocene–Miocene carbonates and siliciclastics, East Java basin, Indonesia. *American Association of Petroleum Geologists (AAPG) Bulletin*, 89, 799–819.
- Siggerud, E.I.H., Steel, R.J., 1999. Architecture and trace-fossil characteristics of a 10,000–20,000 year, fluvial-to-marine sequence, SE Ebro Basin, Spain. *Journal of Sedimentary Research*, 69, 365–383.
- Summa, L.L., Goodman, E.D., Richardson, M., Norton, I.O., Green, A.R., 2003. Hydrocarbon systems of Northeastern Venezuela: plate through molecular scale-analysis of the genesis and evolution of the Eastern Venezuela Basin. *Marine and Petroleum Geology*, 20, 323–349.
- Swift, D.J.P., Phillips, S., Thorne, J.A., 1991. Sedimentation on continental margins: V. Parasequences. In: Swift, D.J.P., Oertel, G.F., Tillman, R.W., Thorne, J.A. (eds.). *Shelf Sand and Sandstone Bodies—Geometry, Facies and Sequence Stratigraphy*. International Association of Sedimentologists Special Publication, 14, 153–187.
- Syahrir, M.R., Hanjoko, T., Adnan, A., Yasser, M., Efendi, M., Budiarsa, A.A., Suyatna, I., 2018. The existence of estuarine coral reef at eastern front of Mahakam Delta, East Kalimantan, Indonesia: a first record. *Aquaculture, Aquarium, Conservation & Legislation*, 11(2), 362–378.
- Tomassetti, L., Petracchini, L., Brandano, M., Trippetta, E., Tomassi, A., 2018. Modeling lateral facies heterogeneity of an upper Oligocene carbonate ramp (Salento, southern Italy). *Marine and Petroleum Geology*, 96, 254–270.
- Tomassetti, L., Petracchini, L., Brandano, M., Mascaro, G., Scrocca, D., 2021. Stratigraphical and sedimentological relationships of the Bolognano Formation (Oligocene–Miocene, Majella Mountain, Central Apennines, Italy) revealed by geological mapping and 3D visualizations. *Geologica Carpathica*, 72, 3–16.
- Tournadour, E., Fournier, E., Etienne, S., Collot, J., Maurizot, P., Patriat, M., Sevin, B., Morgans, H.E.G., Martin-Garin, B., Braga, J.C., 2020. Seagrass-related carbonate ramp development at the front of a fan delta (Burdigalian, New Caledonia): Insights into mixed carbonate-siliciclastic environments. *Marine and Petroleum Geology*, 121, 104581.
- Vail, P.R., Audemard, E., Bowman, S.A., Eisner, P.N., Perez-Cruz, C., 1991. The stratigraphic signatures of tectonics, eustasy and sedimentology – an overview. In: Einsele, G., Ricken, W., Seilacher, A. (eds.). *Cycles and Events in Stratigraphy*. Berlin, Springer-Verlag, 617–659.
- Valencia, F.L., Laya, J.C., 2020. Deep-burial dissolution in an Oligocene–Miocene giant carbonate reservoir (Perla Limestone), Gulf of Venezuela Basin: Implications on microporosity development. *Journal of Marine and Petroleum Geology*, 113, 104144.
- van Buchem, F.S.P., Allan, T.L., Laursen, G.V., Lotfpour, M., Moallemi, A., Monibi, S., Motiei, H., Pickard, N.A.H., Tahmasbi, A.R., Vedrenne, V., Vicent, B., 2010. Regional stratigraphic architecture and reservoir types of the Oligo–Miocene deposits in the Dezful Embayment (Asmari and Pabdeh Formations) SW Iran. In: van Buchem, F.S.P., Gerdes, K.D., Esteban, M. (eds.). *Mesozoic and Cenozoic Carbonate Systems of the Mediterranean and the Middle East: Stratigraphic and Diagenetic Reference Models*. London, The Geological Society, 329 (Special Publications), 219–263.
- Vandenbergh, N., Hilgen, F.J., Speijer, R.P., Ogg, J.G., Gradstein, F.M., Hammer, O., Hollis, C.J., Hooker, J.J., 2012. The Paleogene Period. In: Gradstein, F.M., Ogg, J.G., Schmitz, M.D., Ogg, G.M. (eds.). *The Geologic Time Scale*. Boston, Elsevier, 923–978.
- Van Wagoner, J.C., Posamentier, H.W., Mitchum, R.M., Vail, P.R., Sarg, J.F., Loutit, T.S., Hardenbol, J., 1988. An overview of sequence stratigraphy and key definitions. In: Wilgus, C.K., Hastings, B.S., Kendall, C.G.St.C., Posamentier, H.W., Ross, C.A., Van Wagoner, J.C. (eds.). *Sea Level Changes – An Integrated Approach*. Society for Sedimentary Geology (SEPM) Special Publication, 42, 39–45.
- Vaughan, D.K., 1928. Species of larger arenaceous and orbitoidal foraminifera from the Tertiary deposits of Jamaica. *Journal of Paleontology*, 1(4), 277–298, pls. 43–50.
- Vaughan, T.W., 1933. Studies of American species of foraminifera of the genus *Lepidocyclina*. *Smithsonian Miscellaneous Collection*, 89(10), 1–53.
- Vaziri-Moghaddam, H., Seyrafian, A., Taheri, A., Motiei, H., 2010. Oligocene–Miocene ramp system (Asmari Formation) in the NW of the Zagros basin, Iran: Microfacies, paleoenvironment and depositional sequence. *Revista Mexicana de Ciencias Geológicas*, 27, 56–71.
- Velde, B., 2014. Green clay minerals. In: Halland, H.D., Turekian K.K. (eds.). *Treatise on Geochemistry*. Elsevier, 9, 351–364.
- Watts, A.B., 1981. The U.S. Atlantic continental margin: subsidence history, crustal structure and thermal evolution. In: Bally, A.W., Watts, A.B., Grow, J.A., Manspeizer, W., Bernoulli, D., Schreiber, C., Hunt, J.M. (eds.). *Geology of passive continental margins: history, structure and sedimentologic record (with special emphasis on the Atlantic margin)*. American Association of Petroleum Geologists (AAPG), Education Course Note Series, 19(2), 24pp.
- Wheeler, C.B., 1963. Oligocene and lower Miocene stratigraphy of western and northeastern Falcón basin, Venezuela. *American Association of Petroleum Geologists (AAPG) Bulletin*, 47, 35–68.
- Williams, H.D., Burgess, P.M., Wright, V.P., Della Porta, G., Granjeon, D., 2011. Investigating carbonate platform types: multiple controls and a continuum of geometries. *Journal of Sedimentary Research*, 81(1), 18–37.
- Zachos, J.C., Shackleton, N.J., Revenaugh, J.S., Pälike, H., Flower, B.P., 2001. Climate Response to Orbital Forcing Across the Oligocene–Miocene Boundary. *Science*, 292, 274–278.

APPENDIX

DETAILED FACIES DESCRIPTIONS

Siliciclastic Facies

Estuarine Facies (EsF)

Estuarine facies (Fig. 1) are characterized by deposits influenced by tides, waves and fluvial processes (Dalrymple *et al.*, 1992). In the study area, the occurrence of estuarine strata is restricted to the lower Churuguara Fm., representing the second facies in importance recognized in the southern Falcón Basin (15% of the whole studied sections). This facies type is made up of an alternation of quartz-sandstones, sandstone-shale interbeds and massive shales. The quartz-sandstones are well sorted and medium to very coarse grained containing fewer amounts of chert and sporadic feldspars. The quartz particles are subangular to subrounded, poorly cemented by calcite and exhibiting a high intergranular porosity. The sandstone-shale interbeds consist of very poorly to poorly sorted, fine to medium grained litharenites-sublitharenites to lithic wackes (*sensu* Pettijohn *et al.*, 1972) composed by angular to subangular mono- and polycrystalline quartz, chert, feldspars, other minor lithic fragments and micas. Feldspars commonly occur altered to sericite and kaolinite. Cements include calcite, quartz, and iron oxides. Shallow-marine ichnofossils are abundant and mostly include *Planolites*, *Ophiomorpha*, *Thalassinoides*, and minor *Gyrolithes* and *Skolithos*. The EsF can be subdivided into 3 different subfacies including estuary mouth, lagoon and bayhead delta.

Estuary Mouth Subfacies (EsMS; Fig. 1) is integrated by successions of tabular to cross-stratified sandstones containing minor shale interbeds. The sandstone layers average 10-60cm thick. Both grain size and bed thickness generally increase upwards. The shale layers present tabular and lenticular stratification, averaging 1-10cm in thickness and commonly decrease and thin upwards. The sedimentary structures include planar and cross laminations with bioturbated intervals including *Planolites*, *Ophiomorpha*, *Thalassinoides* and *Skolithos*. The bioturbation is most intense in EsMS in comparison with the other estuarine subfacies. This subfacies contains well-preserved or somewhat reworked shells of bivalves and gastropods.

Lagoon Subfacies (LS; Fig. 1) is made up of massive dark-gray shales, limolites and fine sandstone interbeds. Massive

shales are dominant and alternate with heterolytic-bedded deposits that exhibit wavy, lenticular and flaser beddings. The individual sandstone interbeds range from 2 to 10cm in thickness and display planar and cross laminations. The occurrence of bivalves and gastropods, along with bioturbated levels of *Thalassinoides*, *Ophiomorpha* and *Gyrolithes* are distinctive of these deposits.

Bayhead Delta Subfacies (BDS; Fig. 1) consists of matrix-clean, non-fossiliferous quartz sandstones, and microconglomerates containing quartz, chert, and minor clay pebbles. These units alternate with shales, which are characterized by sporadic vegetal remains and thin coal layers. The facies is distinguished by meter-thick units exhibiting planar, cross, and lenticular bedding, along with channel-fill deposits organized into coarsening upwards sets ranging from 5 to 50cm in thickness. BDS interfingers and laterally transitions into LS.

Delta Facies (DF)

The term delta refers to fluvial-fed clastic wedges that show a marine to non-marine transition (Alexander, 1989). In the northern margin of the Falcón Basin, DF (Fig. 1) constitute the Patiecitos and Guarabal siliciclastic successions, which interfinger with the San Luis platform carbonates towards the South. In the southern Falcón Basin, delta deposits are included in the upper part of the Churuguara Fm., passing laterally into platform carbonates towards the East and South. This facies is build up by coarsening and thickening upwards successions of shales, silty to fine grained sandy limestones, sandstones and conglomerates. The DF has been subdivided into 3 subfacies, including delta top, delta front and prodelta. These clastic successions are the main facies in the northern Falcón Basin, with the 14 % of the studied sections, while in the southern part of the basin, it is the third in importance, constituting also the 14% of the total studied sections.

Delta Top Subfacies (DTS; Fig. 1) is represented by interbedded quartz-pebble oligomictic conglomerates, quartz- and chert-rich sandstones, lignites and greenish-gray red-mottled shales, organized in 0.4-7m thick fining and thinning upwards successions. Shales are dominant and alternate with lenticular to tabular bedded sandstones displaying planar, wavy and cross laminations.

Amalgamated sandstone channels with erosive bases and floodplain sand splays are common. This facies contains plant remains, root marks, and occasionally, well-preserved bivalve shells. The occurrence of laterites, ferruginous horizons and pseudogleys is also common.

Delta Front Subfacies (DFS; **Fig. I**) consists of alternations of poorly- to well-sorted lithic sandstones with scattered skeletal fragments, microconglomerates and minor gray shales, organized in coarsening and thickening upwards successions averaging 2-13m thick. Sandstones and microconglomerates display tabular, lenticular and cross bedding associated with delta channels and amalgamated sandy bars. The dominant lithology corresponds to subrounded to angular, fine to very coarse-grained quartz and chert sandstones, exhibiting parallel, cross and wavy laminations. Skeletal components include highly fragmented and reworked bivalves, gastropods, corals, echinoids, benthic foraminifera (mainly larger and smaller porcelaneous foraminifera and minor small rotaliids) and coralline algae.

Prodelta Subfacies (PS; **Fig. I**) is composed of gray massive and laminated shales with minor interbeddings of fine to very fine-grained sandstones and sheet-like sandy to silty skeletal or micritic limestones. Sedimentary structures include parallel and cross laminations. Bioturbated intervals are common and locally destroy the depositional sedimentary structures. Levels rich in oyster and pectinid bivalves, as well as turritellid gastropods are present. Other skeletal components present are fragmented and reworked molluscs, corals, echinoids, coralline algae detritus, larger porcelaneous foraminifera (soritids, archaiaasinids), small rotaliids, amphisteginids, and minor larger hyaline forms (including nummulitids, miogypsinids and lepidocyclinids). Occasionally, isolated scleractinian colonies in life position occur in the prodelta shales, including plate, foliaceous and columnar growth forms. Sandstone levels thicken and increase upwards, passing and grading into DFS. This facies forms packages ranging from 5-35m thick.

Shallow Marine Glauconite Facies (SMGF)

Shallow marine reworked greensands (**Fig. I**) interfingered with lagoon shales are found in the middle and upper parts of western Churuguara sections. These facies alternate with prodelta and pelagic shale deposits (PS, PSF) and are constituted by an alternation of highly bioturbated gray shales and glauconite-rich sandstones, organized in coarsening and thickening upwards successions ranging from 1 to 13m in thickness. Sandstones consist of fine to medium-grained lithic wackes including glauconite, mono and polycrystalline quartz, chert, micas, mud clasts, and minor feldspars. These green wackes display planar and lenticular stratification, averaging 0.1 to 1.5m in thickness,

and exhibit planar, cross and wavy lamination. Well-preserved and reworked bivalves and gastropods, as well as bioturbated levels with *Thalassinoides*, large-diameter *Ophiomorpha*, *Planolites*, *Gyrolithes* and *Cruziana* are common. These allochthonous glauconite deposits make up less than 1% of the studied sections.

Turbidite Glauconite Facies (TGF)

Deep marine glauconitic sandstones rich in planktonic foraminifera (**Fig. I**) occur in the middle Churuguara and lower Agua Clara fms., at the southern margin of the Falcón Basin. This facies is made up of turbidite successions interfingered within pelagic shales towards the South and East. TGF are commonly organized in finning and thinning upwards successions. The cm- to m-thick sandstone layers are massive, tabular, lenticular or exhibit channel-like shapes. The occurrence of erosive bases with the presence of mud clasts and cobbles are common. Common sedimentary structures include parallel, wavy and cross lamination with occasional slumped beds. Sandstones are fine to medium grained, composed by glauconite grains and minor quartz, chert, feldspars and micas. The matrix is shale with abundant pelagic fauna (mainly globigerinids). Other common skeletal fragments include reworked tests of larger foraminifera, smaller benthic forams, echinoids, coralline algae and other skeletal remains. These turbidite deposits represent the 2% of the whole studied sections.

Pelagic Shale Facies (PSF)

Thick packages of pelagic shales with minor fine sandstones (**Fig. I**) occur in the lower and middle parts of the Churuguara Fm., as well as in the lower Agua Clara Fm., at the southern Falcón Basin. These pelagic successions thicken towards the South and East, and interfinger with TGF northwards and westwards. This facies consists of major black shales with planktonic foraminifera and glauconite, and minor fine laminated and heterolithic sandstones displaying planar, lenticular and channel-like beddings. Sandstones are fine grained, composed by quartz, chert, feldspars, micas, glauconite grains, and skeletal tests (mainly planktonic foraminifera). The matrix of sandstones is rich in shale. These pelagic successions are the most represented facies in the southern basin margin, constituting approximately the 29% of the entire studied sections.

Carbonate Facies

Shoal Facies (ShF)

Shallow marine reworked bioclastic rudstones, floatstones, grainstones and packstones (**Fig. II**) constitute part of the Churuguara Fm., in the southern Falcón

Basin. These shallow marine limestones are organized in decimeter- to meter-thick strata including massive, nodular and wavy beddings, often exhibiting erosive bases. ShF can occur mixed with variable amounts of poorly sorted sandstones, siltstones and shales. Clastic grains are constituted by angulous to subrounded, fine to medium grained quartz, chert, and other lithic fragments. ShF has been subdivided into 2 main subfacies based on the dominant skeletal components. These mixed carbonate-siliciclastic deposits occur in the southern Falcón Basin, constituting less than 3% of the whole studied sections.

Operculinoides Shoal Subfacies (OShS; Fig. II) occurs in the lower Churuguara Fm., interfingering with estuarine siliciclastics (EsF; Fig. I) towards the North and West, and with echinoid rich calcarenites (EF; Fig. II) and Coralline Algal Debris limestones Facies (CADF; Fig. II) towards the South and East. These carbonates are integrated by floatstone to rudstone textures rich in *Operculinoides* sp. mixed with fragments of bivalves and gastropods. In addition, larger porcelaneous foraminifera (soritids, archaiasinids), miogypsinids, amphisteginids and nummulitids occur as accompanying taxa. Other minor skeletal compounds include smaller porcelaneous, hyaline and agglutinated foraminifera, echinoid fragments, serpulids, coralline algae, *Halimeda* sp., coral fragments and other skeletal remains. Bioclasts are often perforated and fragmented. The larger foraminifera tests occur randomly orientated, oriented parallel to the bedding planes, or imbricated. Erosive bases, as well as cross, undulated and lenticular beddings are common. The matrix is bioclastic with variable amounts of micrite and siliciclastic grains. Geopetal structures are common.

Molluscan Shoal Subfacies (MShS; Fig. II) was reorganized in the Churuguara Fm., interfingering with estuarine siliciclastics (EsF; Fig. I) northward and westward, and passing laterally into echinoid rich calcarenites (EF; Fig. II) and coralline algal debris limestones (CADF; Fig. II) towards the South and East. In the upper Churuguara Fm., these deposits locally mark the lower boundary of the siliciclastic Agua Clara Fm. These shallow marine carbonates exhibit floatstone to rudstone textures with a packstone-grainstone matrix dominated by reworked shells of bivalves, gastropods and echinoids. The original aragonitic shells of bivalves and gastropods often occur replaced by calcite. Other minor skeletal remains include coralline algae detritus, *Halimeda* sp., porcelaneous foraminifera (soritids, archaiasinids, peneroplids, miliolids), smaller hyaline foraminifera, miogypsinids, amphisteginids, coral branches and serpulids. Bioclasts occur highly fragmented and often bioperforated. Matrix contains variable amounts of micrite and siliciclastic grains. Geopetal structures are common.

Echinoid Facies (EF)

The echinoid-rich facies (Fig. II) occurs in the lower Churuguara succession, at the southern Falcón Basin, interfingering and grading into carbonate shoal facies towards the West and North. This facies is organized in massive tabular and cross beds (1-5m thick) of locally highly bioturbated calcarenites with scattered well-preserved irregular echinoids (4-7cm in diameter). The texture is dominated by well-sorted, fine-grained grainstone to packstone composed of sand-sized sparite-like carbonate grains, abundant echinoid fragments, and fine to very fine-grained detrital quartz (reaching a maximum content of 10-15%). Other common skeletal components include coralline algae fragments, fine-grained mollusc detritus, well-preserved smaller hyaline foraminifera (rotaliids, lagenids), rare planktonic foraminifera, and very rare fragmented or abraded larger foraminifera. This carbonate texture occurs strongly recrystallized and cemented by syntaxial calcite. Echinoid-rich limestones make up important accumulations in the southern Falcón Basin, comprising 2% of the total studied sections.

Seagrass Facies (SF)

Seagrass skeletal limestones (Fig. II) (*sensu* Brasier, 1975) are organized in 0.1 to 1.5m thick units with massive, tabular, wavy and cross bedding, interfingering and grading into Coral rich Facies (CF; Fig. II) in both San Luis and Churuguara formations. Seagrass limestones also interfinger with the Patiecitos and Guarabal prodelta shales in the northern margin of the Falcón Basin. This facies is represented by poorly- to moderately-sorted bioclastic packstones to grainstones with minor terrigenous grains. The skeletal compounds can occur abraded, encrusted and perforated, and include fragments of molluscs, small and larger porcelaneous foraminifera (soritids, archaiasinids, peneroplids), smaller hyaline foraminifera (rotaliids, lagenids), encrusting foraminifera, echinoid plates and spines with syntaxial calcite overgrowth cement, coralline red algae detritus (common articulated and hook-shaped forms), *Halimeda* sp., coral branches, ostracods, serpulids, and other undetermined skeletal remains. Rare tests of larger hyaline foraminifera also occur. Matrix varies between irregular distributed calcisiltite to micrite or clayey-silty micrite. Geopetal structures commonly occur. Seagrass limestones are poorly represented in the northern and southern Falcón Basin, constituting less than 1% of the whole studied sections in both basin margins.

Coral Facies (CF)

Scleractinian-rich facies (Fig. II), exhibiting boundstone, rudstone and floatstone textures, are present in both San Luis and Churuguara successions. The CF is

further subdivided into 2 different subfacies, representing autochthonous and allochthonous depositional fabrics. These scleractinian-rich deposits form the second most significant in both the northern and southern Falcón Basin, accounting for 4% of the studied sections in the North and 3% in the South.

Coral Boundstone Subfacies (CBS; Fig. II) consists of scleractinian colonies mainly in growth position. Based on the study of 120 coral exposures, 49% of the identified coral growth fabrics correspond to pillarstones, 26% to mixstones, 23% to domestones and 2% to platestones (*sensu* Insalaco, 1998). This facies occurs within prodelta shales in the northern Patiecitos and Guarabal fms. or in proximal carbonate settings within the San Luis and Churuguara fms.

Coral boundstone deposits in prodelta shales are represented by: i) pillarstone, mixstone, and domestone growth fabrics, with sparse to densely packed coral colonies in a micritic skeletal matrix; ii) pillarstone facies displaying a continuous, dense fabric of branching scleractinian colonies within a shaly to silty matrix and iii) minor sparsely platestone to sheetstone growth fabrics in a shaly to sandy matrix. The bioclastic matrix filling the spaces between corals consists of floatstone/rudstone to poorly-sorted packstone and wackestone textures, with varying clastic content. The skeletal fraction includes fragmented molluscs and echinoids, red algae detritus, branching coral fragments, *Halimeda* sp., preserved to fragmented benthic foraminifera, encrusting foraminifera, bryozoans, serpulids, and scarce planktonic foraminifera. Dominant benthic foraminifera include larger and smaller porcelaneous forms (soritids, archaiasinids, miliolids), rotaliids, lagenids, gypsinids and textularids. Less represented forms include miogypsinids, amphisteginids, nummulitids and lepidocyclinids. Scleractinian colonies, as well as skeletal fragments in the matrix may show signs of encrustation and bioerosion. This facies forms cm- to m-thick bioherms and biostromal beds with plane-parallel, massive, nodular, wavy, or sigmoidal stratification, often amalgamating to create coral mounds up to 5-15m thick.

Coral boundstones in proximal carbonate settings are dominated by parallel stratified coral bioherms, and occasionally, by isolated biostromes of branching, columnar and rare massive growth forms. Massive, nodular and wavy beddings were also recognized. Corals commonly occur closely clustered but not in contact, supported by a skeletal matrix. This inter-coral skeletal matrix corresponds to floatstone/rudstone to poorly-sorted packstone textures, which may be silty, sandy or shaly. The most common skeletal components include molluscan remains, fragmented coral branches, coralline algae detritus, fragments of *Halimeda* sp., echinoid spicules and

plates, bryozoans, worm tubes, preserved or fragmented benthic foraminifera, encrusting foraminifera and scarce planktonic foraminifera. Small rhodoliths were also locally observed. The most represented benthic foraminifera include larger and smaller porcelaneous forms (soritids, archaiasinids, miliolids), smaller rotaliids, amphisteginids, textularids and miogypsinids. Secondary foraminifera taxa are nummulitids, lepidocyclinids and lagenids. Intraskelatal geopetal fillings are common. The identified taphonomic signatures include abrasion, fragmentation, bioerosion and encrustation.

Detrital Coral Subfacies (DCS; Fig. II) is made up of scleractinian-rich floatstones to rudstones of branching and columnar coral fragments and scattered small rhodoliths within a skeletal matrix or in a sandy to silty shale. The skeletal matrix corresponds to packstone to grainstone textures of wholly-preserved and fragmented benthic foraminifera, molluscan detritus, coralline algae and *Halimeda* sp. fragments, echinoid spines and plates, bryozoans, worm tubes, encrusting foraminifera, and scarce planktonic foraminifera. The most abundant benthic foraminifera present in the matrix are larger and smaller porcelaneous forms (soritids, archaiasinids, miliolids), hyaline foraminifera (small rotaliids, lagenids, gypsinids, amphisteginids, miogypsinids), and textularids. Rarely nummulitids and lepidocyclinids are also present. Skeletal rests commonly display signs of abrasion, fragmentation, bioerosion, and encrustation. These allochthonous coral deposits are organized in tabular, lenticular and occasional channel-filling sedimentary bodies with thicknesses that range between 0.1 and 7m. The beds internally display massive or nodular bedding. Less frequent stratal arrangements include parallel, wavy or cross bedding with rare erosive bases. This subfacies grades and interfingers with CBS.

Rhodolith Facies (RF)

Rhodolith-rich lithofacies (Fig. II) occur in San Luis and Churuguara formations, including floatstones and minor rudstones of heterometric rhodoliths, commonly 3-6cm in diameter, with laminar concentric to moderately branched morphologies. Most rhodoliths are nucleated around branching coral fragments or other bioclasts, and may contain interlayered bryozoans and encrusting foraminifera. The matrix is made up of poorly sorted packstone and grainstone textures of coralline algae detritus, wholly-preserved to abraded larger foraminifera, scattered coral fragments, broken molluscs, echinoid fragments, ostracods, bryozoans, encrusting foraminifera, scarce planktonic foraminifera, and rare fragments of calcareous green algae (*Halimeda* sp.). Dominant benthic foraminifera correspond to amphisteginids, miogypsinids, nummulitids and lepidocyclinids. Other foraminifera occurrences

include larger and smaller porcelaneous forms (soritids, archaiasinids, miliolids), lagenids, sphaerogypsinids and textularids. *Entobia* multi-chambered borings and other simple borings are common in some rudite-sized allochems. Skeletal fragments can occur abraded, fragmented, bioeroded and encrusted. The fine grains in the matrix correspond to irregularly-distributed micropeloidal micrite. Geopetal structures, as well as shelter and fenestral pores, are common. The matrix may contain a maximum of 15 to 20% of siliciclastic sand to silt. RF displays up to 3m thick packages of nodular, massive or wavy bedded strata. Nodular textures are typically associated with a silty to clayey matrix. Rarely, rhodolith limestones occur as amalgamated channel fillings or display clinoforms with internal parallel, cross and slumped bedding. Rhodolith-rich limestones are rare in both the northern and southern margins of the Falcón Basin, comprising only 1% of the studied sections in each area.

Maerl Facies (MF)

Maerl facies (Fig. II) (*sensu* Nebelsick *et al.*, 2005) occurs in the northern San Luis and southern Churuguara carbonate successions. The facies corresponds to floatstone to rudstone textures with coralline algal branches, scattered rhodoliths and their detritus. Matrix is made up of a skeletal packstone texture containing coralline algae fragments, fragmented molluscs, echinoid plates and spines, commonly well-preserved to slightly abraded larger foraminifera (amphisteginids, miogypsinids, nummulitids and lepidocyclinids), ostracods, bryozoans, encrusting foraminifera and rare planktonic foraminifera (mainly globigerinids). Minor skeletal remains include larger and smaller porcelaneous foraminifera (archaiasinids, miliolids) and other smaller benthic foraminifera (rotaliids and textularids). The facies is organized into massive to slightly stratified sedimentary bodies of 0.2 to 5m thick, which interfinger and grade into the coralline algal debris facies. Branching red algae rudstones are rare in the northern and southern Falcón Basin, representing less than 1% of the studied sections in both basin margins.

Coralline Algal Debris Facies (CADF)

Reworked coralline algal limestones (Fig. II) are broadly represented in both the San Luis and Churuguara formations, and make up tabular, massive or wavy beds that range from 1 to 6m in thickness. This facies is characterized by packstone to grainstone textures, dominated by highly fragmented coralline algae detritus and abraded larger foraminifera, including amphisteginids, miogypsinids, nummulitids, and lepidocyclinids. Other common skeletal grains are fragmented and abraded tests of molluscs, echinoid plates and spines, ostracods, encrusting foraminifera and planktonic foraminifera. Minor bioclasts include rotaliids, lagenids, larger and smaller porcelaneous

foraminifera (soritids, archaiasinids, miliolids), textularids, *Sphaerogypsina*, *Planorbulinella*, worm tubes, bryozoans, scarce fragments of *Halimeda* sp., scattered coral fragments and occasional small rhodoliths. The facies includes levels rich in glauconite grains. The matrix consists of calcisiltite and micropeloidal micrite, with a maximum of 2–3% fine- to very fine-grained sand and silt, composed of quartz and scarce feldspars. Limestones made up of reworked coralline algae and benthic foraminifera are the main carbonate facies in the Falcón Basin, representing the 5% of the total studied sections in the northern basin margin and the 4% in southern part of the basin.

Heterostegina Facies (HF)

Heterostegina accumulations (Fig. II) occur in few localized exposures within the San Luis and Churuguara successions, appearing as strata ranging from decimetera to a few meters in thickness. These strata are interlayered within coral mounds in prodelta shales or with littoral shoals or bars interbedded within rhodalgial and larger foraminifera-rich limestones (MF and CADF). The deposits display massive, wavy, or cross bedding with rudstone to floatstone textures dominated by *Heterostegina* and other fragmented and abraded bioclasts. Subordinated skeletal fragments include other nummulitids, lepidocyclinids, amphisteginids, rare miogypsinids, larger porcelaneous foraminifera (soritids, archaiasinids), coralline algae branches, coral fragments, and coarse mollusc fragments. Larger foraminifera and other platy-shaped bioclasts occur randomly oriented, parallel to the stratification, or imbricated. Matrix exhibits a bioclastic packstone to grainstone texture composed of echinoid plates and spines, fine mollusc detritus, coralline algae fragments, smaller benthic foraminifera, planktonic foraminifera and medium- to fine-grained siliciclastic grains, which constitute up to 3–5% of the composition. The matrix itself is composed of fine-grained bioclastic silt and micrite. In both the northern and southern Falcón Basin, HF represents less than 1% of the total studied sections.

Lepidocyclina Facies (LF)

Lepidocyclina debris (Fig. II) are found in the San Luis and Churuguara carbonate successions, interfingering landwards with rhodalgial and larger foraminifera-rich limestones (MF and CADF), and occasionally with rhodolith floatstones (RF). This facies grades basinwards into Planktonic Foraminifera-rich limestones Facies (PFF; Fig. II). Stratification is massive, plane-parallel or wavy. The beds measure 0.2-0.5m in thickness, with common diffuse bioturbation, glauconite-rich levels and hardground surfaces. This lithofacies is dominated by few species of large-sized *Lepidocyclina* and *Eulepidina*, and less abundant nummulitids, forming

rudstone to floatstone textures with a mud-rich skeletal matrix. Secondary coarse-sized components include amphisteginids, miogypsinids, branching coralline algae, scattered small rhodoliths and bryozoans. The matrix contains abundant coralline algae detritus, planktonic foraminifera, echinoid plates and spines, highly fragmented molluscs, other skeletal fragments, and a variable sand content (up to 1-3 %). The matrix consists of peloidal micrite mixed with bioclastic siltite and shale. Larger foraminifera are randomly oriented, but may also show localized parallel orientation due to compaction effects, evidenced by pressure dissolution features and clay-rich levels. The skeletal remains occur abraded, bioeroded, and fragmented. These larger foraminifera-rich limestones are well represented in the southern Falcón Basin, constituting less than 2% of the total studied sections, whereas in the northern basin margin, they account for less than 1%.

Planktonic Foraminifera Facies (PFF)

Planktonic foraminifera-rich limestones (Fig. II) interfinger and grade landwards with *Lepidocyclina* debris (LF) in both the San Luis and Churuguara carbonate systems. These deposits are organized in massive-tabular strata with a maximum thickness of 0.7m. Their texture is a fine-grained packstone, locally wackestone, dominated by globigerinids. Other minor scattered skeletal remains include abraded and fragmented tests of larger foraminifera (mainly lepidocyclinids and nummulitids), red algae detritus, and rare smaller benthic foraminifera. This facies contains up to 5% of very fine-grained detrital quartz, along with authigenic glauconite and pyrite. The matrix is micrite with variable contents of shale. In both the northern and southern Falcón Basin, planktonic foraminifera-rich limestones constitute less than 1% of the studied sections.



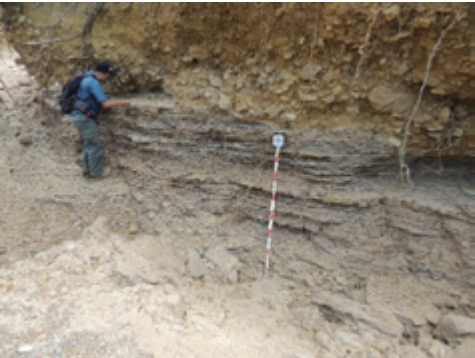

EsF: Estuarine Facies Lithology: Sandstone and shale. Skeletal components: Abraded and fragmented, as well as well preserved, skeletal grains. Texture: Fine to very coarse grained, poorly to well sorted, matrix to grain supported. Stratigraphic features: Massive and bedded; normal, inverse or no gradation; common bioturbation. Field view of the estuarine succession of the Churuguara Fm. (section 17 in Fig. 2). Image width: 265m.	
EsMS: Estuary Mouth Subfacies Lithology: Sandstone and minor shale. Skeletal components: Preserved and fragmented molluscs. Texture: Fine to medium grained, moderate to poorly sorted, matrix and grain supported. Stratigraphic features: Tabular, lenticular and cross beddings; inverse gradation; planar, and cross lamination; common bioturbation. Churuguara Fm. (section 18 in Fig. 2). Image width: 8.7m.	
LS: Lagoon Subfacies Lithology: Shale and less abundant sandstone. Skeletal components: Bivalves and gastropods. Texture: Fine grained, poorly sorted, matrix and minor grain supported. Stratigraphic features: Fine laminated interbeddings; ungraded; planar, lenticular and flaser lamination; common bioturbation. Churuguara Fm. (section 17 in Fig. 2). Image width: 4.9m.	
BDS: Bayhead Delta Subfacies Lithology: Non-fossiliferous, mud-clean sandstone, subordinated clay, shale and sporadic coal interlayers. Skeletal components: Sparse bivalve shells. Texture: Medium to very coarse grained, well sorted, grain supported, matrix clean. Stratigraphic features: Tabular, planar, cross channel-like and lenticular bedded; overall coarsening upwards trends. Churuguara Fm. (section 17 in Fig. 2). Image width: 5.4m.	

FIGURE 1. Description of Lower Miocene siliciclastic Facies and Subfacies of the northern and southern margins of the Falcón Basin. It includes lithology, skeletal components, texture, stratigraphic features and outcrop or thin section views.





DF: Delta Facies Lithology: Shale, sandstone, conglomerate, sandy-shally limestone and limestone. Skeletal components: Fragmented and well-preserved mollusc shells and other skeletal fragments. Texture: Very fine to very coarse grained, poorly to well sorted, matrix to grain supported. Stratigraphic features: Massive and bedded, inverse or normal graded. Isolated coral mounds within delta deposits. Patiecitos, Guarabal and San Luis Fms. (section 7 in Fig. 2 northwards). Image width: 200m.	
DTS: Delta Top Subfacies Lithology: Mottled shale, sandstone, conglomerate and lignite. Skeletal components: Scattered bivalve shells. Texture: Very fine to very coarse grained, poorly to well sorted, matrix or grain supported. Stratigraphic features: Channel, lenticular and sheet-like bedding; normal graded; planar, wavy and cross lamination; scarce bioturbation. Guarabal Fm. El Hueque, near Cabure. Image width: 5.4m.	
DFS: Delta Front Subfacies Lithology: Sandstone, conglomerate and less abundant shale. Skeletal components: Abraded and fragmented bivalves, gastropods, corals, larger foraminifera (soritids) and coralline algae. Texture: Fine to very coarse grained, poorly to well sorted, grain supported, matrix-clean or clayey to silty matrix. Stratigraphic features: Lenticular, cross and planar beddings, inverse gradation, parallel, cross and wavy lamination, moderate bioturbation. Patiecitos Fm. (section 9 in Fig. 2). Image width: 10.5m.	
PS: Prodelta Subfacies Lithology: Shale with minor sandstone and sandy to silty limestone. Skeletal components: Reworked to well preserved molluscs, corals, larger foraminifera (soritids, archaiasinids), echinoids and coralline algae. Texture: Very fine to fine grained, poorly sorted, matrix and rarely grain supported. Stratigraphic features: Massive, finely bedded and laminated, inverse gradation, common bioturbation. Patiecitos Fm. (section 5 in Fig. 2). Image width: 14m.	

FIGURE I. Continued.

SMGF: Shallow Marine Glauconite Facies

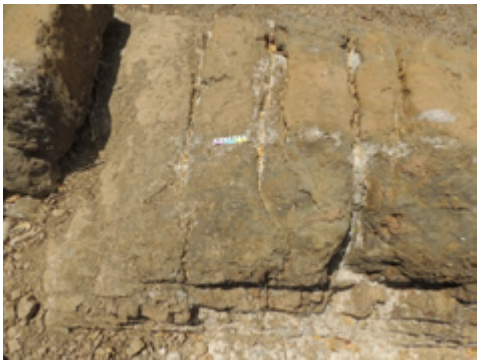
Lithology: Allochthonous glauconitic sandstone, lithic sandstone and shale.

Skeletal components: Often well-preserved bivalves and gastropods.

Texture: Fine to medium grained, poorly sorted, grain and matrix supported, shale-rich matrix. Common mud clasts.

Stratigraphic features: Tabular, lenticular and cross bedding with internal planar, wavy and cross laminations. Common bioturbation destroying sedimentary structures, inverse gradation.

Churuguara Fm. (section 18 in Fig. 2). Image width: 1.9m.



TGF: Turbidite Glauconite Facies

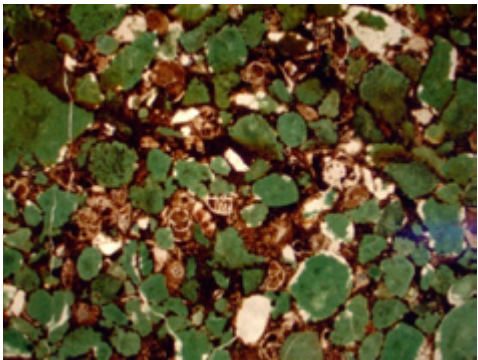
Lithology: Allochthonous glauconitic sandstone.

Skeletal components: Planktonic foraminifera and less abundant reworked benthic foraminifera, echinoids and coralline algae.

Texture: Fine to medium grained, poorly sorted, grain or matrix supported, matrix rich in shale.

Stratigraphic features: Massive, tabular, lenticular or channel-like bedding; normal grading.

Churuguara Fm. Image width: 68.8mm.



PSF: Pelagic Shale Facies

Lithology: Shale with glauconite and minor sandstone.

Skeletal components: Planktonic foraminifera.

Texture: Very fine grained, poorly sorted, and minor grain supported, dominant shale matrix.

Stratigraphic features: Massive and minor laminated, lenticular and channel-like bedding; ungraded.

Churuguara Fm. (section 22 in Fig. 2). Image width: 50m.

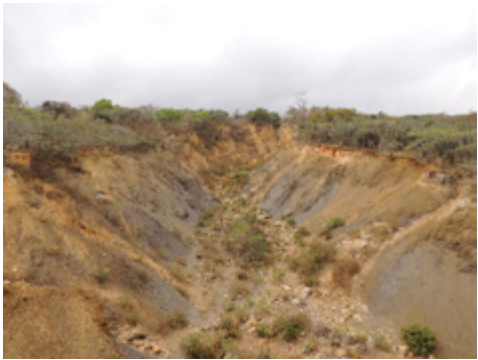


FIGURE I. Continued.


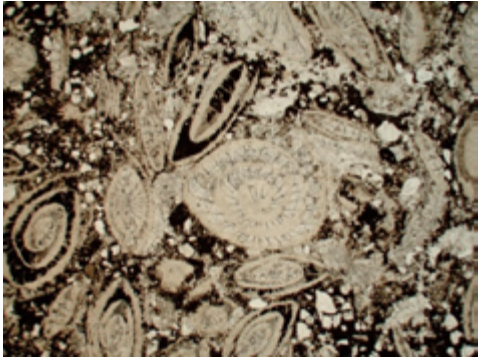
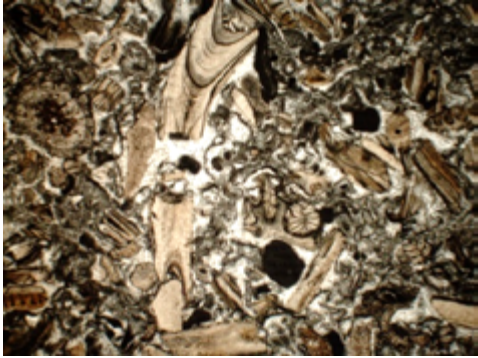
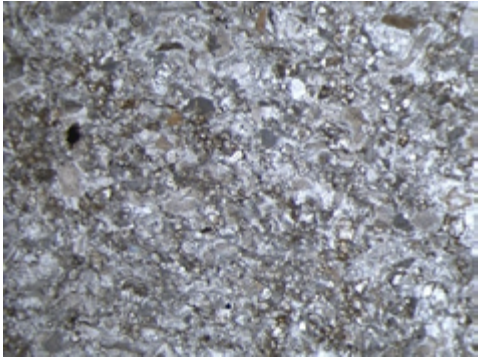
ShF: Shoal Facies Main components: Rudite-sized, highly-abraded skeletal grains (larger foraminifera and/or mollusc shells). Subordinate components: Sand-sized skeletal detritus mixed with siliciclastic grains. Texture: Floatstone to rudstone with skeletal packstone to grainstone matrix. Other sedimentary features: Stratified with common erosive bases. Churuguara Fm. (section 19 in Fig. 2). Image width: 3.5m.	
OShS: Operculinoides Shoal Subfacies Main components: <i>Operculinoides</i> sp. Subordinate components: Reworked fragments of bivalves, gastropods, benthic foraminifera, echinoids, serpulids, coralline algae and calcareous green algae mixed with siliciclastics. Texture: Floatstone to rudstone with skeletal packstone to grainstone matrix. Other sedimentary features: Stratified with common erosive bases, skeletal grains can occur orientated parallel to the bedding or imbricated. Churuguara Fm. Image width: 6.9mm.	
MShS: Molluscan Shoal Subfacies Main components: Reworked molluscs and echinoids. Subordinate components: Red algae detritus, benthic foraminifera, calcareous green algae, coral fragments and worm tubes mixed with siliciclastics. Texture: Floatstone to rudstone with skeletal packstone to grainstone matrix. Other sedimentary features: Stratified with common erosive bases, skeletal fragments can occur orientated parallel to the bedding. Churuguara Fm. Image width: 6.9mm.	
EF: Echinoid Facies Main components: Sand-sized echinoid detritus. Subordinate components: Scattered well-preserved infaunal echinoids, fragmented coralline algae, mollusc detritus, smaller benthic foraminifera, abraded larger foraminifera and fine to very fine-grained detrital quartz. Texture: Well-sorted and cemented grainstone and minor packstone. Other sedimentary features: Massive, tabular, cross-bedded or unbedded. Churuguara Fm. Image width: 8.6mm.	

FIGURE II. Description of Lower Miocene carbonate facies and subfacies of the northern and southern margins of the Falcón Basin with dominant components, subordinate components, texture, other sedimentary features and outcrop or thin section views.

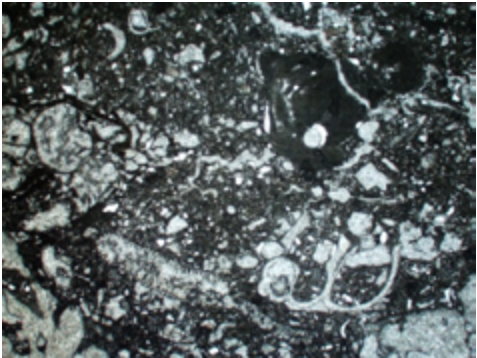

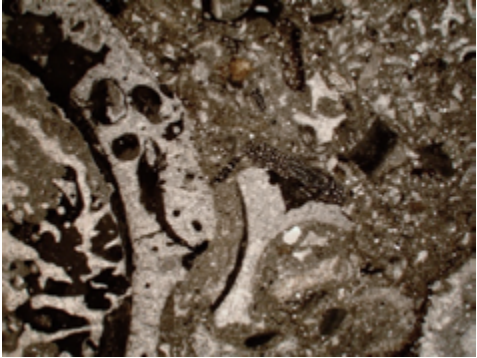
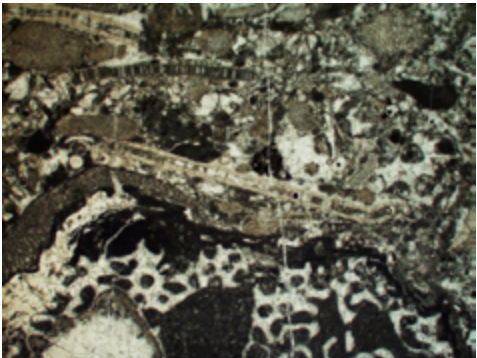
SF: Seagrass Facies Main components: Molluscs, hook-shaped coralline algae, porcelaneous foraminifera (soritids, archaiasinids), hyaline foraminifera and <i>Halimeda</i> sp. Subordinate components: Other minor skeletal fragments and siliciclastic grains. Texture: Poorly sorted packstone to grainstone, matrix of bioclastic silt and clayey to silty micrite. Other sedimentary features: Massive, tabular, wavy and cross-bedded; grading within Coral Facies. San Luis Fm. Image width: 6.9mm.	
CF: Coral Facies Main components: Branching corals. Subordinate components: Nodular, sheet-like and platy corals, molluscs, echinoids, larger foraminifera, coralline algae and other skeletal components. Texture: Floatstone, rudstone and boundstone with a skeletal or siliciclastic matrix. Other sedimentary features: Bedded or unbedded massive deposits. San Luis Fm. Image width: 10.9cm.	
CBS: Coral Boundstone Subfacies Main components: Branching and nodular coral colonies, mainly in growth position. Subordinate components: Sheet-like coral colonies, molluscs, echinoids, coral detritus, coralline algae, porcelaneous foraminifera (soritids, archaiasinids, miliolids), other skeletal remains and siliciclastic grains. Texture: Boundstone within poorly sorted packstone-grainstone or terrigenous matrix. Other sedimentary features: Amalgamated bioherms and biostromes with parallel, massive, nodular, wavy and cross beddings. San Luis Fm. Image width: 6.9mm.	
DCS: Detrital Coral Subfacies Main components: Fragments of branching and columnar coral colonies. Subordinate components: Scattered rhodoliths, larger foraminifera, molluscs, coralline algae, other skeletal rests and siliciclastic grains. Texture: Floatstone and rudstone with packstone, grainstone or poorly sorted terrigenous matrix. Other sedimentary features: Coral fragments commonly encrusted, massive or nodular bedding, no orientation or gradation. San Luis Fm. Image width: 6.9mm.	

FIGURE II. Continued.

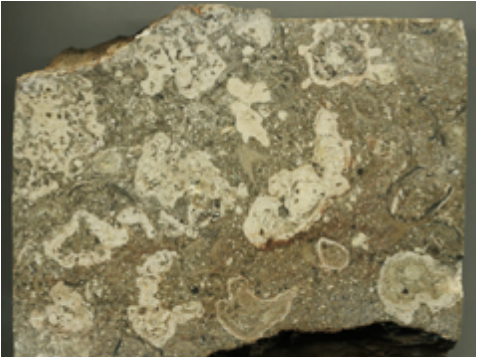
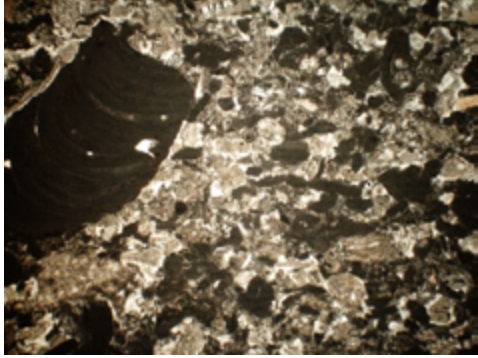
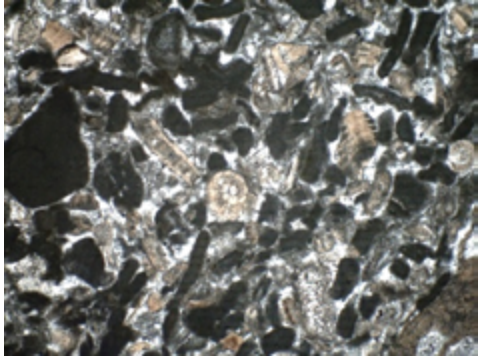
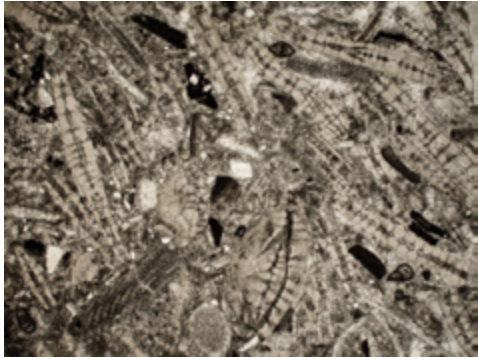
RF: Rhodolith Facies Main components: Rhodoliths and coralline algae detritus. Subordinate components: Amphisteginids, miogypsinids, nummulitids, lepidocyclinids, molluscs, echinoids, and other minor skeletal fragments. Texture: Floatstone to rudstone with a poorly sorted packstone to grainstone matrix. Other sedimentary features: Various rhodolith shapes including spherical, elongated and branching forms, nodular to massive bedding, no orientation or gradation. Churuguara Fm. Image width: 12.6cm.	
MF: Maerl Facies Main components: Coralline algae detritus and branches. Subordinate components: Amphisteginids, miogypsinids, nummulitids, lepidocyclinids, and other minor skeletal rests. Texture: Floatstone to rudstone with packstone matrix. Other sedimentary features: Massive bedded or unbedded; grading within Coralline Algal Debris Facies. Churuguara Fm. Image width: 6.9mm.	
CADF: Coralline Algal Debris Facies Main components: Coralline algae detritus and larger foraminifera (amphisteginids, miogypsinids, nummulitids and lepidocyclinids). Subordinate components: Molluscs, echinoids, rotaliids, lagenids, soritids, archaisinids, miliolids, bryozoans, sporadic small rhodoliths, and other minor skeletal rests. Texture: Packstone to grainstone. Other sedimentary features: Tabular, massive or wavy bedding; no gradation. Churuguara Fm. Image width: 3.3mm.	
HF: Heterostegina Facies Main components: Reworked tests of <i>Heterostegina</i> sp. Subordinate components: Other nummulitids, lepidocyclinids, amphisteginids, miogypsinids, soritids, archaisinids, coralline algae detritus, coral fragments, and abraded molluscs. Common detrital grains. Texture: Floatstone-rudstone within a skeletal to siliciclastic matrix. Other sedimentary features: Both chaotic and horizontally orientated fabrics; massive, wavy or cross bedding. San Luis Fm. Image width: 6.9mm.	

FIGURE II. Continued.

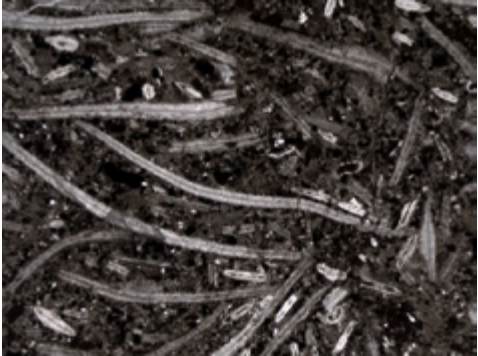
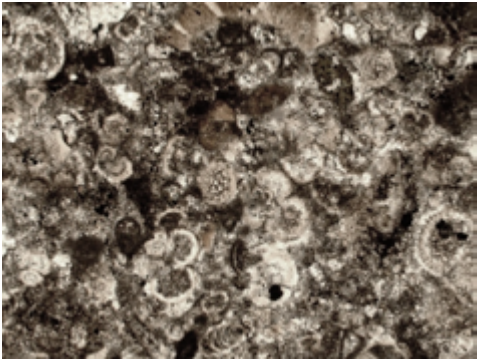
LF: <i>Lepidocyclina</i> Facies	
Main components: Large and flat <i>Lepidocyclina</i> and <i>Eulepidina</i> tests.	
Subordinate components: Nummulitids, other minor skeletal fragments and glauconite grains.	
Texture: Rudstone with bioclastic packstone matrix; common micropeloidal micrite to shally-rich matrix.	
Other sedimentary features: Randomly or horizontal orientated fabrics; bedded or unbedded; grading with the Planktonic Foraminifera Facies.	
Churuguara Fm. Image width: 23.4mm.	
PFF: Planktonic Foraminifera Facies	
Main components: Globigerinid planktonic foraminifera.	
Subordinate components: Larger foraminifera, coralline algae fragments, and glauconite grains.	
Texture: Wackestone-packstone with a micritic-shally matrix.	
Other sedimentary features: No bedding or grading.	
San Luis Fm. Image width: 1.7mm.	

FIGURE II. Continued.